VOLUME 3

MIT Quantum Science and Engineering Consortium

QSEC Quarterly

Winter 2022

Contents

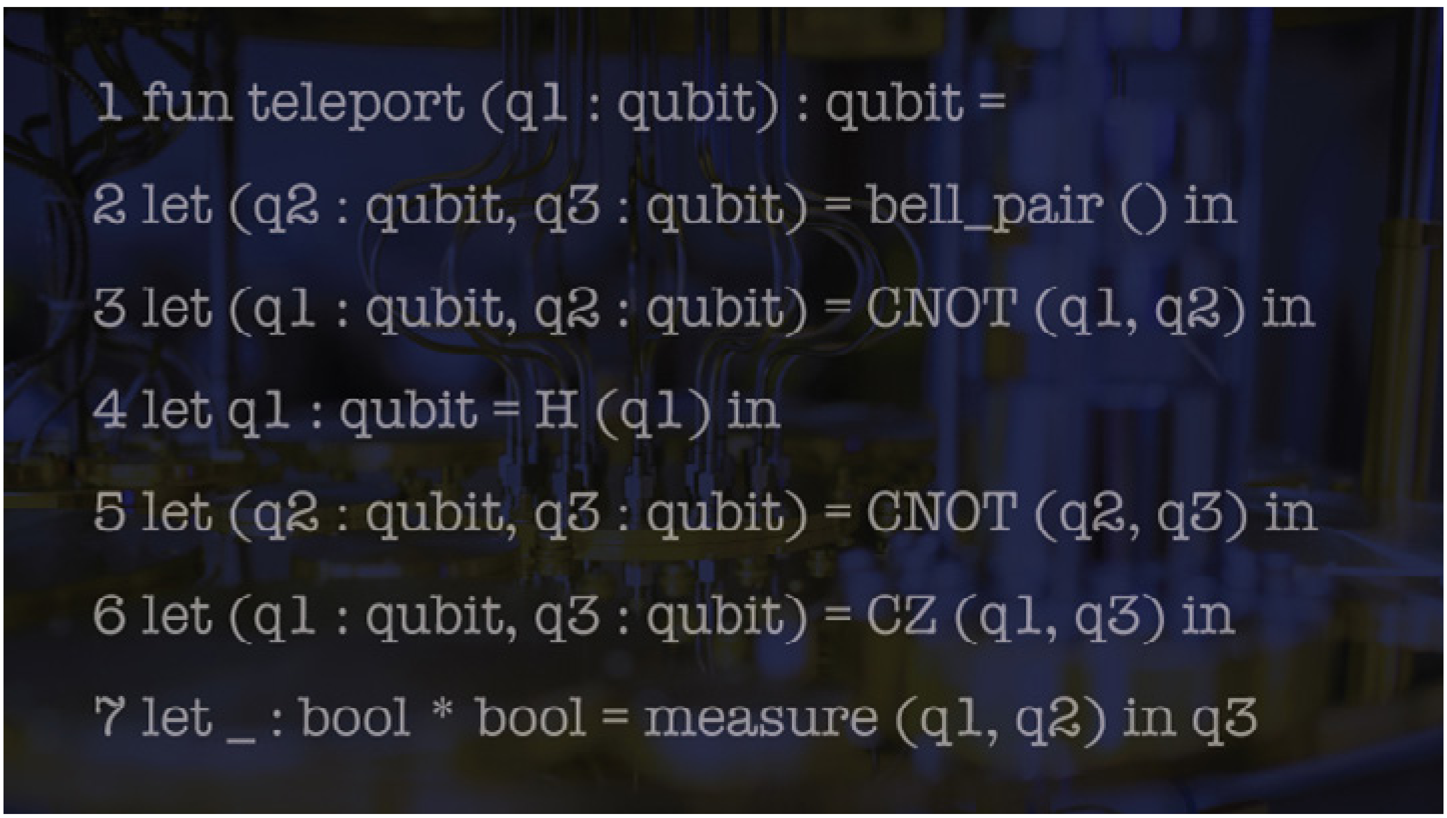

Image: RLE

A new language for quantum computing
Now out in MIT News from MIT-CQE Doc Bedard Fellow, Chris McNally: "Twist: Sound Reasoning for Purity and Entanglement in Quantum Programs" by Charles Yuan, Chris McNally and MIT Prof. Michael Carbin. “Twist is an MIT-developed programming language that can describe and verify which pieces of data are entangled to prevent bugs in a quantum program."

FROM THE DIRECTOR

It is our pleasure to present the Winter 2022 edition of the Quantum Science and Engineering Consortium (QSEC) newsletter.

The spring term is well underway at MIT and with it a number of exciting developments for the MIT quantum community.

We held our first annual QSEC meeting on February 6th, a day-long event with more than 40 students and faculty attending presenting 36 posters to our QSEC membership. The day also featured fantastic plenary talks by Dr. Junsgang Kim (CTO, Ion-Q) and Dr. Isaac Chuang (Professor, MIT). We'd like to extend our thanks to MIT's iQuISE graduate student group for helping to organize this event.

In addition, we are pleased to announce the QSEC Connector, a web interface aiming to connect the QSEC membership and Lincoln Laboratory to MIT students who are interested in internships in quantum. And, thank you to Chihiro Watanabe for leading its development. Please reach out to Paula Jorgensen for more information.

Wishing you all a productive and prosperous spring 2022!

William D. Oliver

William D. Oliver
william.oliver@mit.edu

DIRECTOR
MIT Center for Quantum Engineering (CQE)

PROFESSOR
of Electrical Engineering and Computer Science and of Physics

LINCOLN LABORATORY FELLOW

MIT-CQE Mission

MIT's Center for Quantum Engineering is dedicated to the academic pursuit and practice of science and engineering to accelerate the practical application of quantum technologies for the betterment of humankind.

CQE PI FEATURE

From Neutrino Hunter to Qubits Whisperer

JOSEPH FORMAGGIO
Professor of Physics
Division Head, Experimental Nuclear and Particle Physics

Joseph Formaggio, a professor of physics, explores the nature of neutrinos and their deep connection between particle physics, quantum mechanics and cosmology. Neutrinos are a fundamental particle, that is, basic building blocks of the universe. Every second, trillions of these particles pass through your body. Their mass is so tiny, and they interact so weakly with other matter, that it is nearly impossible to detect them, making it very difficult to study their properties.

Formaggio leads multiple research projects to understand neutrino properties and how they fit into our understanding of the universe. He is a leading member of the KATRIN and Project 8 experiments, which use the process of tritium beta decay —originally proposed by Enrico Fermi— to measure the mass of the neutrino directly.

In a recent milestone that will bear on future discoveries in nuclear and particle physics, KATRIN scientists established a new upper limit on the mass of the neutrino subatomic particle: 0.8 eV/c2. Published in Nature Physics (https://www.nature.com/articles/s41567-021-01463-1), the discovery has pushed our understanding of neutrinos' mass.

"The idea of using radioactive decays to measure neutrino masses is as old as the idea of the neutrino itself," says Formaggio. "[Enrico] Fermi himself devised the technique back in the 1930s. But only now do we have the capabilities to make use of the technique to extract the neutrino mass with such precision."

Formaggio's group develops novel detector technologies and techniques to better understand the properties of neutrinos and other rare and exotic particles. The group developed the technique of cyclotron radiation emission spectroscopy to accurately measure the energy of electrons emitted in beta decay; a technique now used by the Project 8 experiment.

The Formaggio group is also developing new cryogenic bolometers to better understand neutrino interactions at extremely low energies. Such detectors are part of the upcoming Ricochet experiment, which aims to study the process of coherent neutrino scattering using neutrinos created in nuclear reactors. More recently, the group has been exploring the potential role of quantum sensors and quantum readout systems for the purpose of detecting neutrinos and other weakly interacting particles.

One may be curious how a neutrinos hunter took a hard left and landed into the Quantum Computing field. "I guess you could say there are two common themes in my work: I like to take techniques or methods that are usually seen in one field and I apply it to my field or vice versa. The other is that I often pursue projects where I am explicitly told that there's no way something will work, and then I make it work." Formaggio's approach clearly works; he has produced a successful track record of surprising discoveries across multiple fields.

In 2019 Formaggio was conversing with MIT-CQE Director, MIT Prof. Will Oliver over lunch about the many sources of decoherence that could destabilize a qubit, such as fluctuating magnetic and electric fields, thermal energy, and even interference between qubits. "Everyone is having a problem with getting qubits to last a really long time. The longer they last, the more computations you can do." Oliver suggested radiation may be a problem. "Your walls have radiation, there's cosmic rays that cause radiation." So Formaggio thought, "you've come to the right guy."

So Oliver and Formaggio teamed up to see how they might nail down the effect of low-level environmental radiation on qubits. "Cosmic ray radiation is hard to get rid of," Formaggio says. "It's very penetrating, and goes right through everything like a jet stream. If you go underground, that gets less and less. It's probably not necessary to build quantum computers deep underground, like neutrino experiments, but maybe deep basement facilities could probably get qubits operating at improved levels."

Many told Formaggio it couldn't be radiation. But through experimentation the team reported that the low-level, otherwise harmless background radiation that is emitted by trace elements in concrete walls and incoming cosmic rays are enough to cause decoherence in qubits. They found that this effect, if left unmitigated, will limit the performance of qubits to just a few milliseconds.

Given the rate at which scientists have been improving qubits, they may hit this radiation-induced wall in just a few years. To overcome this barrier, scientists will have to find ways to shield qubits — and any practical quantum computers — from low-level radiation, perhaps by building the computers underground or designing qubits that are tolerant to radiation's effects.

"These decoherence mechanisms are like an onion, and we've been peeling back the layers for the past 20 years, but there's another layer that left unabated is going to limit us in a couple years, which is environmental radiation," says Oliver. "This is an exciting result, because it motivates us to think of other ways to design qubits to get around this problem." Formaggio is intrigued by the types of sensitivities these experiments can produce and hopes there will be more interplay between the two fields.

While the pandemic delayed his plans, Formaggio envisions a sabbatical in France in his future. "I'll have an opportunity to work on one of my experiments based there while continuing to make Project 8, a long-term experiment, bigger and better." While he continues to push his detector explorations further, he wants to write and recharge there too.

Formaggio holds a BS degree from Yale University in physics and PhD from Columbia University where he did his dissertation on neutrino physics. Prior to his arrival to MIT in 2005, Formaggio joined the Sudbury Neutrino Observatory as a postdoctoral fellow at the University of Washington, where he was later appointed as a research assistant professor.

Sources and credits: Interview with Prof. Joseph Formaggio and excerpts from MIT News: "On the hunt for neutrinos" by Anne Trafton, "Cosmic Rays may soon stymie quantum computing" by Jennifer Chu, "A new upper limit on the mass of neutrinos" by Laboratory for Nuclear Science, and Formaggio Physics page profile.

CQE STUDENT FEATURE

Engineering Quantum Systems (EQuS) group: Chris McNally

Research group name: The Engineering Quantum Systems (EQuS) group

Research Advisor: MIT-CQE Director, MIT Prof. William D. Oliver

Hometown, Country: Boston, Massachusetts, USA

Academic History Prior to coming to MIT: BS in Mathematics and Physics at McGill University in beautiful Montreal, Quebec.

What brought you to MIT? Growing up in Massachusetts, I met a fair number of people who'd been through MIT. It was clear to me that there was something distinctly special about them, and that "MIT people" are the sort of people to emulate. I also attended some memorable ESP programs back then. So, MIT meant something to me from early on. After undergrad, I joined Danielle Braje's lab at Lincoln Laboratory as assistant staff. She and her team are amazing experimentalists, and I was incredibly lucky to be able to work with and learn from them. Being at Lincoln also brought me into contact with the quantum engineering groups on campus. Not only was their research output inspiring, graduate students from those groups were already some of my colleagues. Their example and help made it seem possible to apply.

CHRIS MCNALLY
CQE-LPS Doc Bedard Fellow.
This three-year graduate fellowship i
s awarded through the MIT Center for Quantum Engineering. It is funded by the Laboratory of Physical Sciences and recognizes the achievements and technical leadership of Dr. Fernand (Doc) Bedard, a pioneer of cryogenic computing.

What interests you the most about your research? At MIT I've been able to collaborate with people from a remarkable range of backgrounds, from condensed matter to programming language theory. Even within the EQuS group–which is focused on superconducting quantum circuits–our research runs from basic materials science to quantum algorithms. That's what makes Quantum engineering an exciting field to be in today. In part because of the limitations of present-day qubit devices, we have to push in every direction at once. And, for researchers, it's not enough to have one tool in your belt. I came to MIT as an (apprentice) experimental physicist, but an early device calibration project sent me down a deep programming rabbit hole which, in turn, has recently led to some exciting new explorations in computer science proper.

What are your future plans? I recently completed a summer internship at LPS in Maryland as part of the Doc Bedard fellowship program. Not only was it a reprieve from a year-long lockdown, but a welcome interlude before the "back half" of the PhD. It was a great opportunity to discover entirely new research problems.

In the long term, I'm undecided between industry, an academic postdoc, or something else entirely. So far in grad school, I've had a few opportunities–like the LPS internship–to see "outside," including a couple of weeks here and there in industry. Academia isn't all there is to the world, but it's been very rewarding so far.

AROUND THE INSTITUTE

Meet our MIT-CQE Principal Investigators

RAYMOND ASHOORI
Physics

MARC BALDO
EECS

JOHN BARRY
Lincoln Laboratory

KARL BERGGREN
EECS

RAFAEL GOMEZ-BOMBARELLI
DMSE

DON BORONSON
Lincoln Laboratory

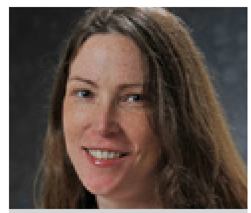

DANIELLE BRAJE
Lincoln Laboratory

COLIN BRUZEWICZ
Lincoln Laboratory

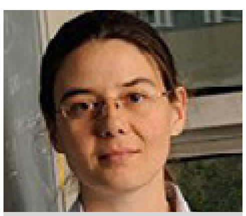

PAOLA CAPPELLARO
NSE

JOSEPH CHECKELSKY
Physics

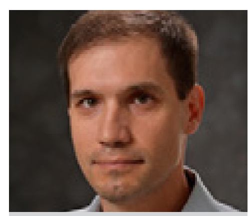

JOHN CHIAVERINI
Lincoln Laboratory

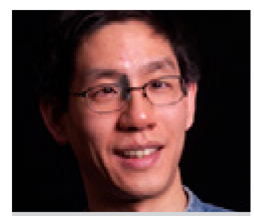

ISAAC CHUANG
EECS, Physics

MICHAEL CUSUMANO
Sloan School

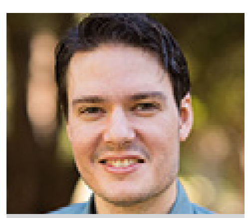

RICCARDO COMIN
Physics

ERIC DAULER
Lincoln Laboratory

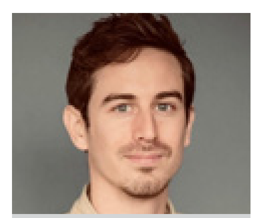

DANE DEQUILETTES
Lincoln Laboratory

Meet our MIT-CQE Principal Investigators

BENJAMIN DIXON
Lincoln Laboratory

DIRK ENGLUND
EECS

EDWARD FARHI
Physics

RICHARD FLETCHER
Physics

JOSEPH A. FORMAGGIO
Physics

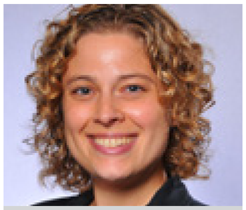

DANNA FREEDMAN
Chemistry

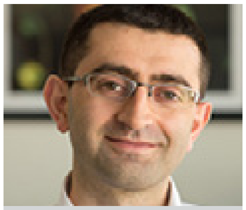

NUH GEDIK
Physics

MARK GOUKER
Lincoln Laboratory

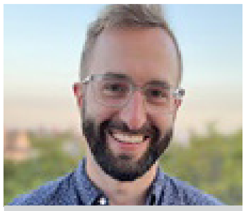

JEFF GROVER
RLE

SIMON GUSTAVSSON
RLE

SCOTT HAMILTON
Lincoln Laboratory

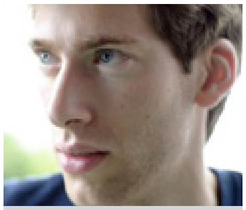

ARAM W. HARROW
Physics

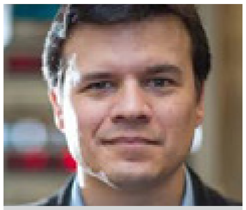

PABLO JARILLO-HERRERO
Physics

LONG JU
Physics

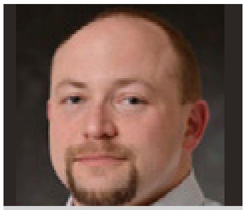

ANDREW J. KERMAN
Lincoln Laboratory

WOLFGANG KETTERLE
Physics

Meet our MIT-CQE Principal Investigators

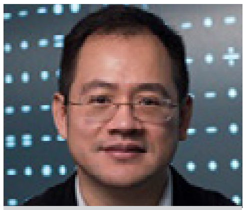

JU LI
NSE MSE

MINGDA LI
NSE

LUQIAO LIU
EECS

SETH LLOYD
ME, ES, Physics

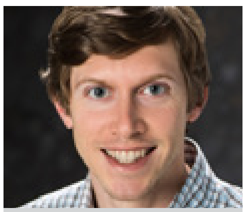

ROBERT McCONNELL
Lincoln Laboratory

ANAND NATARAJAN
EECS

JELENA NOTAROS
EECS

KEVIN OBENLAND
Lincoln Laboratory

KEVIN P. O'BRIEN
EECS

WILLIAM D. OLIVER
EECS, Physics, Lincoln Laboratory

TERRY ORLANDO
EECS

LINH PHAM
Lincoln Laboratory

RAJEEV RAM
EECS

MOLLIE SCHWARTZ
Lincoln Laboratory

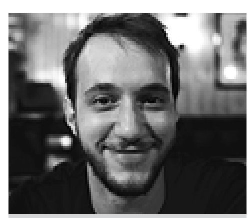

KYLE SERNIAK
Lincoln Laboratory

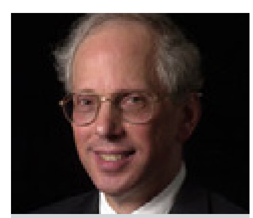

JEFFREY H. SHAPIRO
EECS

Meet our MIT-CQE Principal Investigators

PETER SHOR
Mathematics

MICHAEL SIPSER
Mathematics

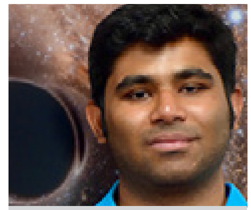

VIVISHEK SUDHIR
ME

TIMOTHY SWAGER
Chemistry

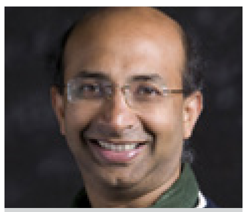

SENTHIL TODRARI
Physics

TROY VAN VOORHIS
Chemistry

VLADAN VULETIC
Physics

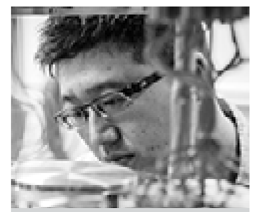

JOEL I-JAN WANG
RLE

LINDLEY WINSLOW
Physics

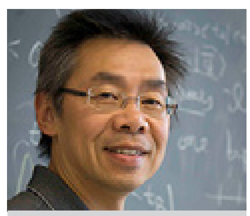

FRANCO N. C. WONG
RLE

WAYNE WOODS
Lincoln Laboratory

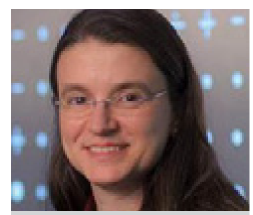

BILGE YILDIZ
NSE MSE

JONILYN YODER
Lincoln Laboratory

MARTIN ZWIERLEIN
Physics

RAYMOND ASHOORI, *Physics*

“Cascade of isospin phase transitions in Bernal bilayer graphene at zero magnetic field”
Sergio C. de la Barrera, Samuel Aronson, Zhiren Zheng, Kenji Watanabe, Takashi Taniguchi, Qiong Ma, Pablo Jarillo-Herrero, Raymond Ashoori
arXiv:2110.13907 (2021)

MARC BALDO, *EECS*

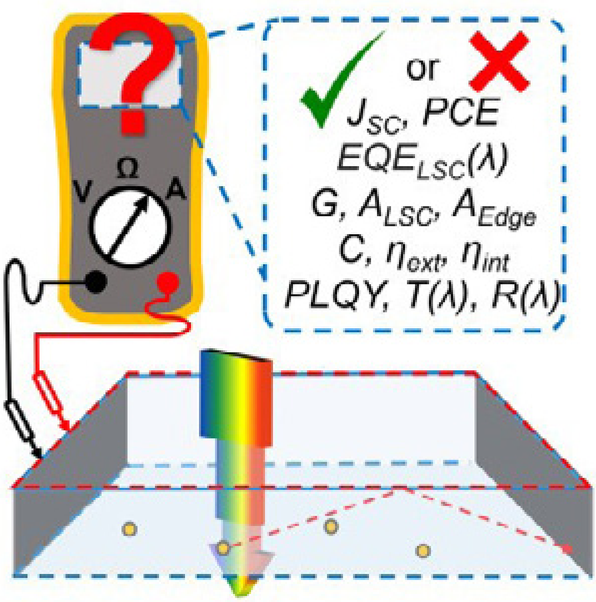

“Consensus statement: Standardized reporting of power-producing luminescent solar concentrator performance”
Chenchen Yang, Harry A. Atwater, Marc A. Baldo, ..., et al.
Joule (2022)

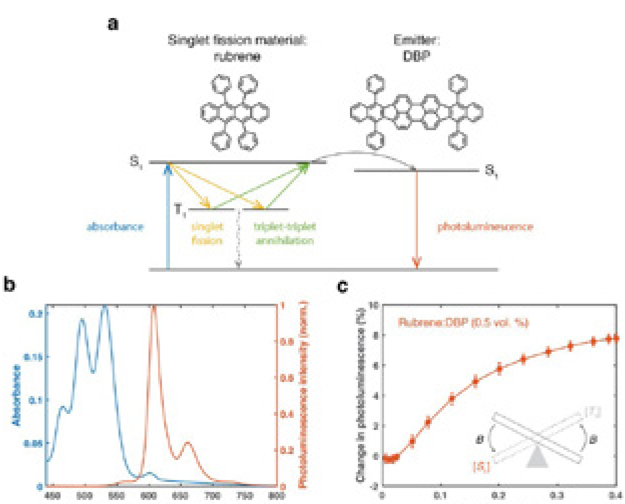

“Magnetic field-switchable Laser Via Optical Pumping of Rubrene”
Collin F. Perkinson, Markus Einzinger, Joseph Finley, Moungi G. Bawendi, Marc A. Baldo
Adv. Mater (2021)

KARL BERGGREN, *EECS*

"Electron Emission Regimes of Planar Nano Vacuum Emitters"
Marco Turchetti, Yujia Yang, Mina R. Bionta, Alberto Nardi, Luca Daniel, Karl K. Berggren, Phillip D. Keathley
arxiv.org/abs/2201.04043 (2022)

"Improved heralded single-photon source with a photon-number-resolving superconducting nanowire detector"
Samantha I. Davis, Andrew Mueller, Raju Valivarthi, Nikolai Lauk, Lautaro Narvaez, Boris Korzh, Andrew D. Beyer, Marco Colangelo, Karl K. Berggren, Matthew D. Shaw, Neil Sinclair, Maria Spiropulu
arxiv.org/abs/2112.11430 (2021)

"A Superconducting Nanowire-based Architecture for Neuromorphic Computing"
Authors: Andres E. Lombo, Jesus E. Lares, Matteo Castellani, Chi-Ning Chou, Nancy Lynch, Karl K. Berggren
arXiv:2112.08928 (2021)

"Broadband solenoidal haloscope for terahertz axion detection"
Jesse Liu, Kristin Dona, Gabe Hoshino, Stefan Knirck, Noah Kurinsky, Matthew Malaker, David Miller, Andrew Sonnenschein, Pete Barry, Karl K. Berggren, Daniel Bowring, Gianpaolo Carosi, Clarence Chang, Aaron Chou, Mohamed Hassan, Rakshya Khatiwada, Samantha Lewis, Juliang Li, Sae Woo Nam, Omid Noroozian, Tony X. Zhou
arXiv:2111.12103 (2021)

"Secondary Electron Count Imaging in SEM"
Akshay Agarwal, John Simonaitis, Vivek K. Goyal, Karl K. Berggren
arxiv.org/abs/2111.01862 (2021)

"New Constraints on Dark Matter from Superconducting Nanowires"
Yonit Hochberg, Benjamin V. Lehmann, Ilya Charaev, Jeff Chiles, Sae Woo Nam, Karl K. Berggren arxiv.org/abs/2110.01586 (2021)

"First Constraints on Dark Photon Dark Matter with Superconducting Nanowire Detectors in an Optical Haloscope"
Jeff Chiles, Ilya Charaev, Robert Lasenby, Masha Baryakhtar, Junwu Huang, Alexana Roshko, George Burton, Marco Colangelo, Ken Van Tilburg, Asimina Arvanitaki, Sae Woo Nam, Karl K. Berggren
arxiv.org/abs/2110.01582 (2021)

KARL BERGGREN, *EECS*

"PHz Electronic Device Design and Simulation for Waveguide-Integrated Carrier-Envelope Phase Detection"
Dario Cattozzo Mor, Yujia Yang, Felix Ritzkowsky, Franz X. Kärtner, Karl K. Berggren, Neetesh Kumar Singh, Phillip D. Keathley
arxiv.org/abs/2109.12558 (2021)

"50 Ω transmission lines with extreme wavelength compression based on superconducting nanowires on high-permittivity substrates"
Daniel F. Santavicca, Marco Colangelo, Carleigh R. Eagle, Maitri P. Warusawithana, and Karl K. Berggren
Appl. Phys. Lett. 119, 252601 (2021) | arxiv.org/abs/2111.01006

RAFAEL GOMEZ-BOMBARELLI, *DMSE*

"Excited state, non-adiabatic dynamics of large photoswitchable molecules using a chemically transferable machine learning potential"
Simon Axelrod, Eugene Shakhnovich, Rafael Gómez-Bombarelli
arxiv.org/abs/2108.04879 (2021)

PAOLA CAPPELLARO, *NSE*

[Optimal control of a quantum sensor: From an analytic solution to a fast algorithm]
S. Hernández-Gómez, F. Balducci, G. Fasiolo, P. Cappellaro, N. Fabbri, A. Scardicchio
arXiv:2112.14998

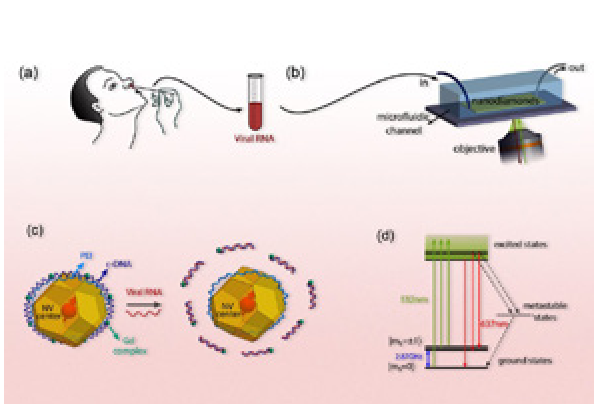

"SARS-CoV-2 Quantum Sensor Based on Nitrogen-Vacancy Centers in Diamond"
Changhao Li, Rouhollah Soleyman, Mohammad Kohandel, and Paola Cappellaro
https://news.mit.edu/2021/quantum-sensor-detect-covid-1220, https://pubs.acs.org/doi/10.1021/acs.nanolett.1c02868, arXiv:2111.05472

Using mathematical simulations, MIT researchers have shown that it would be possible to design a sensor, based on quantum physics, that could detect the SARS-CoV-2 virus.

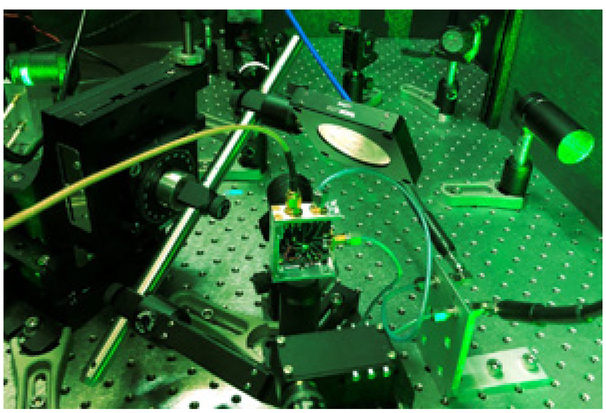

"Observation of symmetry-protected selection rules in periodically driven quantum systems"
Guoqing Wang, Changhao Li, Paola Cappellaro
MIT News | PhysRevLett.127.140604 | arXiv:2105.12209 (2021)

Photo: Guoqing Wang/MIT
Instrumentation setup in the Quantum Engineering Group at MIT to study dynamical symmetries with qubits in diamond crystals

JOSEPH CHECKELSKY, *Physics*

“Snapshots of a light-induced metastable hidden phase driven by the collapse of charge order”

Frank Y. Gao, Zhuquan Zhang, Linda Ye, Yu-Hsiang Cheng Zi-Jie Liu, Joseph G. Checkelsky, Edoardo Baldini, Keith A. Nelson
arXiv:2112.11015 (2021)

“Signatures of Bosonic Landau Levels in a Finite Momentum Superconductor”

A. Devarakonda, T. Suzuki, S. Fang, J. Zhu, D. Graf, M. Kriener, L. Fu, E. Kaxiras, J. G. Checkelsky
MIT News | Nature 599, 51-56 (2021)

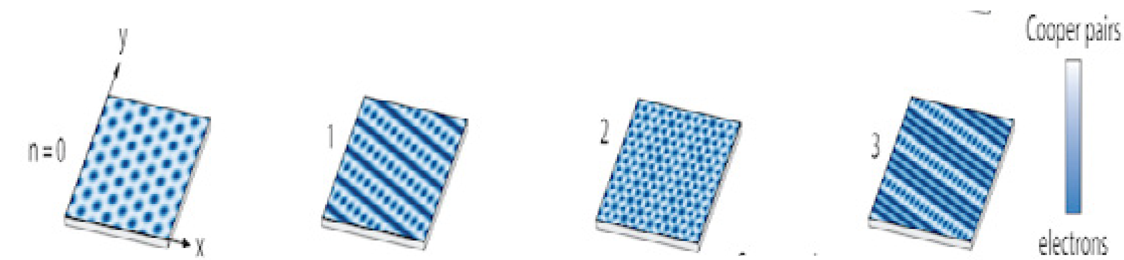

Diagram illustrating three different patterns of superconnectivity realized in a new material synthesized at MIT.

“Evidence of two-dimensional at band at the surface of antiferromagnetic kagome metal FeSnP”

M. Han, H. Inoue, S. Fang, C. John, L. Ye, M. K. Chan, D. Graf, T. Suzuki, M. P. Ghimire, W. J. Cho, E. Kaxiras, J. G. Checkelsky”
Nature Communications 12, 5345 (2021)

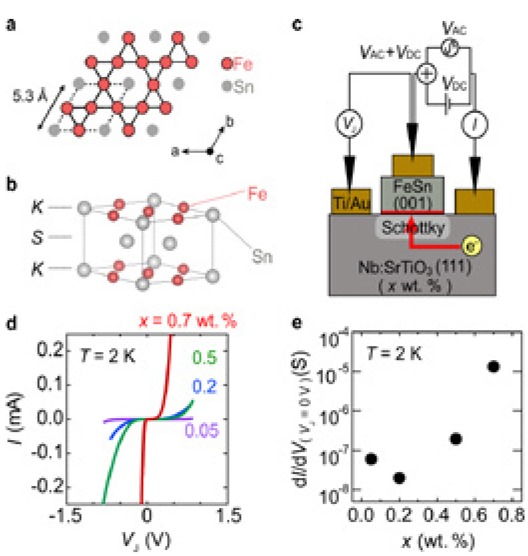

a Top view of the Fe kagome layer (Fe3Sn). Dashed lines delineate the crystallographic unit cell. b Crystal structure of FeSn, consisting of kagome layers (K) and Sn honeycomb (stanene) layers (S) stacked along the c-direction. c Schematic of the three-terminal planar Schottky tunneling measurement setup. AC (VAC) and DC (VDC) voltages are applied onto the tunneling electrode and the junction voltage (VJ) and the tunnel current (I) are measured. d Current-voltage (I–V) characteristics of FeSn/Nb:STO junctions with different Nb concentrations, all measured at temperature T = 2 K. e Nb concentration-dependent zero bias differential tunneling conductance (dI/dV(VJ = 0 V)) at T = 2 K.

JOSEPH CHECKELSKY, *Physics*

“Ferromagnetic helical nodal line and Kane-Mele spin-orbit coupling in kagome metal Fe3Sn2”

Shiang Fang, Linda Ye, Madhav Prasad Ghimire, Mingu Kang, Junwei Liu, Min-yong Han, Liang Fu, Manuel Richter, Jeroen van den Brink, Efthimios Kaxiras, Riccardo Comin, and Joseph G. Checkelsky

Phys. Rev. B 105, 035107 (2022) | arXiv:2103.08803 (2021)

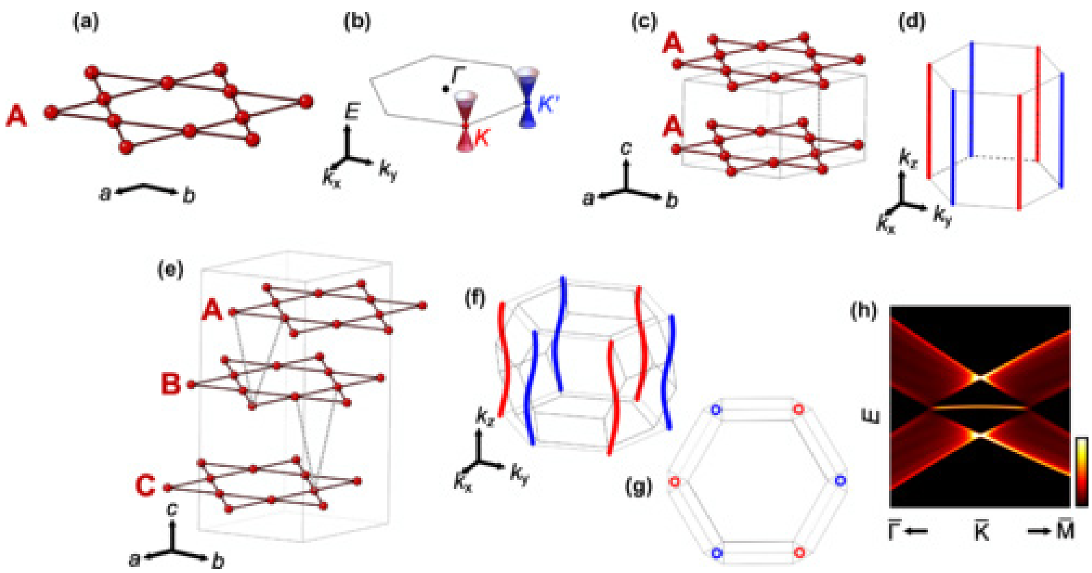

Nodal lines and three-dimensional stacking of the kagome lattice. (a) The two-dimensional (2D) kagome lattice and (b) associated Dirac fermions in the hexagonal Brillouin zone (BZ). Blue and red Dirac fermions at K and K′ possess opposite chiralities. (c) Schematic of a three-dimensional (3D), A-A stacked kagome lattice, and (d) the corresponding vertical nodal lines in the hexagonal prism BZ. (e) Schematic of an A-B-C stacking of the kagome lattice and the corresponding helical nodal lines are shown in (f) and (g) from both an isometric (f) and a top (g) perspective. In (c) and (e), the dashed lines represent the interplane hopping t1 while the in-plane kagome bonds are characterized by an hopping integral t0. In (f), we show the rhombohedral BZ along with a hexagonal prism extended from the 2D BZ illustrated in (b). (h) Surface spectra weight of the A-B-C kagome tight-binding model. A drumhead surface state (DSS) can be identified as the flat and bright intensity within the projection of the helical nodal line to the surface BZ

ISAAC CHUANG, *EECS, Physics*

"omg blueprint for trapped ion quantum computing with metastable states"
D. T. C. Allcock, W. C. Campbell, J. Chiaverini, I. L. Chuang, E. R. Hudson, I. D. Moore, A. Ransford, C. Roman, J. M. Sage, D. J. Wineland
Applied Physics Letters 119 (21), 214002 (2021) | arxiv.org/abs/2109.01272 (2021)

"Learning Noise via Dynamical Decoupling of Entangled Qubits"
Trevor McCourt, Charles Neill, Kenny Lee, Chris Quintana, Yu Chen, Julian Kelly, V. N. Smelyanskiy, M. I. Dykman, Alexander Korotkov, Isaac L. Chuang, A. G. Petukhov
arXiv:2201.11173 (2022)

"Active Learning of Quantum System Hamiltonians yields Query Advantage"
Arkopal Dutt, Edwin Pednault, Chai Wah Wu, Sarah Sheldon, John Smolin, Lev Bishop, Isaac L. Chuang
arXiv:2112.14553 (2021)

"Efficient Fully-Coherent Hamiltonian Simulation"
John M. Martyn, Yuan Liu, Zachary E. Chin, Isaac L. Chuang
arXiv:2110.11327 (2021)

"A Grand Unification of Quantum Algorithms"
John M. Martyn, Zane M. Rossi, Andrew K. Tan, Isaac L. Chuang
PRX Quantum 2, 040203 (2021) | arxiv.org/abs/2105.02859v3 (2021)

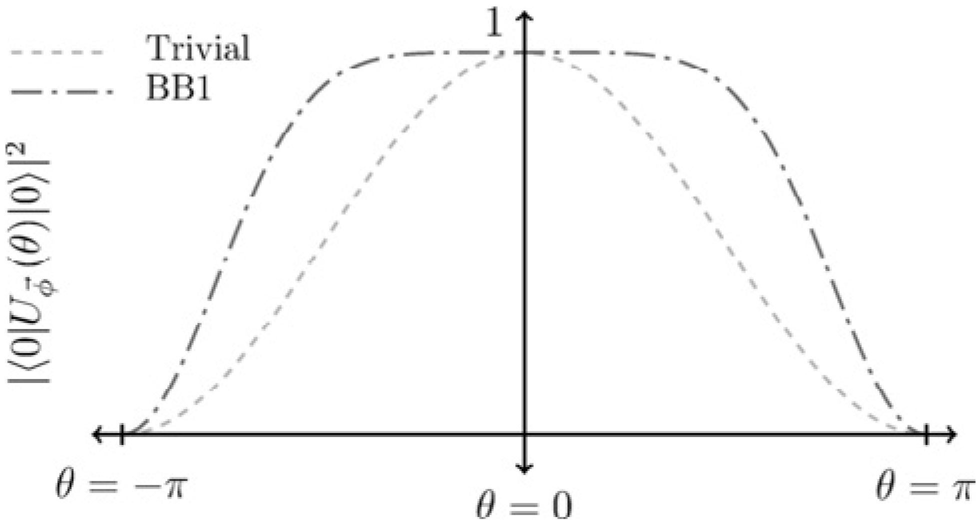

The transition probabilities for |0⟩→|0⟩ after the application of exp(iθX/2) (uniform dashed) and the QSP sequence for the BB1 protocol (dotted dashed). The latter transition probability is seen to be near one for a wider range of θ.

RICCARDO COMIN, *Physics*

"Ultrafast signatures of spin and orbital order in antiferromagnetic α-Sr2CrO4"
Min-Cheol Lee, Connor Occhialini, Jiarui Li, Zhihai Zhu, Nicholas S. Sirica, La Moyne T. Mix, Dmitry A. Yarotski, Riccardo Comin, Rohit P. Prasankumar
arXiv:2110.14004 (2021)

"Twofold van Hove singularity and origin of charge order in topological kagome superconductor CsV3Sb5"

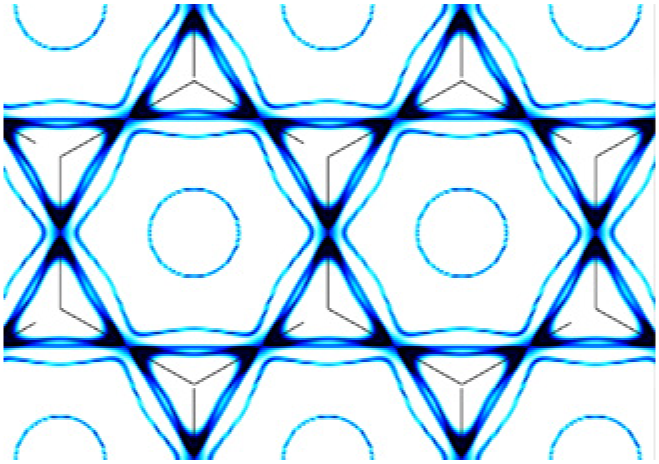

Mingu Kang, Shiang Fang, Jeong-Kyu Kim, Brenden R. Ortiz, Sae Hee Ryu, Jimin Kim, Jonggyu Yoo, Giorgio Sangiovanni, Domenico Di Sante, Byeong-Gyu Park, Chris Jozwiak, Aaron Bostwick, Eli Rotenberg, Efthimios Kaxiras, Stephen D. Wilson, Jae-Hoon Park & Riccardo Comin
MIT News (2022) | Nature Physics, 1-8 (2022)

A visualization of the zero-energy electronic states – also known as "Fermi surface" – from the kagome material studied by MIT's Riccardo Comin and colleagues

Randomized probe imaging through deep k-learning
Z Guo, A Levitan, G Barbastathis, R Comin
Optics Express 30 (2), 2247-2264 (2022)

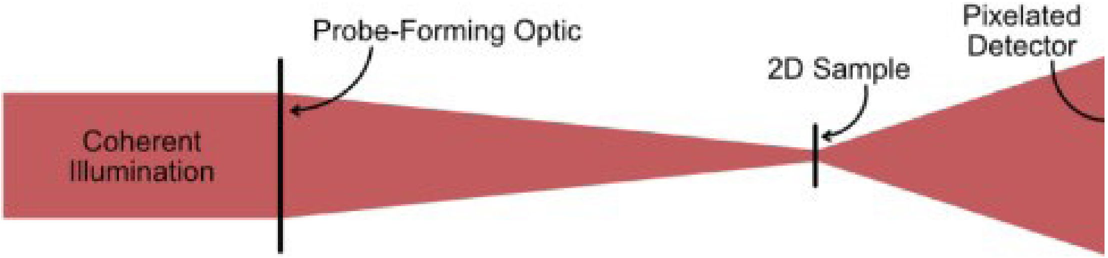

A conceptual diagram of the layout used in an RPI experiment.

RICCARDO COMIN, *Physics*

[Maskless Fourier transform holography]

K Keskinbora, AL Levitan, R Comin

[Optics Express 30 (1), 403-413 (2021)]

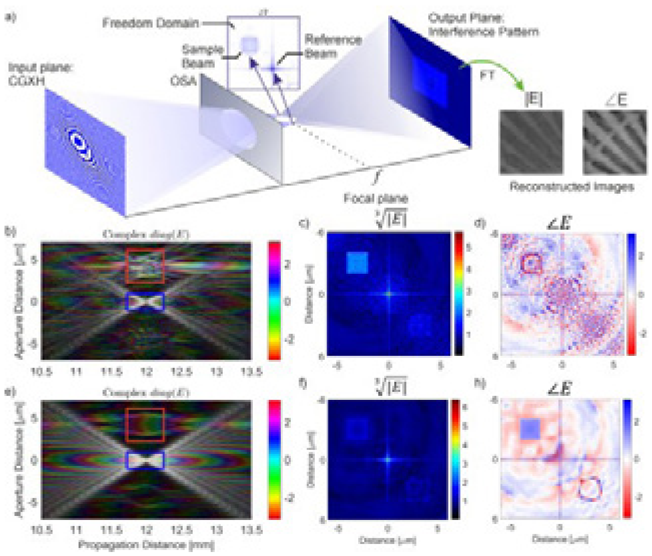

Schematic description of the proposed experiment. a In the StIXH experiment, a computer-generated X-ray hologram is illuminated by a coherent plane wave. Two separate beams with tailored complex-amplitudes are simultaneously projected onto the sample in lieu of the transmission mask, by a computer-generated hologram. A spatial filter called an order sorting aperture eliminates the spurious diffraction orders. The sample is illuminated by structured light at the focal plane (f), and the sample beam is imprinted with sample information such as chemical, structural, electronic/magnetic properties. An area detector captures the far-field interference pattern of the sample and the reference beams. A Fourier transform of the interference pattern yields the amplitude and phase images of the sample. b A 2D diagonal slice of the complex field created by a hologram synthesized using GSA, along the propagation direction near the focal plane (12 mm). Note the scrambled phase of the sample beam and the intensity variation (marked red) in relation to the reference beam (marked blue). c, d The amplitude and phase of the structured illumination pattern of a GSA hologram at f exhibit speckle noise in the sample beam as a result of constructive and destructive interference within this region due to the random phase. e Slice of the complex field of a DC-GSA hologram at f. Notice how the sample-beam has a flat phase at the focal plane in contrast to b. f, h The amplitude and phase of DC-GSA holograms at f clearly show relatively flat phase and intensity distribution.

DANE DEQUILETTES, *Lincoln Laboratory*

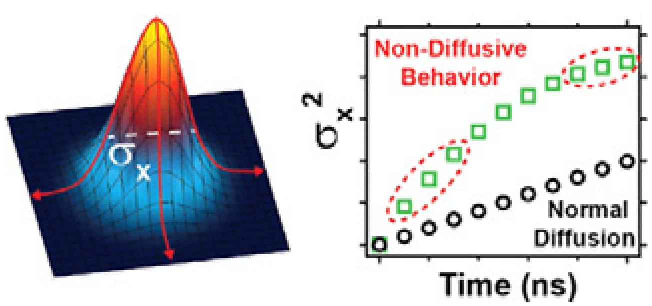

[“Impact of Photon Recycling, Grain Boundaries, and Nonlinear Recombination on Energy Transport in Semiconductors”]

Dane W deQuilettes, Roberto Brenes, Madeleine Laitz, Brandon T Motes, Mikhail M Glazov, Vladimir Bulović

[ACS Photonics.1c01186 (2021)]

DIRK ENGLUND, *EECS*

"High-speed programmable photonic circuits in a cryogenically compatible, visible-NIR 200 mm CMOS architecture"
Mark Dong, Genevieve Clark, Andrew J. Leenheer, Matthew Zimmermann, Daniel Dominguez, Adrian J. Menssen, David Heim, Gerald Gilbert, Dirk Englund, Matt Eichenfield
Nature Photonics (2021) | arXiv:2105.12531 (2021)

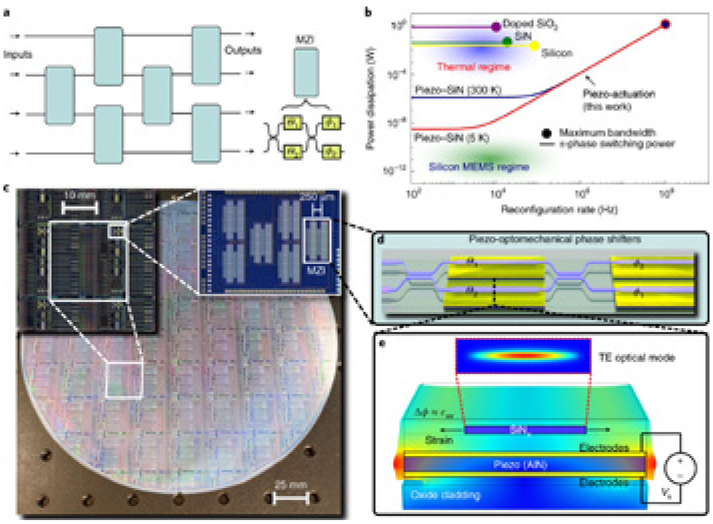

a, Schematic of a four-mode programmable circuit consisting of cascaded MZIs for SU(4) operations. b, Trade space diagram of the power–reconfiguration rate for other CMOS-compatible photonic technologies and our piezo-actuated photonics. c, Microscopy images of a fully processed 200 mm wafer with insets showing the zoomed-in view of a reticle and a 4 × 4 MZM. d, Three-dimensional concept art of an MZI with piezo-optomechanical phase shifters. e, Cross-sectional diagram of our phase shifter, illustrating how an applied voltage across the piezo results in strain imparted to the optical waveguide.

"Waveguide-Integrated Mid-Infrared Photodetection using Graphene on a Scalable Chalcogenide Glass Platform"
Jordan Goldstein, Hongtao Lin, Skylar Deckoff-Jones, Marek Hempel, Ang-Yu Lu, Kathleen A. Richardson, Tomas Palacios, Jing Kong, Juejun Hu, Dirk Englund
arXiv:2112.14857 (2021)

DIRK ENGLUND, *EECS*

[“The potential and global outlook of integrated photonics for quantum technologies”]

Emanuele Pelucchi, Giorgos Fagas, Igor Aharonovich, Dirk Englund, Eden Figueroa, Qihuang Gong, Hübel Hannes, Jin Liu, Chao-Yang Lu, Nobuyuki Matsuda, Jian-Wei Pan, Florian Schreck, Fabio Sciarrino, Christine Silberhorn, Jianwei Wang, Klaus D. Jöns
Nature Reviews Physics (2021)

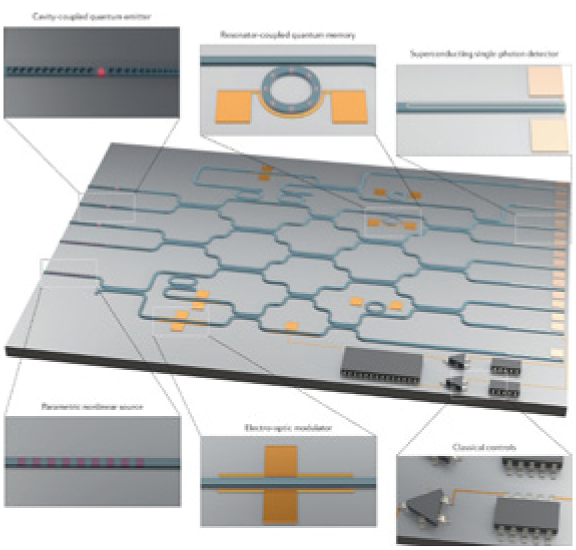

Quantum photonic integrated circuits (qPICs) are the devices realizing the various applications of integrated quantum photonics. They can be monolithically, hybrid or heterogeneously integrated and can harness the current progress of classical photonic integration platforms. qPIC architecture includes nonlinear optics (such as periodically poled structure) and quantum light sources (red dots/defects) in nanobeam cavities, quantum memories (optical resonators including ions/atoms), electro-optic modulators/switches and single-photon detectors (superconducting nanowires), classical controls (electronic components) and active and passive photonic elements. Some components are not represented in the figure due to space limitations, such as filter and classical pump sources.

“A vertically-loaded diamond microdisk resonator spin-photon interface”

Yuqin Duan, Kevin C. Chen, Dirk R. Englund, and Matthew E. Trusheim
Optics Express Vol. 29, Issue 26, pp. 43082-43090 (2021) | arXiv:2105.05695 (2021)

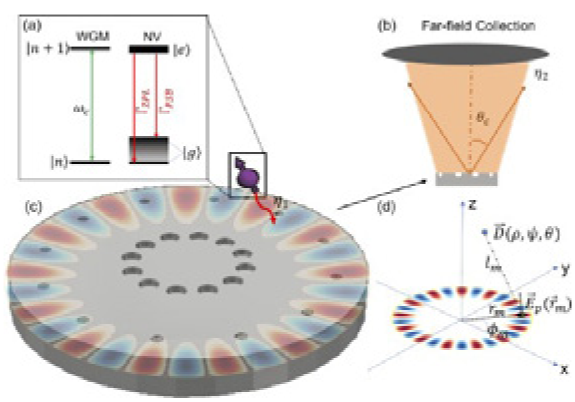

VLDMoRt concept. An NV center is coupled to a WGM resonator with efficiency $\eta 1\eta 1$, which in turn emits into the far-field collection mode with efficiency $\eta 2\eta 2$ through an embedded perturbative grating. (a) The WGM is on-resonance with the NV center’s ZPL. (b) Side view of VLDMoRt coupling to free space with emission angle $\theta c\theta c$. (c) The VLDMoRt design with a WGM excited. Red and blue represents the WGM near-field, and concentric, periodic pertubative gratings at two radii are shown. (d) Schematic diagram of the scattering model for far-field intensity analysis.

DIRK ENGLUND, *EECS*

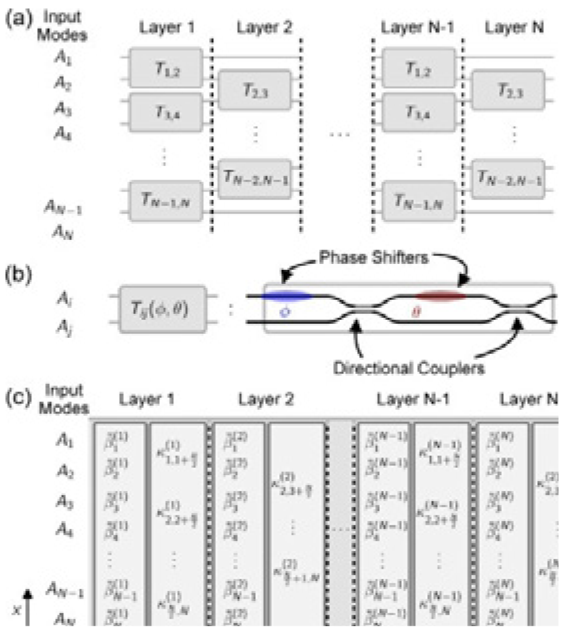

[**"Universal linear optics by programmable multimode interference"**](#)
Hugo Larocque and Dirk Englund
Optics Express Vol. 29, Issue 23, pp. 38257-38267 (2021) | arXiv:2107.06107 (2021)

SU(2) mesh architectures (a) Schematics of an SU(N) transformation decomposed into a rectangular mesh of SU(2) transformations TijTij. (b) Mach-Zehnder interferometer (MZI) used in integrated photonic platforms for implementing individual TijTijs in the mesh. These building blocks consist of two phase shifters, where one of them is book-ended by directional couplers. (c) MMI approach to realizing SU(N) transformations. The latter are achieved by segmenting the waveguide into layers where programmed refractive index variations first alter the propagation constants βm,nβm,n of modes m,nm,n to β (l) m,nβ~m,n(l) and subsequently couples them as parametrized by the coupling strength κ(l)mnκmn(l).

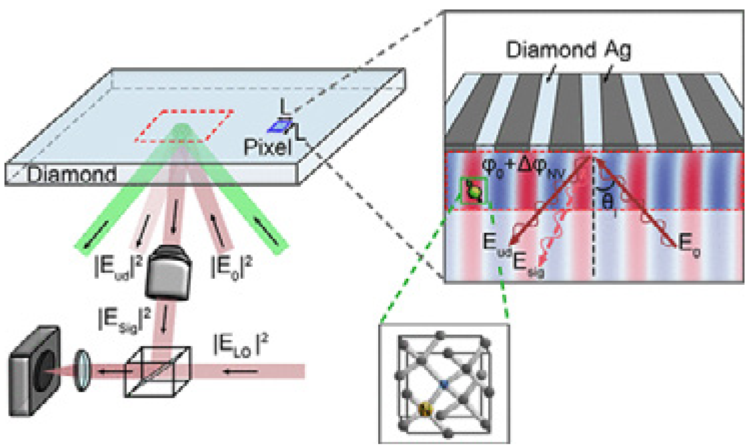

"Absorption-Based Diamond Spin Microscopy on a Plasmonic Quantum Metasurface"
Laura Kim, Hyeongrak Choi, Matthew Trusheim, and Dirk Englund
ACS Photonics 8, 11, 3218–3225 (2021) | arXiv:2011.04885 (2020)

"Infinitely Scalable Multiport Interferometers"
Ryan Hamerly, Saumil Bandyopadhyay, Dirk Englund
arXiv: 2109.05367 (2021)

DIRK ENGLUND, *EECS*

"Hardware error correction for programmable photonics"

Saumil Bandyopadhyay, Ryan Hamerly, Dirk Englund

Optica Vol. 8, Issue 10, pp. 1247-1255 (2021) | arXiv:2103.04993 (2021)

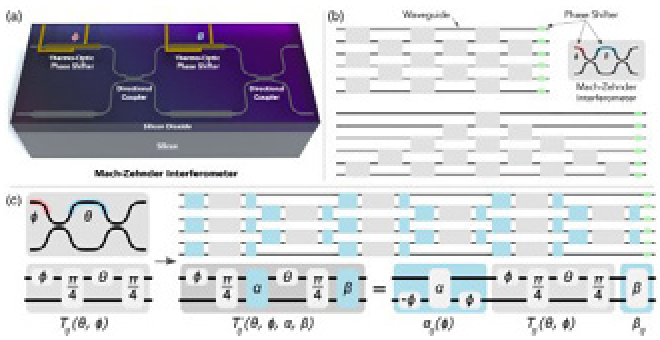

(a) A Mach–Zehnder interferometer (MZI) on the silicon-on-insulator platform is composed of two 50-50 splitters, implemented with directional couplers, and an external phase shifter ϕϕ and internal phase shifter θθ implemented with thermo-optic phase shifters. These devices act as electrically controlled 2×22×2 optical gates in programmable photonics. (b) Arbitrary higher-dimensional matrix operations can be implemented by connecting N(N−1)/2N(N−1)/2 MZIs in a rectangular (top) or triangular (bottom) configuration. The Reck (triangular) and Clements (rectangular) decompositions [17,18] describe a procedure for computing the phase settings for each MZI, but they assume the components are ideal. (c) A realistic MZI implemented on a photonics platform will have splitting errors α,βα,β for the two directional couplers within the interferometer. The effect of these hardware errors is to left- and right-multiply each programmable 2×22×2 unitary Tij(θ,ϕ)Tij(θ,ϕ) implemented by an MZI by error matrices βij,αij(ϕ)βij,αij(ϕ). Applying the standard decomposition for ideal components to these imperfect optical gates will not produce the correct gate operation.

"Controlled-Phase Gate by Dynamic Coupling of Photons to a Two-Level Emitter"

Stefan Krastanov, Kurt Jacobs, Dirk R. Englund, Mikkel Heuck

arXiv:2110.02960 (2021)

"Investigation of the Stark Effect on a Centrosymmetric Quantum Emitter in Diamond"

Lorenzo De Santis, Matthew Trusheim, Kevin Chen, Dirk Englund

Phys. Rev. Lett. 127, 147402 (2021) | arXiv:2102.01322 (2021)

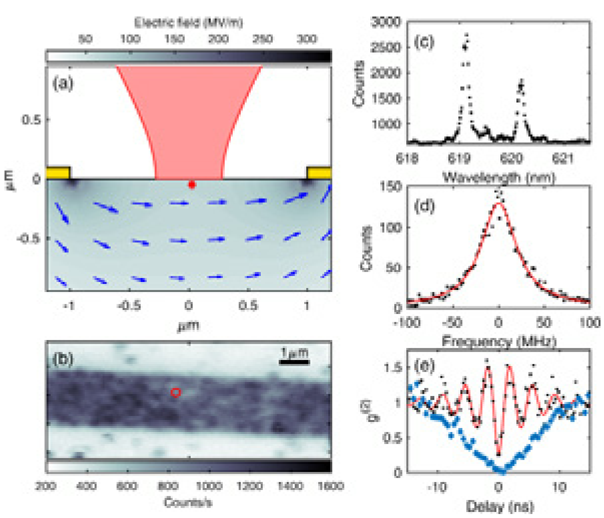

(a) Side view of the sample layout, showing two gold electrodes and the electric field distribution simulated with COMSOL for an external bias of 200 V. A red circle indicates the emitter location (76 nm below the surface). (b) Confocal PL scan of the sample, showing an ensemble of emitters in the exposed diamond, enclosed between two electrodes. The red circle locate the SnV emitter analyzed here. (c) Typical emission spectrum obtained under non-resonant excitation. (d) PLE spectrum of the transition to the lower ground state of an SnV, showing a linewidth of 47 MHz. (e) Second order correlation measurement performed under weak (blue diamonds) and strong driving (black dots).

DIRK ENGLUND, *EECS*

“Alignment-free photonic interconnects”
Saumil Bandyopadhyay and Dirk Englund
ArXiv: 2110.12851 (2021)

“Quantum Control of the Tin-Vacancy Spin Qubit in Diamond”
Romain Debroux, Cathryn P. Michaels, Carola M. Purser, Noel Wan, Matthew E. Trusheim, Jesús Arjona Martínez, Ryan A. Parker, Alexander M. Stramma, Kevin C. Chen, Lorenzo de Santis, Evgeny M. Alexeev, Andrea C. Ferrari, Dirk Englund, Dorian A. Gangloff, and Mete Atatüre
Phys. Rev. X 11, 041041 (2021) | arXiv:2106.00723 (2021)

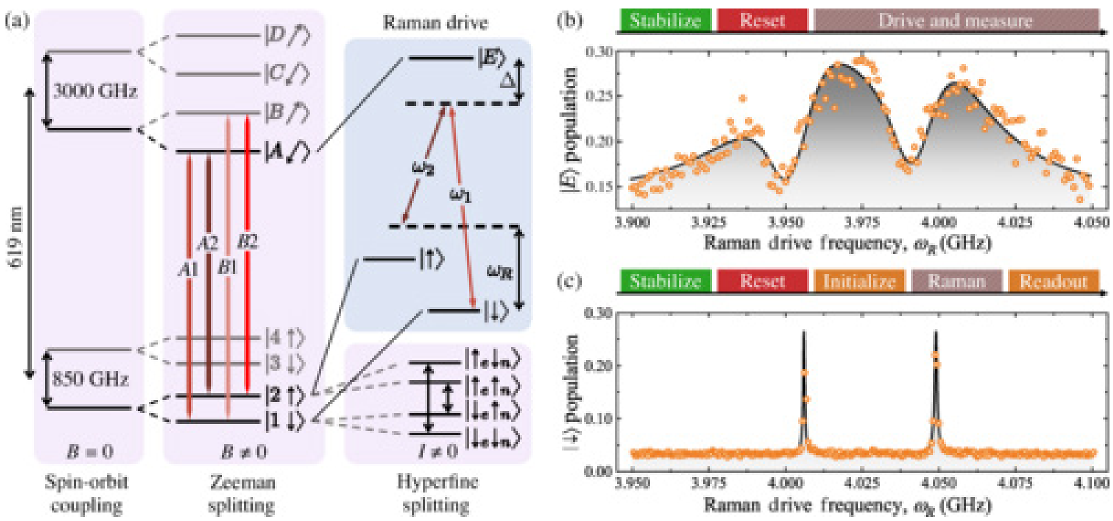

SnV and Raman drive. (a) Lilac panels: energy levels of the SnV split by spin-orbit coupling (left), Zeeman splitting (middle), and hyperfine splitting (right). Blue panel: qubit defined by the |↓⟩ and |↑⟩ electronic levels. An optical lambda scheme is defined by two optical fields ω1 and ω2 detuned by Δ from the excited state |E⟩. The Raman drive frequency ωR=ω1−ω2 is the energy offset between the two fields. (b) |E⟩ population plotted in orange circles as a function of ωR for Δ=0 and 200 mT magnetic field strength applied at 54.7° relative to the SnV symmetry axis. The pulse sequence consists of an approximately 10−μW green stabilization pulse for 50 μs, B2 reset pulse for 30 μs, and Raman drive with p=40(4) nW for 2 μs. The solid curve is a three-level model describing coherent population trapping. (c) |↓⟩ population plotted in orange circles as a function of ωR for Δ=600 MHz at 204-mT magnetic field strength. After the stabilize and reset pulses, the sequence includes an initialization pulse for 30 μs, a Raman drive with p=40(4) nW for 1 μs, and a readout pulse on A1 for 30 μs. The solid curve is a two-Lorentzian fit resulting in an average linewidth of 900(200) kHz and spin resonances split by 42.6(4) MHz.

JOSEPH A. FORMAGGIO, *Physics*

“Improved eV-scale Sterile-Neutrino Constraints from the Second KATRIN Measurement Campaign”
M. Aker, D. Batzler, A. Beglarian, ..., J. A. Formaggio, et al.
arXiv:2201.11593 (2022)

“Viterbi Decoding of CRES Signals in Project 8”
A. Ashtari Esfahani, Z. Bogorad, S. Böser, ..., J. A. Formaggio, et al.
arXiv:2112.05265 (2021)

“Ricochet Progress and Status”
Ricochet Collaboration, G. Beaulieu, V. Belov, ..., J. A. Formaggio, et al.
arXiv:2111.06745 (2021)

“Direct neutrino-mass measurement with sub-electronvolt sensitivity”
The KATRIN Collaboration, Joe Formaggio, et. Al
MIT News (2022) | Nature Physics 18, 160–166 (2022) | arXiv:2105.08533

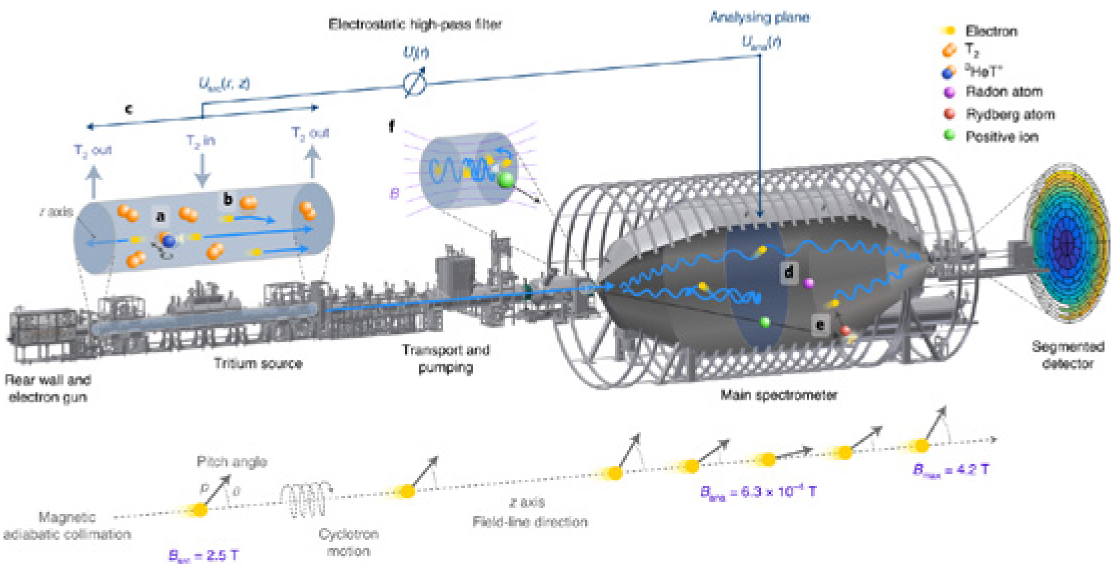

The main components are labelled. The transport of β-electrons and magnetic adiabatic collimation of their momenta p are illustrated. a–f, View into the tritium source depicts three systematic effects: molecular excitations during β-decay (a), scattering of electrons off the gas molecules (b) and spatial distribution of the electric potential in the source Usrc(r, z) (c). The view into the spectrometer illustrates the main background processes arising from radon decays inside the volume of the spectrometer 47,48,49 (d), highly excited Rydberg atoms sputtered off from the structural material via α-decays of 210Po (refs. 44,45,46) (e) and positive ions created in a Penning trap between the two spectrometers 57 (f). Low-energy electrons, created in the volume as a consequence of radon decays or Rydberg-atom ionizations, can be accelerated by qUana towards the focal-plane detector, making them indistinguishable from signal electrons 66.

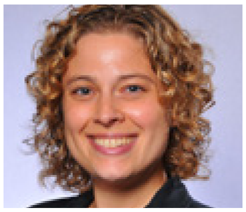

DANNA FREEDMAN, *Chemistry*

“Controlled n-Doping of Naphthalene Diimide-Based Two-Dimensional Polymers”
Evans, A. M.; Collins, K. A.; Xun S.; Allen, T. G.; Jhulki S.; Castano, I.; Smith, H. L.; Strauss, M. J.; Oanta, A. K.; Liu, L.; Sun, L.; Reid, O. G.; Sini, G.; Puggioni, D.; Rondinelli, J. M.; Rajh, T.; Gianneschi, N. C.; Kahn, A.; Freedman, D. E.; Li, H.; Barlow, S.; Rumbles, G.; Brédas, J.; Marder, S. R.; Dichtel W. R.
Adv. Mater., 2101932. (2021)

“Tunable Cr4+ Molecular Color Centers”
Laorenza, D. W.; Kairalapova, A.; Bayliss, S. L.; Goldzak, T.; Green, S. M.; Weiss, L. R.; Deb, P.; Mintun, P. J.; Collins, K. A.; Awschalom, D. D.; Berkelbach, T. C.; Freedman, D. E.
J. Am. Chem. Soc., 143, 21350-21363. (2021)

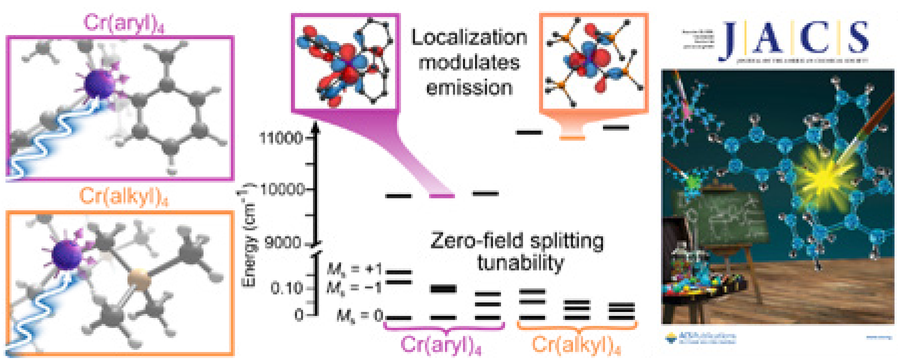

“Strong Magnetocrystalline Anisotropy Arising from Metal–Ligand Covalency in a Metal–Organic Candidate for 2D Magnetic Order”
Wang, Y.; Ziebel, M. E.; Sun, L.; Gish, J. T.; Pearson, T. J.; Lu, X.; Thorarinsdottir, A. E.; Hersam, M. C.; Long, J. R.; Freedman, D. E.; Rondinelli, J. M.; Puggioni, D.; Harris, T. D.
Chem. Mater. 33, 8712-8721. (2021)

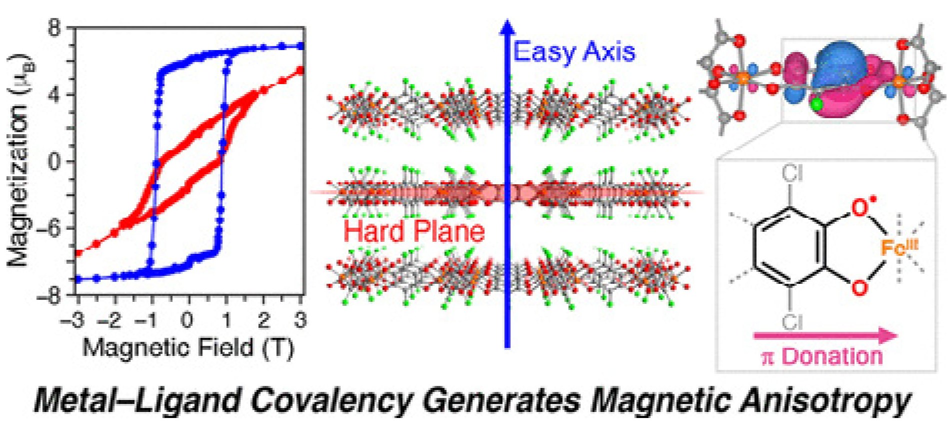

NUH GEDIK, *Physics*

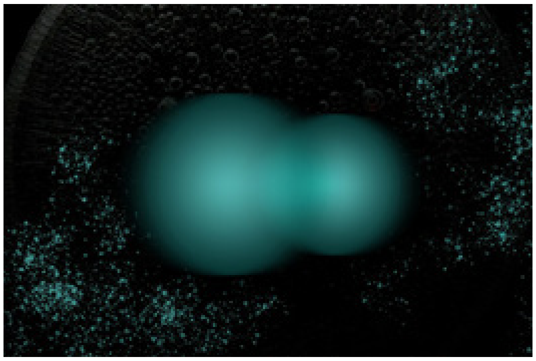

Image: Christine Daniloff, MIT
MIT physicists have detected a hybrid particle in an unusual, two-dimensional magnetic material. The hybrid particle is a mashup of an electron and a phonon.

"Magnetically brightened dark electron-phonon bound states in a van der Waals antiferromagnet"
Emre Ergeçen, Batyr Ilyas, Dan Mao, Hoi Chun Po, Mehmet Burak Yilmaz, Junghyun Kim, Je-Geun Park, T. Senthil & Nuh Gedik
MIT News (2022)| Nature communications 13 (1), 1-7 (2022)

"Terahertz Field-Induced Reemergence of Quenched Photoluminescence in Quantum Dots"
Jiaojian Shi, Frank Y. Gao, Zhuquan Zhang, Hendrik Utzat, Ulugbek Barotov, Ardavan Farahvash, Jinchi Han, Jude Deschamps, Chan-Wook Baik, Kyung Sang Cho, Vladimir Bulović, Adam P. Willard, Edoardo Baldini, Nuh Gedik, Moungi G. Bawendi, Keith A. Nelson
arXiv:2112.08533 (2021)

"Unconventional hysteretic transition in a charge density wave"
B. Q. Lv, Alfred Zong, D. Wu, A.V. Rozhkov, Boris V. Fine, Su-Di Chen, Makoto Hashimoto, Dong-Hui Lu, M. Li, Y.-B. Huang, Jacob P. C. Ruff, Donald A. Walko, Z. H. Chen, Inhui Hwang, Yifan Su, Xiaozhe Shen, Xirui Wang, Fei Han, Hoi Chun Po, Yao Wang, Pablo Jarillo-Herrero, Xijie Wang, Hua Zhou, Cheng-Jun Sun, Haidan Wen, Zhi-Xun Shen, N. L. Wang, Nuh Gedik
MIT News | Physical Review Letters 128 (3), 036401 (2022) | arxiv.org/abs/2106.09774 (2021)

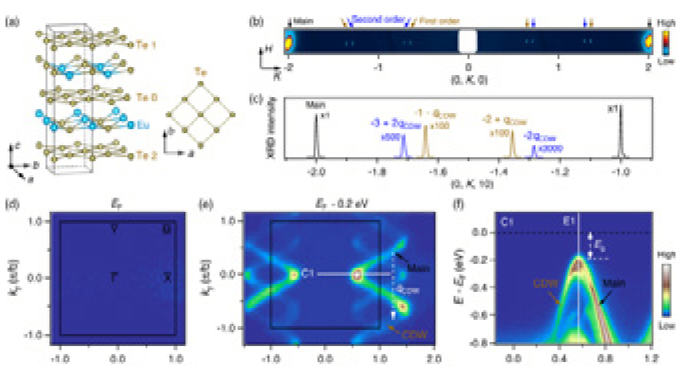

Incommensurate CDW in EuTe4. (a) Crystal structure of EuTe4. Black lines denote the primary unit cell, which contains two motifs of the Te square lattice (right panel): bilayer (Te 1 and Te 2) and monolayer (Te 0). (b) Room temperature x-ray diffraction pattern taken with 30.6 keV photon energy in transmission mode. (c) Room temperature high-resolution x-ray intensity cut along the (0, K, 10) direction, taken with 11 keV photons in reflection geometry. (d) Room temperature Fermi surface map, showing no intensity contrast. (e) ARPES constant energy contour at 0.2 eV below EF, measured at T=20 K. (f) Band dispersions at 55 K, corresponding to the C1 cut in (e). Photon energy used was 90 eV in (d),(e) or 24 eV in (f).

NUH GEDIK, *Physics*

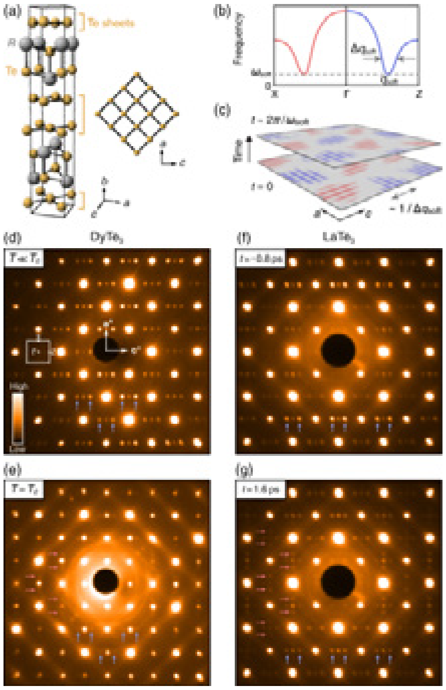

“Role of equilibrium fluctuations in light-induced order”
A Zong, PE Dolgirev, A Kogar, Y Su, X Shen, JAW Straquadine, X Wang, ...
Physical review letters 127 (22), 227401 (2021) | arXiv:2110.00865 (2021)

Competing charge density waves in rare-earth tritellurides. (a) Left: schematic of the layered structure of RTe3, where dashed lines indicate the primary unit cell. Right: enlarged view of the nearly square-shaped Te sheets that host the CDW instabilities. (b) Schematic phonon dispersion right above Tc along Γ−X and Γ−Z, featuring two Kohn anomalies at qsoft. (c) Schematic of fluctuating CDWs right above Tc. (d),(e) Equilibrium electron diffractions of DyTe3 [Tc=306(3) K 24] taken at 100 K (d) and 307 K (e). (f),(g) Time-resolved diffractions of LaTe3 (f) before and (g) 1.6 ps after photoexcitation by an 80-fs, 800-nm laser pulse with an incident fluence of 2.1 mJ/cm2, measured at 307 K. Blue and red arrows indicate the CDW peaks along the c and a axis, respectively. Difference in intensities of lattice Bragg peaks in (d) and (e) results from slight sample drift and tilt during the warm-up process.

“A versatile sample fabrication method for ultrafast electron diffraction”
Ya-Qing Bie, Alfred Zong, X Wang, Pablo Jarillo-Herrero, Nuh Gedik
Ultramicroscopy 230, 11338 (2021)

MARK GOUKER, *Lincoln Laboratory*

“Wafer-Scale Characterization of a Superconductor Integrated Circuit Fabrication Process, Using a Cryogenic Wafer Prober”
Joshua T. West, Arthur Kurlej, Alex Wynn, Chad Rogers, Mark A. Gouker, Sergey K. Tolpygo
arXiv:2112.00705 (2021)

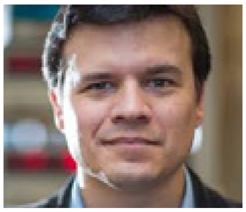

PABLO JARILLO-HERRERO, *Physics*

“Materials and devices for fundamental quantum science and quantum technologies”
Marco Polini, Francesco Giazotto, Kin Chung Fong, Ioan M. Pop, Carsten Schuck, Tommaso Boccali, Giovanni Signorelli, Massimo D’Elia, Robert H. Hadfield, Vittorio Giovannetti, Davide Rossini, Alessandro Tredicucci, Dmitri K. Efetov, Frank H. L. Koppens, Pablo Jarillo-Herrero, Anna Grassellino, Dario Pisignano
arXiv:2201.09260 (2022)

“Magic-Angle Multilayer Graphene: A Robust Family of Moiré Superconductors”
Jeong Min Park, Yuan Cao, Liqiao Xia, Shuwen Sun, Kenji Watanabe, Takashi Taniguchi, Pablo Jarillo-Herrero
arXiv:2112.10760 (2021)

“Interfacial ferroelectricity in rhombohedral-stacked bilayer transition metal dichalcogenides”
Xirui Wang, Kenji Yasuda, Yang Zhang, Song Liu, Kenji Watanabe, Takashi Taniguchi, James Hone, Liang Fu, Pablo Jarillo-Herrero
Nature Nanotechnology (2022) arXiv:2108.07659 (2021)

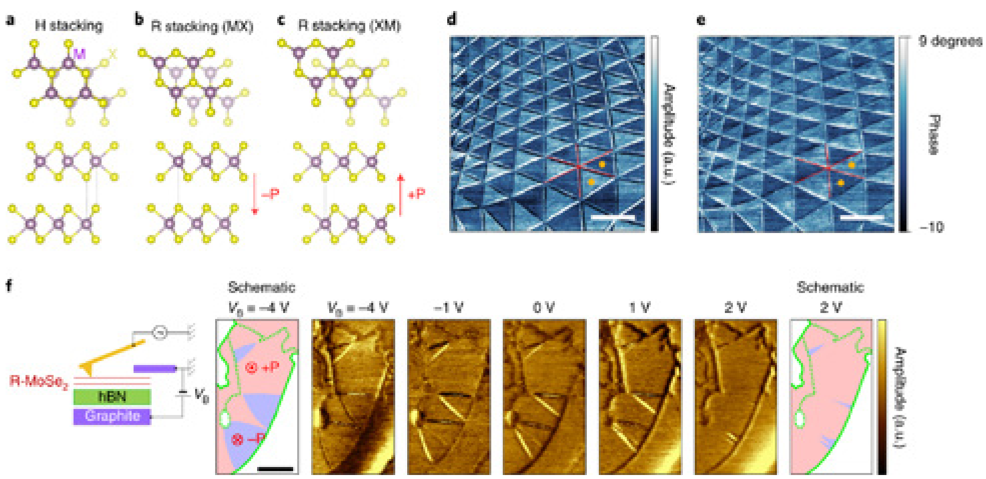

a, H-stacked bilayer TMD. The two layers are stacked in antiparallel configuration, and the inversion symmetry is restored as a whole with zero net polarization. M, metal atom (W or Mo). X, chalcogen atom (S or Se). b,c, MX (b) and XM (c) stacking forms of R-stacked bilayer TMD. The two layers are stacked in parallel, and an out-of-plane polarization exists due to the vertical alignment of different atoms. −P (b) and +P (c) denote downward and upward polarization, respectively. d,e, Amplitude (d) and phase (e) images of vertical piezoelectric force microscopy (PFM) on MoSe2 device p1. The adjacent triangular domains (orange dots) exhibit finite PFM contrast. Scale bars, 200 nm. f, Schematic illustration of lateral PFM measurement on gated MoSe2 device p2 (left). The thickness of BN is 13.7 nm. Amplitude image of lateral PFM under different bottom gate voltages VB. Schematic of the domain configuration is illustrated for VB = −4 V (left) and VB = 2 V (right), as a guide to the eyes. The area surrounded by the solid green curves is the bilayer MoSe2 region. The wrinkles, cracks and bubbles are shown with dotted green curves. The red and blue regions correspond to up and down domains, respectively. Scale bar, 300 nm. a.u., arbitrary units.

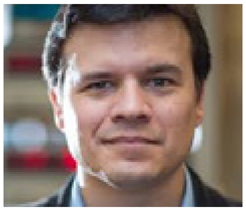

PABLO JARILLO-HERRERO, *Physics*

["Fractional Chern insulators in magic-angle twisted bilayer graphene"]

Yonglong Xie, Andrew T. Pierce, Jeong Min Park, Daniel E. Parker, Eslam Khalaf, Patrick Ledwith, Yuan Cao, Seung Hwan Lee, Shaowen Chen, Patrick R. Forrester, Kenji Watanabe, Takashi Taniguchi, Ashvin Vishwanath, Pablo Jarillo-Herrero, Amir Yacoby

Nature 600, 439–443 (2021) arXiv:2107.10854 (2021)

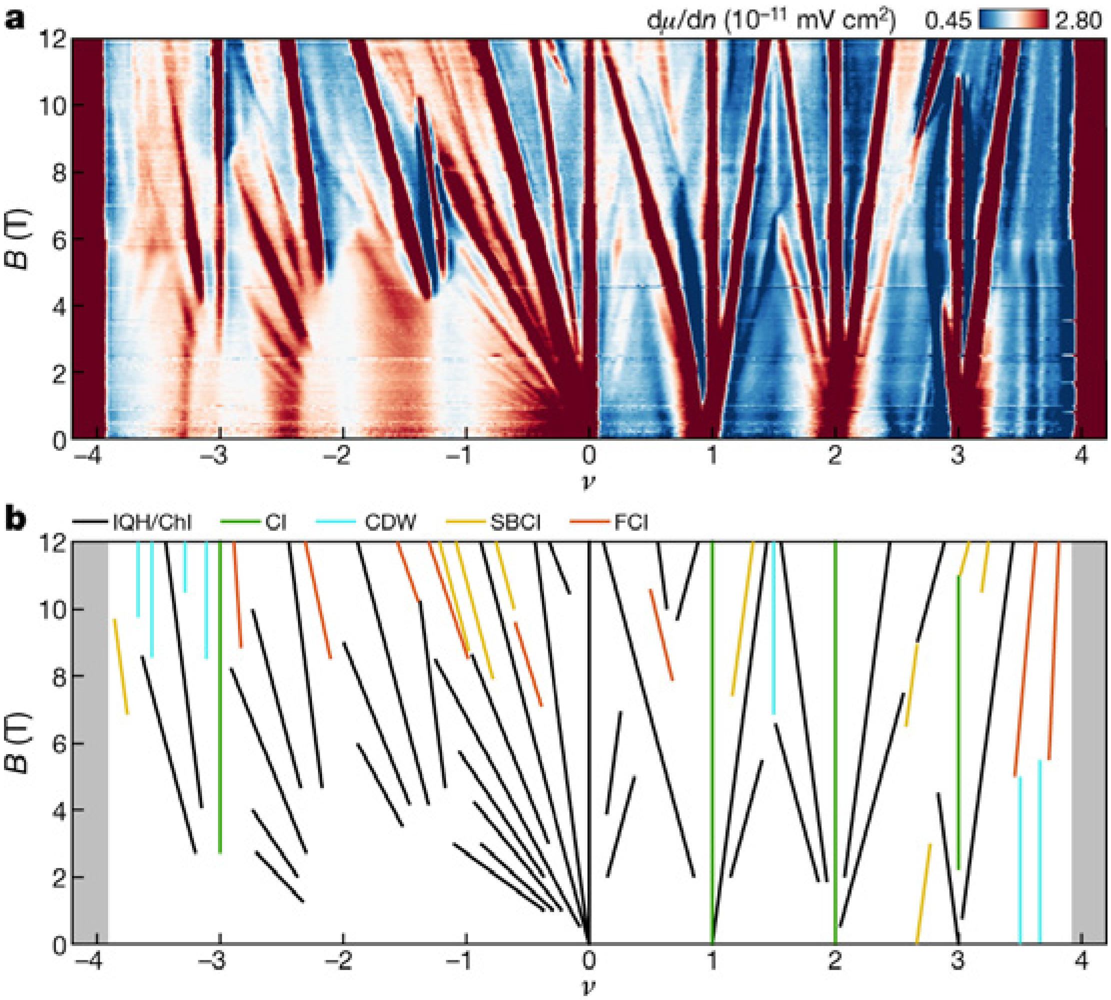

a, Local inverse compressibility dμ/dn measured as a function of magnetic field B and electrons per moiré unit cell ν. b, Wannier diagram identifying the incompressible peaks present in a. Black lines correspond to ChIs and integer quantum Hall (IQH) states; green lines correspond to correlated insulators (CIs) emanating with nonzero integer s and t = 0; blue lines correspond to CDWs with integer t = 0 and fractional s; yellow lines correspond to SBCIs with nonzero integer t and fractional s; and orange lines correspond to FCIs with fractional t and fractional s. Grey shaded regions correspond to the gaps to the remote bands.

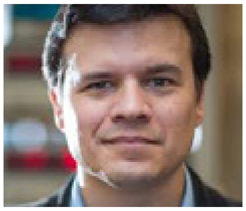

PABLO JARILLO-HERRERO, *Physics*

"Observation of interband collective excitations in twisted bilayer graphene"
Niels C.H. Hesp, Iacopo Torre, Daniel Rodan-Legrain, Pietro Novelli, Yuan Cao, Stephen Carr, Shiang Fang, Petr Stepanov, David Barcons-Ruiz, Hanan Herzig-Sheinfux, Kenji Watanabe, Takashi Taniguchi, Dmitri K. Efetov, Efthimios Kaxiras, Pablo Jarillo-Herrero, Marco Polini, Frank H.L. Koppens
Nature Physics 17, 1162–1168 (2021) arXiv:1910.07893 (2019)

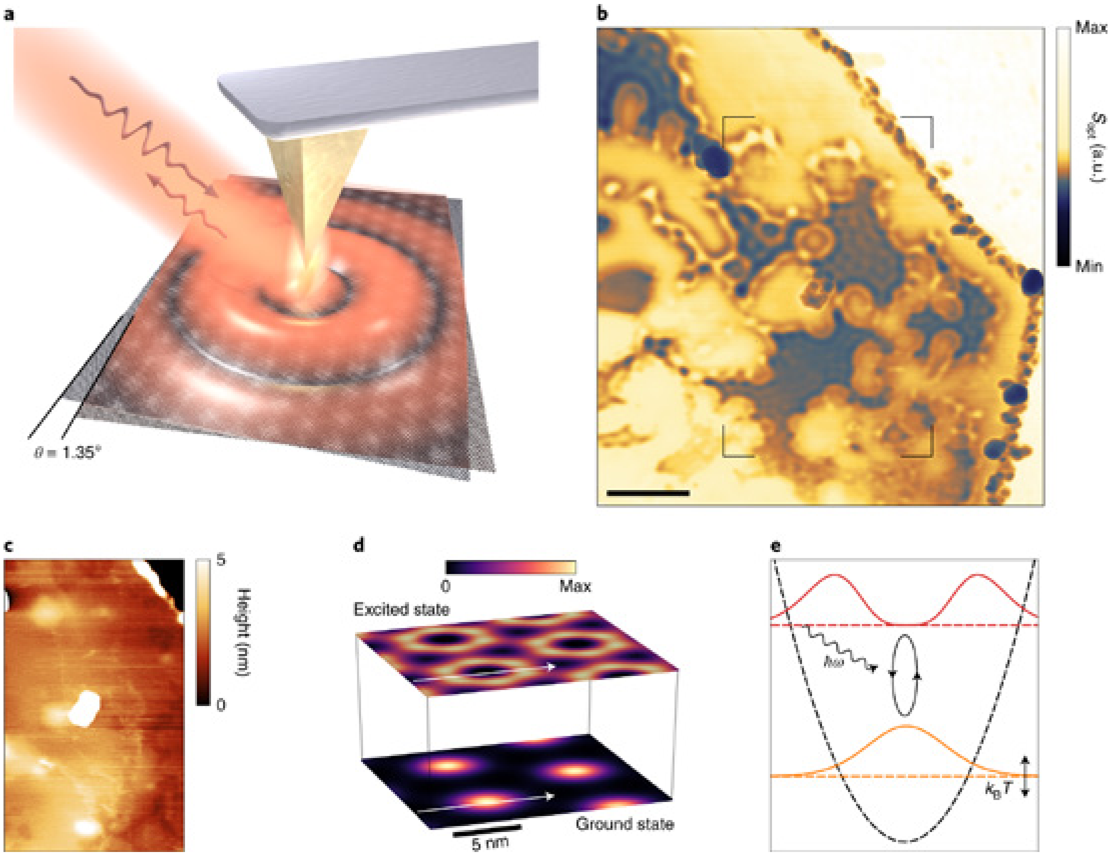

a, Illustration of the s-SNOM experiment: an AFM metallic tip is illuminated by infrared light, which provides sufficient momentum to launch a collective excitation in TBG. The plasmon can, in turn (for example, by reflection from an edge or interface), scatter into light at the tip. This scattered light is detected by a photodetector. The curved arrows indicate the light impinging on the tip (coming from the laser) as well as the scattered light (going to the detector). b, Image of the near-field amplitude obtained by scanning the AFM tip and recording the photodetector signal. Propagating collective excitations are visible in certain areas as periodic interference fringes. The illumination photon energy is ħω = 219 meV and the scale bar is 500 nm. c, AFM image of the marked region in b. d, Square modulus of the wavefunction |⟨r|k = K,ν⟩|2, plotted in arbitrary units, associated with one of the flat bands (bottom) and the first excited band (top), evaluated at the K point of the moiré superlattice Brillouin zone. These states are mostly localized around the regions with local AA stacking (which form a triangular lattice) and are involved in the relevant optical transitions. e, Linecuts of the wavefunctions along the white arrows in c represented in a harmonic confinement potential6 (black dashed line), with the coloured horizontal dashed lines indicating the energies of the states. An interband transition occurs between the lower-energy state and excited state. A similar transition is happening, for holes, between the corresponding pair of states, approximately related to the illustrated ones by electron–hole symmetry.

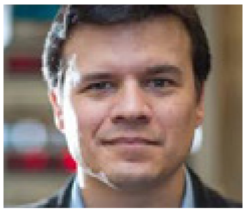

PABLO JARILLO-HERRERO, *Physics*

"Unconventional sequence of correlated Chern insulators in magic-angle twisted bilayer graphene"

Andrew T. Pierce, Yonglong Xie, Jeong Min Park, Eslam Khalaf, Seung Hwan Lee, Yuan Cao, Daniel E. Parker, Patrick R. Forrester, Shaowen Chen, Kenji Watanabe, Takashi Taniguchi, Ashvin Vishwanath, Pablo Jarillo-Herrero, Amir Yacoby

Nature Physics (2021) arXiv:2101.04123 (2021)

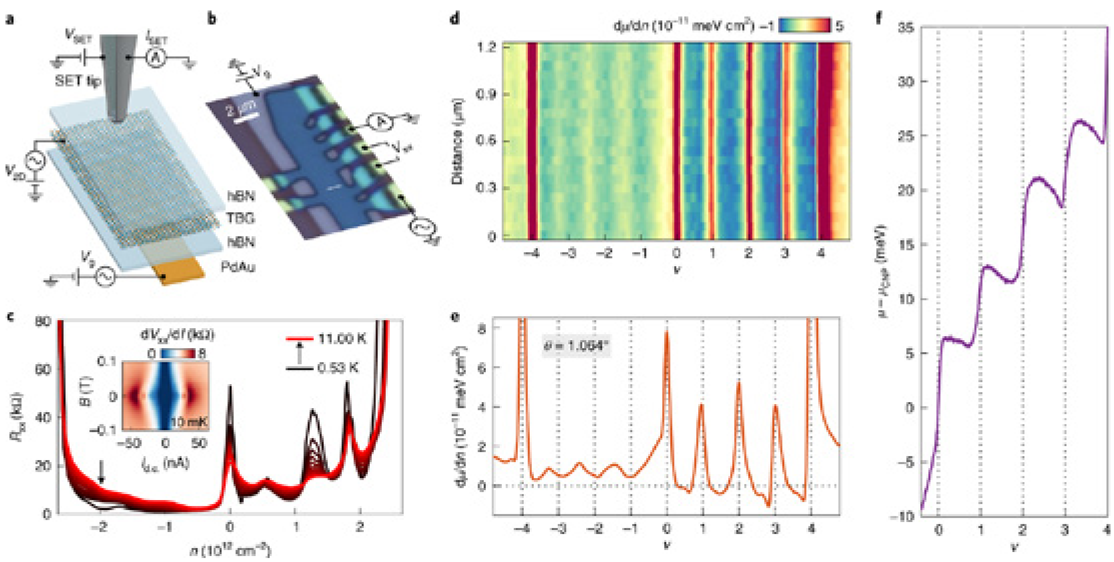

a, Schematic of the scanning SET measurement setup. VSET is the voltage bias applied across the SET. ISET is the SET current. V2D and Vg are voltages applied to twisted bilayer graphene (TBG) and the back gate, respectively. b, Optical image of the device and configuration used for transport measurement. The longitudinal voltage drop is denoted Vxx. c, Four-terminal longitudinal resistance Rxx as a function of carrier density measured at different temperatures ranging from 0.53 K (black trace) to 11.00 K (red trace) using the circuit shown in b. Inset: dilution refrigerator (T ≈ 10 mK) measurement of the differential resistance as a function of the applied d.c. bias current Id.c. and out-of-plane magnetic field B measured at density n = −1.97 × 1012 cm−2 (indicated by the arrow in the main plot). d, Local inverse compressibility dμ/dn as a function of moiré band filling factor ν measured along the white dashed line (1.2 μm) in b. e, Spatially averaged dμ/dn obtained from d, showing incompressible peaks precisely aligned at ν = 0, 1, 2 and 3. f, Spatially averaged chemical potential μ relative to its value at the CNP, denoted μCNP, as a function of moiré band filling factor ν, showing steps at precisely ν = 0, 1, 2 and 3. At these locations, we find the gaps Δν at filling factors ν = 0, 1, 2 and 3 to be Δ0 = 9 meV, Δ1 = 9 meV, Δ2 10 meV and Δ3 = 9 meV, respectively (Methods provides the gap extraction procedure).

From the Director
CQE PI Feature
CQE Student Feature
Around the Institute
Beyond the Institute
Quantum Conferences

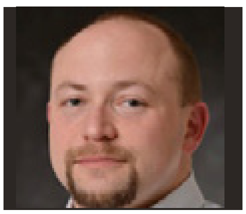

LONG JU, *Physics*

"Weyl Fermion Magneto-Electrodynamics and Ultra-low Field Quantum Limit in TaAs"

Zhengguang Lu, Patrick Hollister, Mykhaylo Ozerov, Seongphill Moon, Eric D Bauer, Filip Ronning, Dmitry Smirnov, Long Ju, BJ Ramshaw

Science advances 8 (2), eabj1076 (2022) | arXiv:2111.06182 (2021)

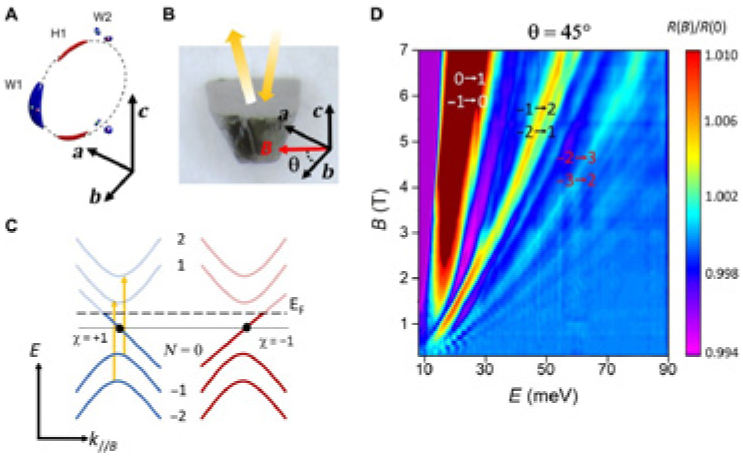

MEASUREMENT SCHEME AND INTER-LL TRANSITIONS IN TAAS.
(A) Fermi surface of TaAs featuring Weyl pockets W1 and W2 and a trivial hole pocket H1—each distributed around the nodal line, represented by the dashed circle, which would be present with zero spin-orbit coupling [reprinted with permission from (21), copyright 2016 by the American Physical Society]. There are four such nodal lines and accompanying pockets arranged at the edges of the Brillouin zone in TaAs. (B) TaAs crystal with the flat surface in the ab plane. The schematic indicates the measurement geometry: The magnetic field is applied in the ab plane at an angle θ from the a axis. Reflected infrared light is collected in the Voigt configuration. (C) Schematic band structure for a pair of Weyl points with chirality χ = ±1 in a magnetic field. LLs labeled by index N are formed in the plane perpendicular to B field, while the momentum parallel to the magnetic field, k//B, is still a good quantum number. The zeroth LLs at both Weyl points disperse as linear, one-dimensional (1D) bands. Inter-LL transitions obey optical selection rules Δ|N| = ±1. (D) 2D color plot of the infrared reflectivity in a magnetic field, normalized by the reflectivity at zero field (taken at θ = 45°). Sharp peaks that evolve with magnetic field are labeled by the proposed LL index of initial and final states. Because of the diverging density of states (DOS) at the band edge for each of the N > 0 LLs, peaks in (D) are dominated by inter-LL transitions at k//B = ±kw where the Weyl points are located.

ANDREW J. KERMAN, *Lincoln Laboratory*

"Demonstration of long-range correlations via susceptibility measurements in a one-dimensional superconducting Josephson spin chain"

Daniel M Tennant, Xi Dai, Antonio J Martinez, Robbyn Trappen, Denis Melanson, M A Yurtalan, Yongchao Tang, Salil Bedkihal, Rui Yang, Sergei Novikov, Jeffery A Grover, Steven M Disseler, James I Basham, Rabindra Das, David K Kim, Alexander J Melville, Bethany M Niedzielski, Steven J Weber, Jonilyn L Yoder, Andrew J Kerman, Evgeny Mozgunov, Daniel A Lidar, Adrian Lupascu

arXiv:2111.04284 (2021)

WOLFGANG KETTERLE, *Physics*

“Rotational Coherence Times of Polar Molecules in Optical Tweezers”

S. Burchesky, L. Anderegg, Y. Bao, S.S. Yu, E. Chae, W. Ketterle, K.K. Ni, and J.M. Doyle
Phys. Rev. Lett., arxiv.org/abs/2105.15199

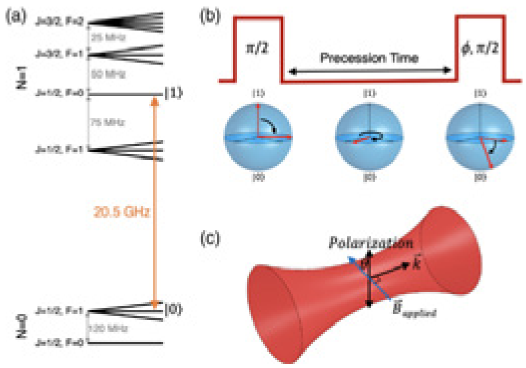

CaF structure. (a) The X-state level structure of CaF. Quantum numbers N, J, and F denote rotation, electron spin+rotation, and total angular momentum, respectively. The lower and upper qubit states are labeled |0⟩ and |1⟩. (b) The Ramsey pulse sequence uses a 10 μs π/2 pulse to create a coherent superposition of |0⟩ and |1⟩ states. The Bloch vector precesses, accumulating phase until the second π/2 pulse with a phase shift (ϕ) rotates the Bloch vector back into the measurement basis prior to imaging the N=1 population. (c) The tweezer light polarization and applied magnetic field lie in the plane perpendicular to the k vector of the tweezer light.

“Transverse spin dynamics in the anisotropic Heisenberg model realized with ultracold atoms”

N. Jepsen, W.W. Ho, J. Amato-Grill, I .Dimitrova, E. Demler, and W. Ketterle
Phys. Rev. X 11, 041054 (2021) |arXiv:2103.07866 (2021)

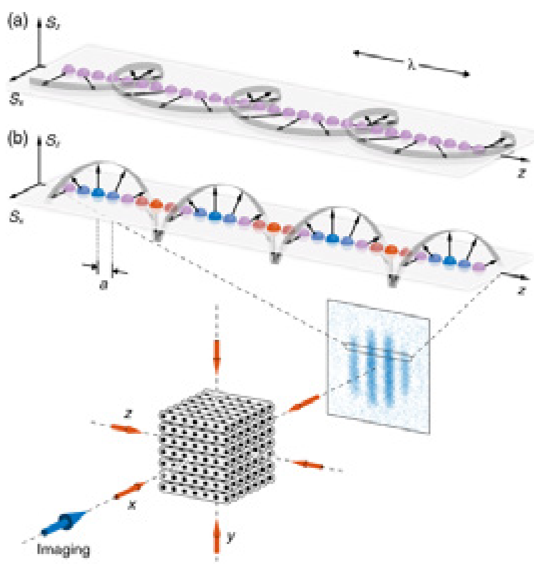

Geometry of the experiment. The initial state is a transverse (a) or longitudinal (b) spin helix where the spin vector winds within the Sx–Sy plane (a) or Sz–Sx plane (b). The transverse helix (a) is a pure phase modulation of spin |↑⟩ and |↓⟩ states, whereas the longitudinal helix (b) also involves population modulation. Deep optical lattices along the x and y directions create an array of independent spin chains. The z lattice is shallower and controls spin dynamics along each chain.

“Pauli blocking of light scattering in degenerate fermions”

Y. Margalit, Y.-K. Lu, F.C. Top, and W. Ketterle
MIT News (2021)| SCIENCE Vol 374, Issue 6570 (2021) | physicsworld (2021) | physicsworld finalist breakthrough of the year (2021) |ScienceNews (2021) | NewScientist (2021) | arXiv:2103.06921

WOLFGANG KETTERLE, *Physics*

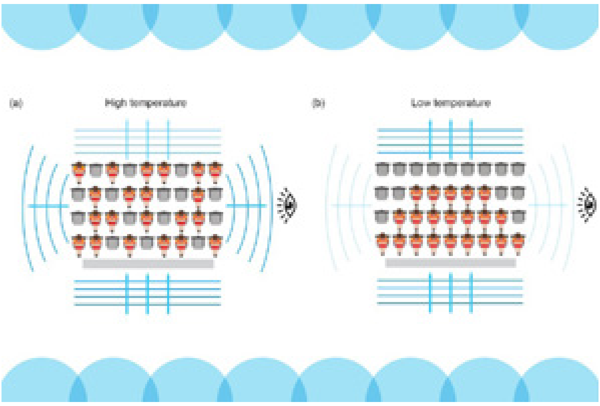

The principle of Pauli blocking can be illustrated by an analogy of people filling seats in an arena. Each person represents an atom, while each seat represents a quantum state. At high temperatures (a), atoms are seated randomly, so every particle can scatter light. At low temperatures (b), atoms crowd together. Only those with more room near the edge can scatter light.

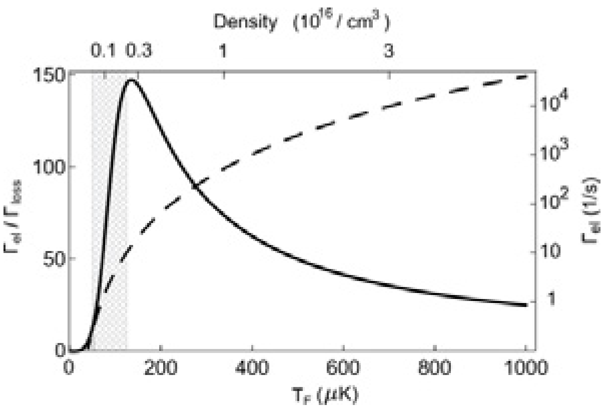

"Spin-polarized fermions with p-wave interactions"
F.C. Top, Y. Margalit, and W: Ketterle
Phys. Rev. A 104, 043311 (2021) | arXiv:2009.05913 (2020)

The ratio of good (elastic) to bad (inelastic) collisions, and the elastic collision rate for 6Li atoms near zero field, far away from the p-wave Feshbach resonance. The solid line shows the ratio for an harmonically trapped cloud with T=TF assuming a vacuum lifetime of 60 seconds. The dashed line is the elastic collision rate. In this work, we have explored the shaded region.

"Catching Bethe phantoms and quantum many-body scars: Long-lived spin-helix states in Heisenberg magnets"
Paul Niklas Jepsen, Yoo Kyung Lee, Hanzhen Lin, Ivana Dimitrova, Yair Margalit, Wen Wei Ho, Wolfgang Ketterle
arXiv:2110.12043 (2021)

"Preparation of the spin-Mott state: a spinful Mott insulator of repulsively bound pairs"
Julius de Hond, Jinggang Xiang, Woo Chang Chung, Enid Cruz-Colón, Wenlan Chen, William Cody Burton, Colin J. Kennedy, Wolfgang Ketterle
arXiv:2110.00354 (2021)

"Control of reactive collisions by quantum interference"
Hyungmok Son, Juliana J. Park, Yu-Kun Lu, Alan O. Jamison, Tijs Karman, Wolfgang Ketterle
arXiv:2109.03944 (2021)

MIT Center for Quantum Engineering
MIT Quantum Science and Engineering Consortium

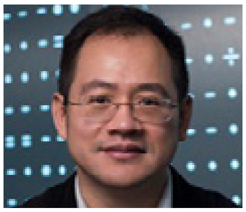

JU LI, *NSE MSE*

“Deep neural network battery life and voltage prediction by using data of one cycle only”

Chia-Wei Hsu, Rui Xiong, Nan-Yow Chen, Ju Li, Nien-Ti Tsou
Applied Energy 306, 118134 (2022)

“Stable two-dimensional lead iodide hybrid materials for light detection and broadband photoluminescence”

Mohamed Saber Lassoued, Yuan-Chao Pang, Qian-Wen Li, Xinkai Ding, Bo Jiao, Hua Dong, Guijiang Zhou, Shujiang Ding, Zhicheng Zhang, Zhaoxin Wu, Gaoyang Gou, Zongyou Yin, Ju Li, Yan-Zhen Zheng
Materials Chemistry Frontiers 6 (1), 71-77 (2022)

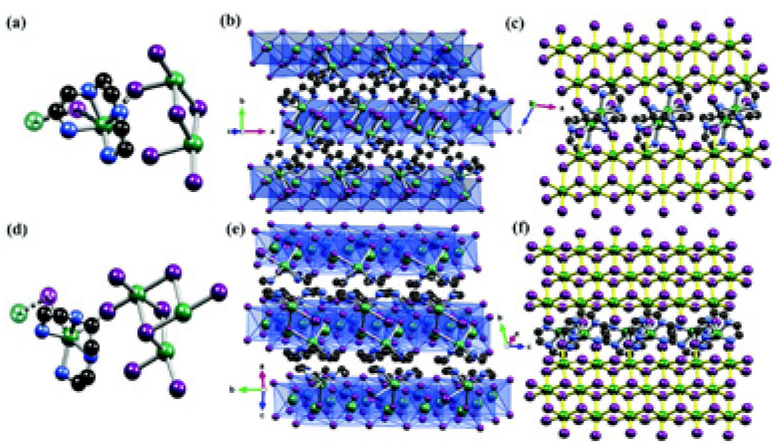

Asymmetric units of 1Pb (a) and 2Pb (d). Crystal structure of the compounds of 1Pb (b) and 2Pb (e). Zoom of 1Pb layer (c) and 2Pb layer (f). Hydrogen atoms are omitted for clarifications. The colors are used to indicate the following: Lead: dark green, iodine: violet, carbon: black and nitrogen: blue.

“Electrochemically stable lithium-ion and electron insulators (LEIs) for solid-state batteries”

Kai Pei, So Yeon Kim, Ju Li
Nano Research 15 (2), 1213-1220 (2022)”

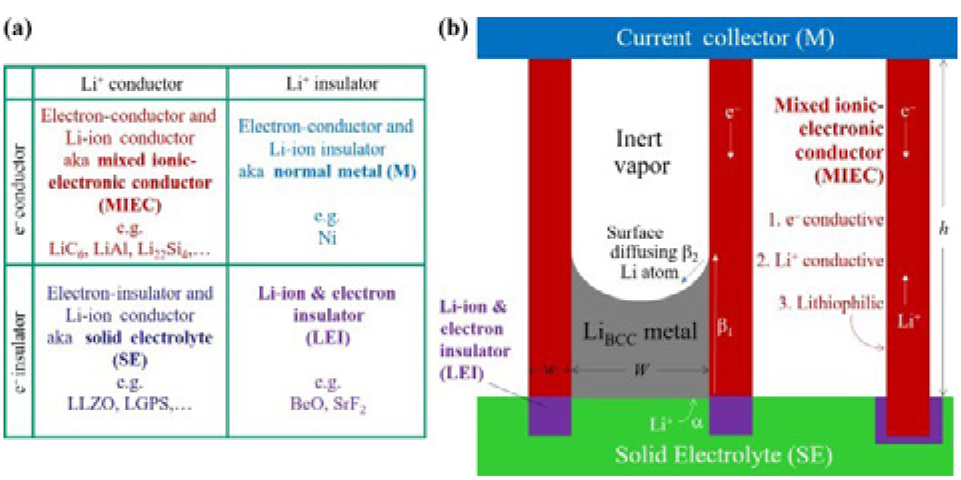

From the Director
CQE PI Feature
CQE Student Feature
Around the Institute
Beyond the Institute
Quantum Conferences

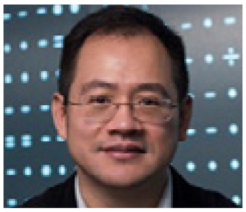

JU LI, *NSE MSE*

[“Healing of donor defect states in monolayer molybdenum disulfide using oxygen-incorporated chemical vapour deposition”]

Pin-Chun Shen, Yuxuan Lin, Cong Su, Christina McGahan, Ang-Yu Lu, Xiang Ji, Xingzhi Wang, Haozhe Wang, Nannan Mao, Yunfan Guo, Ji-Hoon Park, Yan Wang, William Tisdale, Ju Li, Xi Ling, Katherine E Aidala, Tomás Palacios, Jing Kong

Nature Electronics, 1-9 (2021)

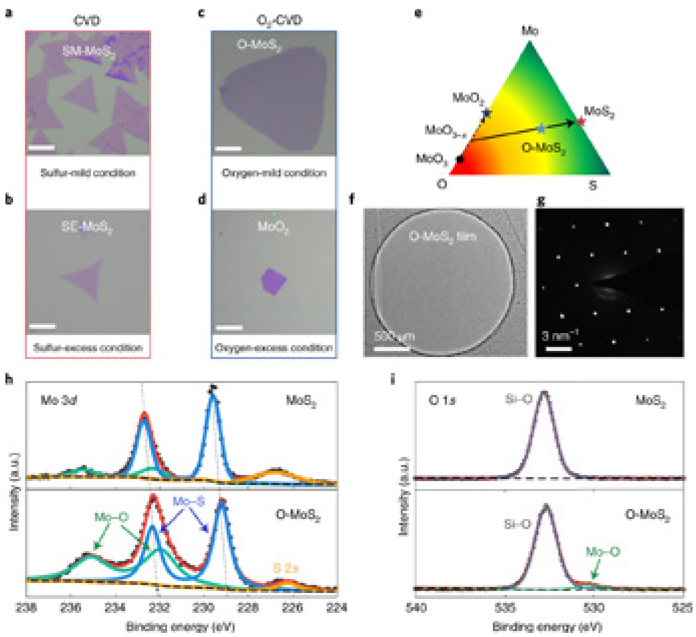

a, Optical image of a typical monolayer MoS2 crystal grown without oxygen under the sulfur-mild condition, showing a triangular shape. b, Optical image of a monolayer MoS2 crystal grown without oxygen under a sulfur-excess condition. The crystal shows inward curved edges (concave shape). c, Optical image of a monolayer MoS2 grown in an oxygen-mild environment. The crystal shows outward curved edges (convex shape). d, Optical image of a metallic layered MoO2 flake obtained at a high flow rate of oxygen. Scale bars, 10 μm (a–d). e, Ternary phase diagram of MoS2, indicating the possible reaction routes for CVD growth of MoS2. The star symbols represent the products obtained in this work. f, A TEM image of O-MoS2. g, A selected-area electron diffraction pattern of the monolayer O-MoS2 film. The sixfold-symmetric diffraction points correspond to the hexagonal lattice structure of monolayer MoS2, indicating the highly crystalline nature of the as-grown crystals. h,i, XPS data of Mo 3d (h) and O 1s (i) for a typical CVD MoS2 film grown under the sulfur-mild condition and an O-MoS2 film, showing the presence of Mo–O bonds in O-MoS2. The dashed lines highlight the shift in binding energies. The redshifted binding energies in the O-MoS2 film indicate the less n-type doping in O-MoS2. The weak intensity of Mo–O peaks in a typical CVD MoS2 film is likely to be associated with the physisorption of oxygen in the environment 30 or MoOx clusters deposited onto the substrate during the growth.

“Dislocation-Mediated Hydride Precipitation in Zirconium”

Si-Mian Liu, Akio Ishii, Shao-Bo Mi, Shigenobu Ogata, Ju Li, Wei-Zhong Han

Small, 2105881 (2021)

“Sliding ferroelectricity in 2D van der Waals materials: Related physics and future opportunities”

Menghao Wu, Ju Li

Proceedings of the National Academy of Sciences 118 (50) (2021)

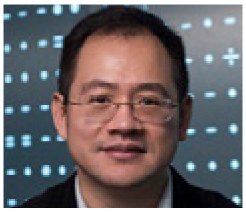

JU LI, *NSE MSE*

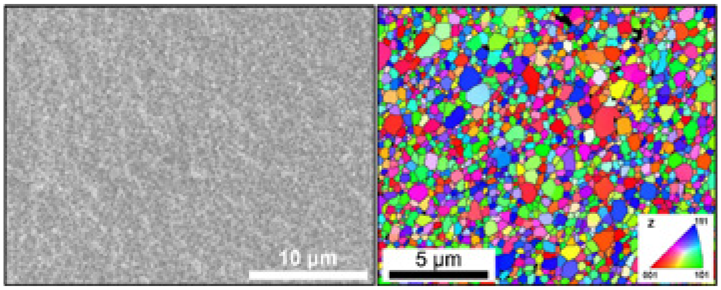

“Towards pressureless sintering of nanocrystalline tungsten”
Xingyu Li, Lin Zhang, Yanhao Dong, Mingli Qin, Zichen Wei, Zhongyou Que, Junjun Yang, Xuanhui Qu, Ju Li
Acta Materialia 220, 117344 (2021)

“Peristalsis-like migration of carbon-metabolizing catalytic nanoparticles”
Peng-Han Lu, De-Gang Xie, Bo-Yu Liu, Fei Ai, Zhao-Rui Zhang, Ming-Shang Jin, Xiao Feng Zhang, En Ma, Ju Li, Zhi-Wei Shan
Extreme Mechanics Letters 49, 101463 (2021)

“Lithium Plating Mechanism, Detection, and Mitigation in Lithium-Ion Batteries”
Xianke Lin, Kavian Khosravinia, Xiaosong Hu, Ju Li, Wei Lu
Progress in Energy and Combustion Science 87, 100953 (2021)

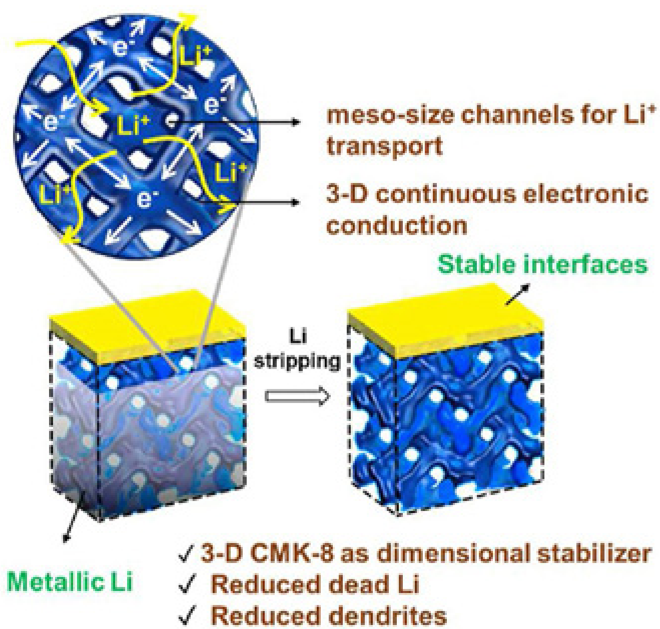

“High-voltage lithium-metal battery with three-dimensional mesoporous carbon anode host and ether/carbonate binary electrolyte”
Egy Adhitama, Purna Chandra Rath, Achmad Prayogi, Jagabandhu Patra, Tai-Chou Lee, Ju Li, Jeng-Kuei Chang
Carbon 184, 752-763 (2021)

“Supercritical CO_2-Assisted SiOx/Carbon Multi-Layer Coating on Si Anode for Lithium-Ion Batteries”
Rahmandhika Firdauzha Hary Hernandha, Purna Chandra Rath, Bharath Umesh, Jagabandhu Patra, Chih-Yang Huang, Wen-Wei Wu, Quan-Feng Dong, Ju Li, Jeng-Kuei Chang
Advanced Functional Materials 31 (40), 2104135 (2021)

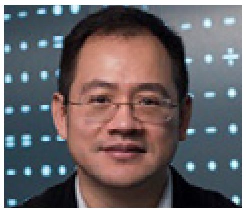

JU LI, *NSE MSE*

"Friction and Adhesion Govern Yielding of Disordered Nanoparticle Packings: A Multiscale Adhesive Discrete Element Method Study"
X Liu, JA Lefever, D Lee, J Zhang, RW Carpick, J Li
Nano Letters 21 (19), 7989-7997 (2021)

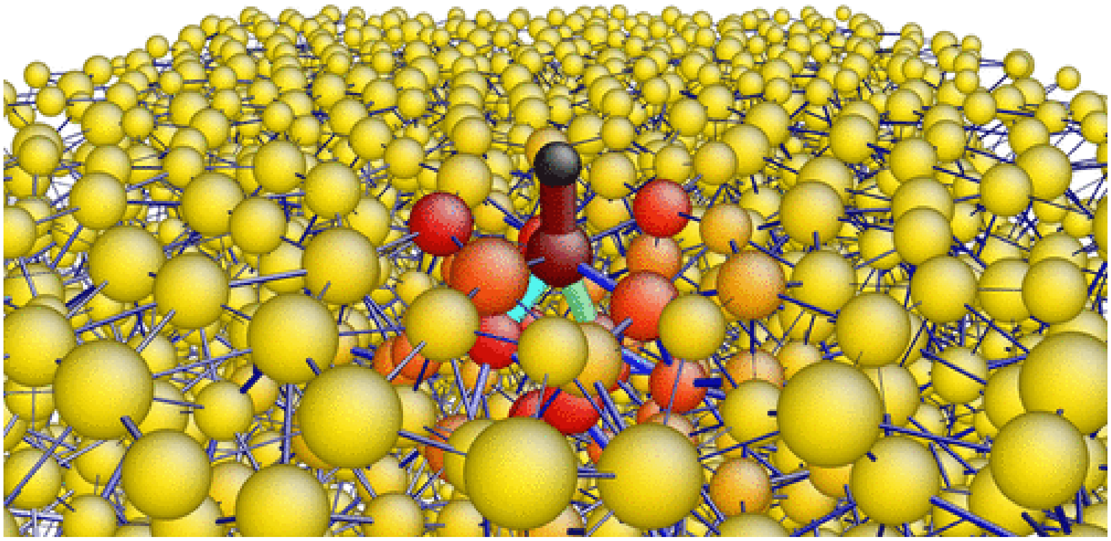

"Electrochemically Engineered, Highly Energy-Efficient Conversion of Ethane to Ethylene and Hydrogen below 550° C in a Protonic Ceramic Electrochemical Cell"
Wei Wu, Lu-Cun Wang, Hongqiang Hu, Wenjuan Bian, Joshua Y Gomez, Christopher J Orme, Hanping Ding, Yanhao Dong, Ting He, Ju Li, Dong Ding
ACS Catalysis 11 (19), 12194-12202 (2021)

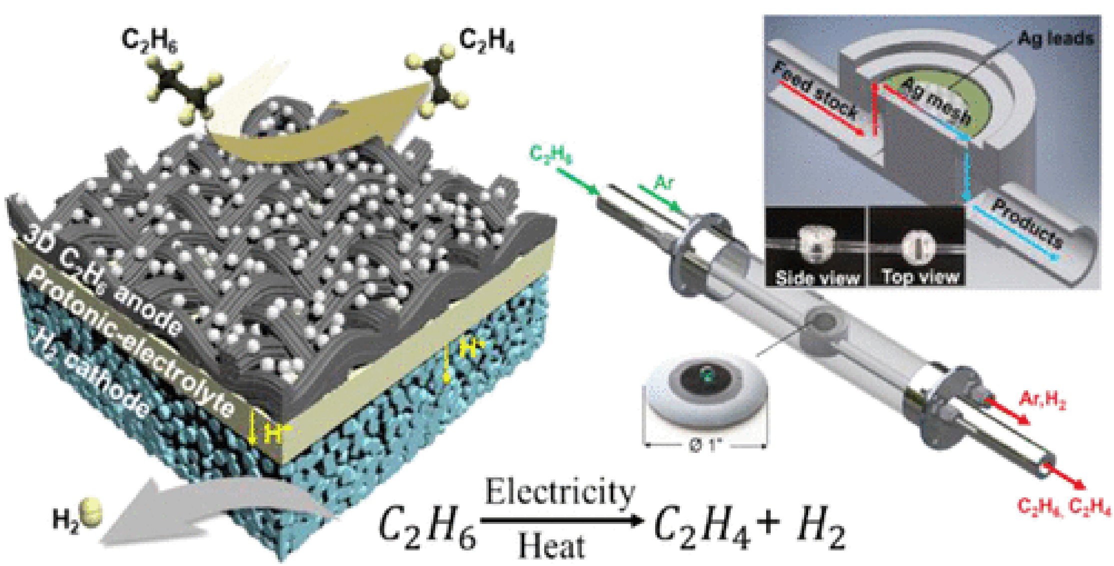

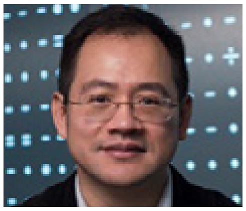

JU LI, *NSE MSE*

"Atomic-scale investigation of Lithiation/Delithiation mechanism in High-entropy spinel oxide with superior electrochemical performance"
Chih-Yang Huang, Chun-Wei Huang, Min-Ci Wu, Jagabandhu Patra, Thi Xuy-en Nguyen, Mu-Tung Chang, Oliver Clemens, Jyh-Ming Ting, Ju Li, Jeng-Kuei Chang, Wen-Wei Wu
Chemical Engineering Journal 420, 129838 (2021)

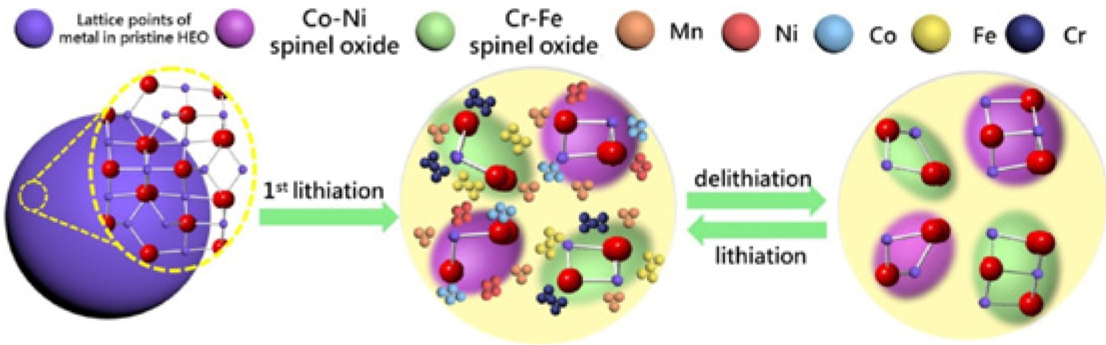

"A new approach of using Lorentz force to study single-asperity friction inside TEM"
Huanhuan Lu, Zhangjie Wang, Di Yun, Ju Li, Zhiwei Shan
Journal of Materials Science & Technology 84, 43-48 (2021)

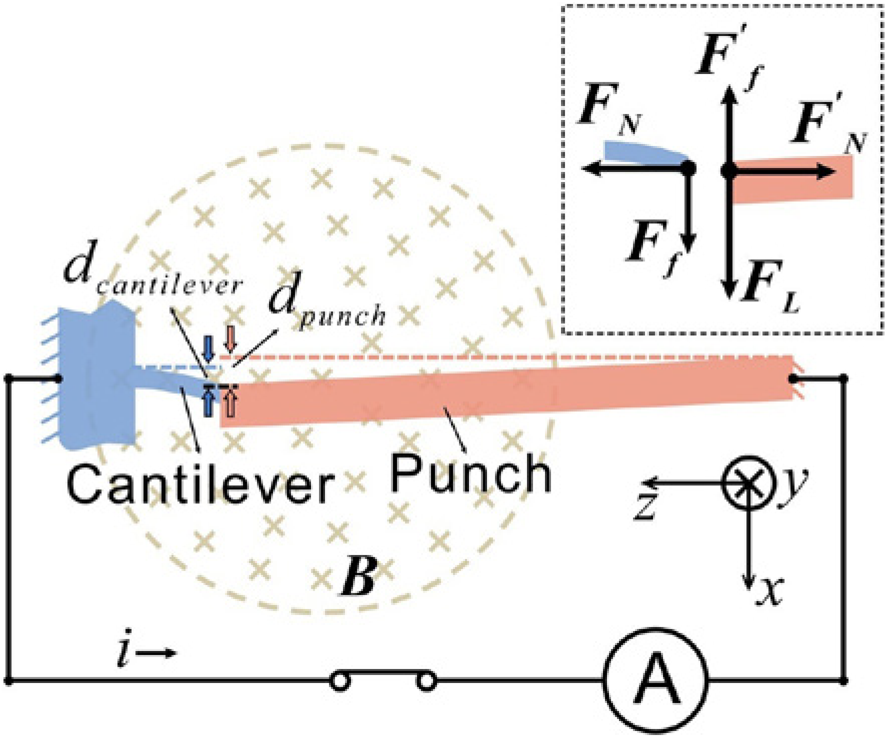

MINGDA LI, *NSE*

“Observation of dynamical transformation plasticity in metallic nanocomposites through a precompiled machine-learning algorithm”
Kang Pyo So, Myles Stapelberg, Yu Ren Zhou, Mingda Li, Michael P. Short & Sidney Yip
Mater. Res. Lett. 10, 14 (2022)

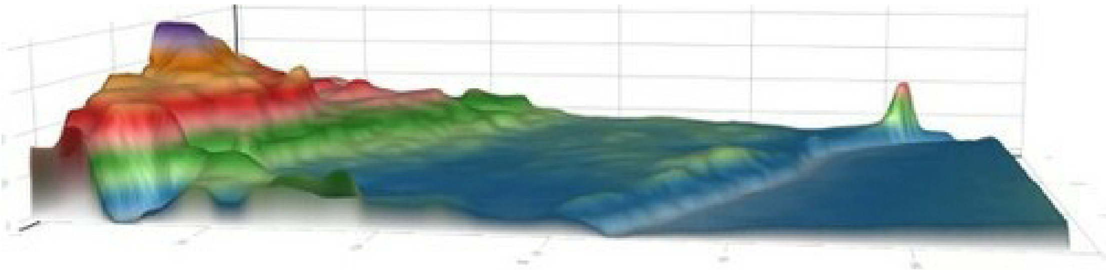

Schematic of the data processing pipeline for image frames from in situ TEM videos. This platform facilitates information extraction from low-quality images through sparse and compressed sensing algorithms and 3D visualization. (A) image frames in the video, (B) sparse and compressed sensing k-space reconstruction with an edge-preserving regularizer, (C) 2D image reconstruction, and (D) 2D vector map for 3D reconstruction. (E) a color-coded 3D surface plot to visualize the four stages of microstructure evolution in nanocomposites.

“Topological Signatures in Nodal Semimetals through Neutron Scattering”
Thanh Nguyen, Yoichiro Tsurimaki, Ricardo Pablo-Pedro, Grigory Bednik, Tong-tong Liu4, Anuj Apte, Nina Andrejevic and Mingda Li
New J. Phys. 24, 013016 (2022)

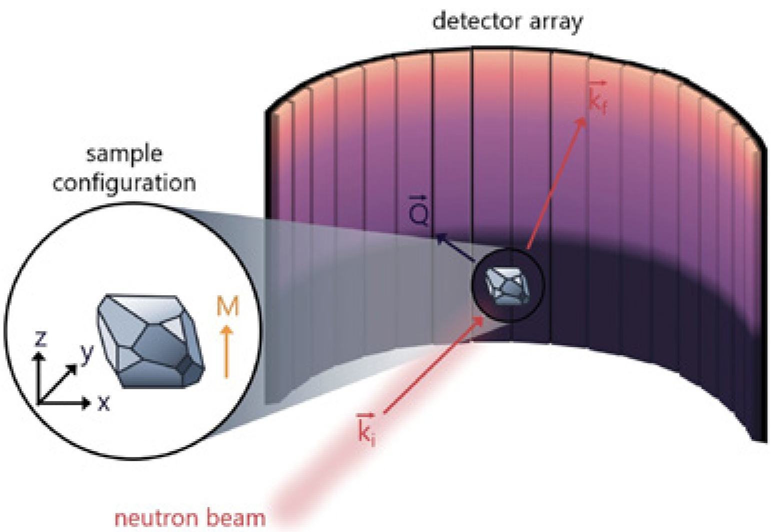

Experimental configuration. Nodal signatures of topology can be observed in the neutron spectra, e.g. extended non-analytical lines of intensity, in the case of a time-of-flight neutron experiment schematically shown here.

MINGDA LI, *NSE*

"One-way express ticket to quantum criticality"

Mingda Li and Yao Wang
Nature Materials, 21, 3 (2022) (Invited News & Views article)

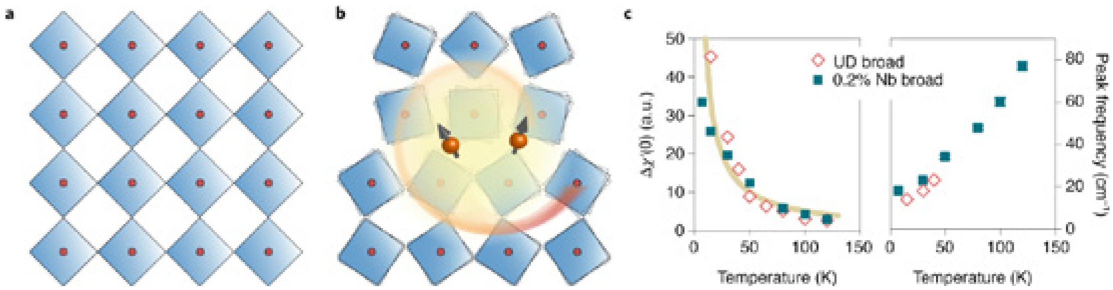

a,b, Crystal structure of a perfect crystal (a) and a plastically deformed crystal (b), in which enhanced quantum fluctuations can be induced through dislocation formation. This mediates stronger coupling of Cooper pairs (red electron pairs) and thereby enhances superconductivity. c, The Raman susceptibility ($\Delta\chi'(0)$; left) and the Raman phonon frequency data (right) as a function of temperature in plastically deformed STO without carrier doping (UD; red diamonds) and with Nb doping (green squares). The divergence of the susceptibility with a 1/T dependence and phonon softening at low temperature indicate entering into a quantum critical regime. These behaviours are insensitive to the carrier doping levels, which further hints at a structural and phononic, rather than purely electronic, origin. a.u., arbitrary units. Panel c reproduced with permission from ref. 5, Springer Nature Ltd.

"Restriction-in-Motion of Surface Ligands Enhances Photoluminescence of Quantum Dots – Experiment and Theory"

Justin M. Fang, Sayan Basu, Mingda Li, Kuo-Chih Shih, Jun Wang,Mircea Cotlet, Xudong Wang, Jing Zhao,T. J. Mountziaris, Joseph J. LoTurco, Mu-Ping Nieh
Advanced Materials Interfaces (2022)

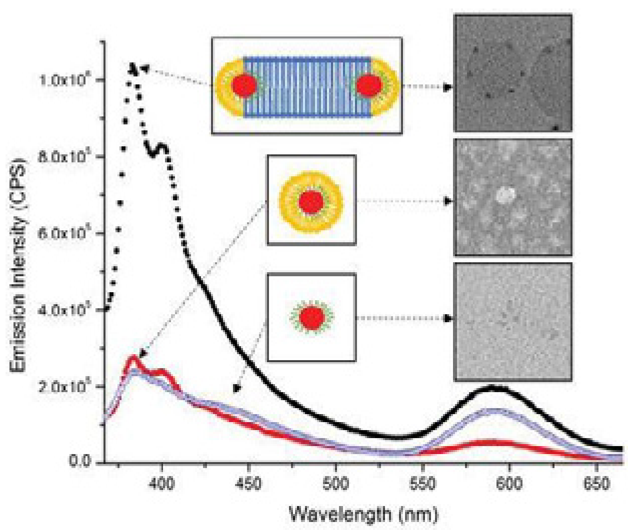

The relationship between emission and ligand restriction of a series of ZnSe/ZnS quantum dots (QDs) encapsulated in nanoparticles is investigated systematically via experiments and quantum theory. The QDs have a ZnSe core and a ZnS shell, capped with hydrophobic ligands (triotylphosphine oxide/hexadecylamine), allowing them to be entrapped in a model biomembrane, bicelle, made of zwitterionic dipalmitoyl and dihexanoyl phosphatidylcholines and charged dipalmitoyl phosphatidylglycerol. Enhanced photoluminescence is observed upon encapsulation, depending on the QD-to-lipid ratio. Transmission electron microscopy and small-angle X-ray scattering confirm that QDs are preferably situated at the rim of bicellar discs. A simplified quantum dissipation heat-bath theory is proposed to correlate the enhancement with slower nonradiative processes caused by the restriction-in-motion (RIM) of the surface ligands. However, Förster resonance energy transfer due to QD aggregation counteracts the effect.

MINGDA LI, *NSE*

“Extended Kohler’s rule of magnetoresistance”

Jing Xu, Fei Han, Ting-Ting Wang, Laxman R. Thoutam, Samuel E. Pate, Mingda Li, Xufeng Zhang, Yong-Lei Wang, Roxanna Fotovat, Ulrich Welp, Xiuquan Zhou, Wai-Kwong Kwok, Duck Young Chung, Mercouri G. Kanatzidis, and Zhi-Li Xiao

Phys. Rev. X 11, 041029 (2021) | arXiv:2109.08089 (2021)

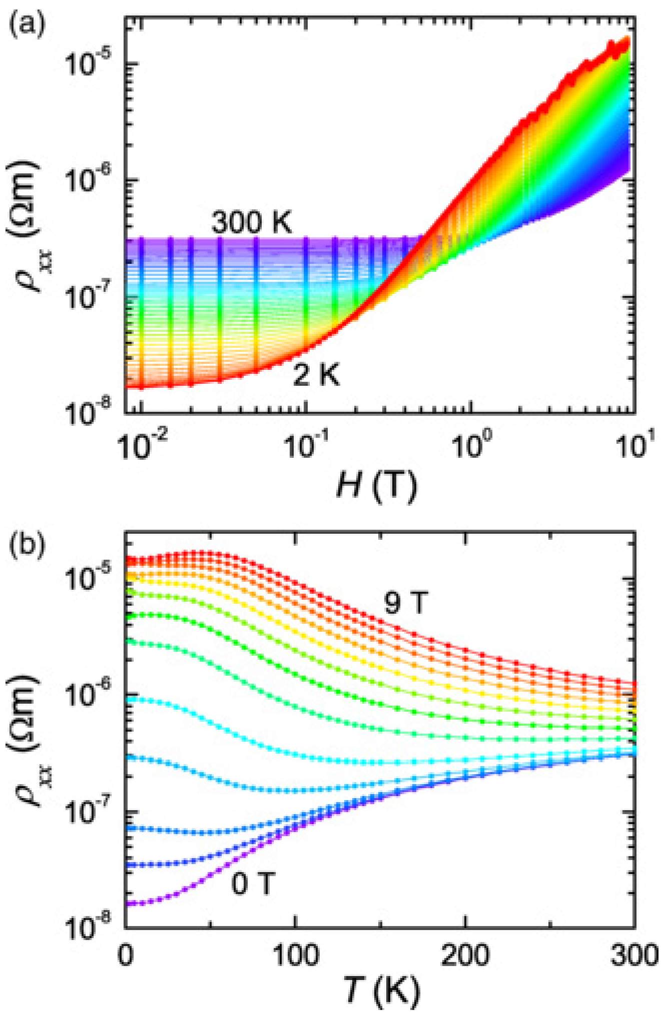

Magnetoresistance of TaP. (a) Magnetic field dependence ρxx(H) measured at temperatures of T=2 K and from 5 to 150 K in intervals of 5 K and from 160 to 300 K in intervals of 10 K (from red to purple). (b) Temperature dependence ρxx(T) constructed from ρxx(H) in (a) at magnetic fields of H=0, 0.1, 0.2, and 0.5 T and from 1 to 9 T in intervals of 1 T (from purple to red). The data are taken from sample TP1.

LUQIAO LIU, *EECS*

"Efficient Spin-Orbit Torques in an Antiferromagnetic Insulator with Tilted Easy Plane"
P Zhang, CT Chou, H Yun, BC McGoldrick, JT Hou, KA Mkhoyan, L Liu
arXiv:2201.04732 (2022)

"Tunable Magnonic Chern Bands and Chiral Spin Currents in Magnetic Multilayers"
Zhongqiang Hu, Liang Fu, Luqiao Liu
arXiv:2201.00312 (2022)

"Ising Machine Based on Electrically Coupled Spin Hall Nano-Oscillators"

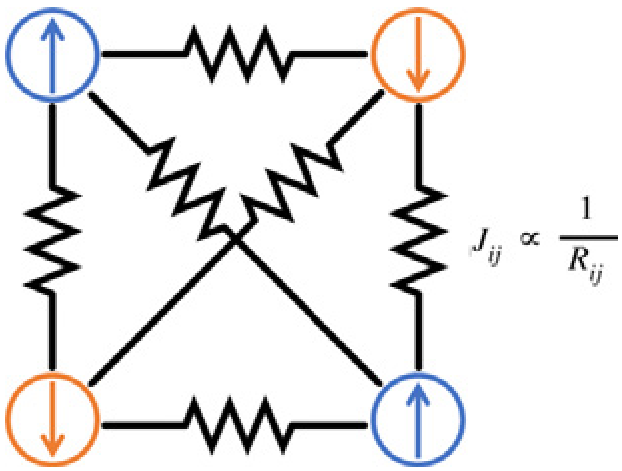

Brooke C. McGoldrick, Jonathan Z. Sun, Luqiao Liu
Physical Review Applied 17 (1), 014006 (2022) | arXiv:2110.08885 (2021)

Schematic of the all-to-all electrically coupled network of four oscillators that can be mapped to the Ising model. Nodes represent oscillators that encode spin values si=+1 ("spin up") or si=−1 ("spin down") in their phases. For resistive coupling, the Ising model coefficients are proportional to the conductances linking each pair of oscillators [5].

"Current-induced switching of a ferromagnetic Weyl semimetal Co2MnGa"
J Han, BC McGoldrick, CT Chou, TS Safi, JT Hou, L Liu
Applied Physics Letters 119 (21), 212409 (2021)

"Proposal for a Spin-Torque-Oscillator Maser Enabled by Microwave Photon-Spin Coupling"
Justin T. Hou, Pengxiang Zhang, and Luqiao Liu
Physical Review Applied 16 (3), 034034 (2021)

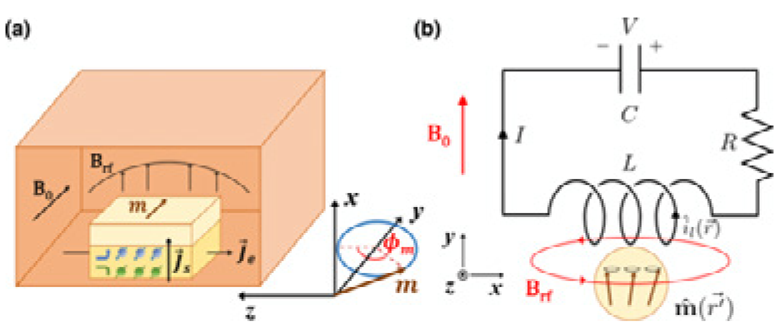

A schematic of the considered device structure. A magnetic oscillator driven by spin-orbit torque is placed inside a microwave cavity and inductively coupled to the cavity photon mode. (b) The effective circuit diagram. The microwave cavity is modeled as a serial LCR circuit. The magnetic thin film is coupled with the LCR circuit through the rf magnetic field Brf generated by the inductor current. No external signals are used to drive the LCR circuit.

SETH LLOYD, *ME, ES, Physics*

“Quantum algorithm for dense kernel matrices using hierarchical splitting”
Quynh The Nguyen, Bobak Toussi Kiani, Seth Lloyd
arXiv:2201.11329 (2022)

“Determination of the parton distribution functions of the proton using diverse ATLAS data from pp collisions at s√=7, 8 and 13 TeV”
Atlas Collaboration, ... , Seth Lloyd, et. All
arXiv:2112.11266 (2021)

“Quantum algorithms for group convolution, cross-correlation, and equivariant transformations”
Grecia Castelazo, Quynh T. Nguyen, Giacomo De Palma, Dirk Englund, Seth Lloyd, Bobak T. Kiani
arXiv: 2109.11330 (2021)

ROBERT McCONNELL, *Lincoln Laboratory*

“High-Fidelity Ion State Detection Using Trap-Integrated Avalanche Photodiodes”
David Reens, Michael Collins, Joseph Ciampi, Dave Kharas, Brian F. Aull, Kevan Donlon, Colin D. Bruzewicz, Bradley Felton, Jules Stuart, Robert J. Niffenegger, Philip Rich, Danielle Braje, Kevin K. Ryu, John Chiaverini, Robert McConnell
arXiv:2202.01715 (2022)

“Cooling of an Integrated Brillouin Laser below the Thermal Limit”
William Loh, Dave Kharas, Ryan Maxson, Gavin N. West, Alexander Medeiros, Danielle Braje, Paul W. Juodawlkis, Robert McConnell
arXiv:2112.00846 (2021)

ANAND NATARAJAN, *EECS*

"Quantum soundness of testing tensor codes"
Zhengfeng Ji, Anand Natarajan, Thomas Vidick, John Wright, Henry Yuen
arXiv:2111.08131 (2021)

"Quantum search-to-decision reductions and the state synthesis problem"
Sandy Irani, Anand Natarajan, Chinmay Nirkhe, Sujit Rao, Henry Yuen
arXiv:2111.02999 (2021)

KEVIN P. O'BRIEN, *EECS*

"Randomized compiling for scalable quantum computing on a noisy superconducting quantum processor"
Akel Hashim, Ravi K. Naik, Alexis Morvan, Jean-Loup Ville, Bradley Mitchell, John Mark Kreikebaum, Marc Davis, Ethan Smith, Costin Iancu, Kevin P. O'Brien, Ian Hincks, Joel J. Wallman, Joseph Emerson, and Irfan Siddiqi
Phys. Rev. X 11, 041039 (2021) | arXiv:2010.00215 (2021)

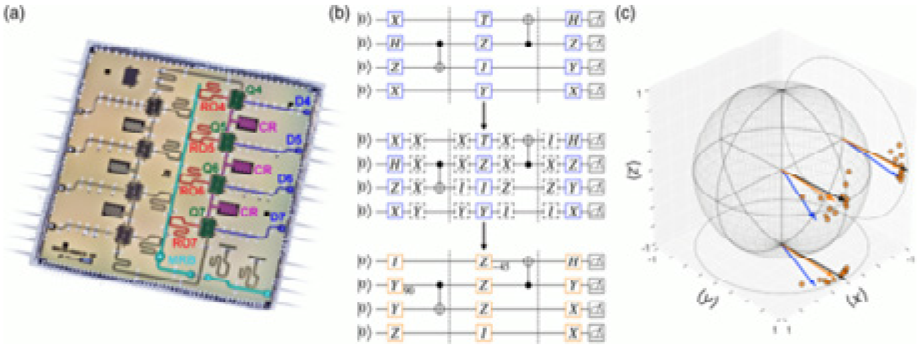

Experimental realization of noise tailoring via randomized compiling on a superconducting quantum processor. (a) False-colored micrograph of our eight-qubit superconducting quantum processor. In this work, we use four transmon qubits [33] (green) with independent microwave control lines (blue). Two-qubit cross-resonance [34, 35, 36, 37] gates are mediated by coupling resonators (CR, purple) between nearest neighbors. The qubits are simultaneously measured via dispersive coupling [38] to independent readout resonators (RO, red) coupled to a multiplexed readout bus (MRB, cyan). (b) Randomization of a quantum circuit. The bare circuit (top), split into K interleaved cycles of easy and hard gates (separated by dashed lines), (middle) is converted into a logically equivalent circuit by inserting random single-qubit twirling gates between each easy and hard cycle, inverting them in the following cycle, and (bottom) then compiling the twirling gates into a new easy-gate cycle. (c) Experimental single-qubit state-tomography results demonstrating noise tailoring. The black vector is the ideal (noiseless) final state of the qubit, but coherent errors cause an over-rotation in the measured state (blue vector). The orange vector represents the final state of the combined distribution of N=12 randomizations (orange data points), which has a lower purity because of the tailored stochastic noise. RC significantly mitigates the impact of coherent errors, as indicated by a reduction in the TVD from $d_{TV,bare}=0.170(8)$ to $d_{TV,RC}=0.029(2)$ in the $\{|+\rangle,|-\rangle\}$ basis, from $d_{TV,bare}=0.069(4)$ to $d_{TV,RC}=0.060(1)$ in the $\{|+i\rangle,|-i\rangle\}$ basis, and from $d_{TV,bare}=0.073(8)$ to $d_{TV,RC}=0.008(2)$ in the $\{|0\rangle,|1\rangle\}$ (computational) basis. This improvement is not captured by the bare (F=0.862) and RC (F=0.879) state fidelities, which are approximately equal.



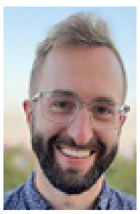

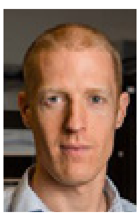


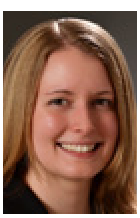

WILLIAM D. OLIVER, *EECS, Physics, Lincoln Laboratory;* **JEFF GROVER**, *RLE;* **SIMON GUSTAVSSON**, *RLE;* **TERRY ORLANDO**, *EECS;* **MOLLIE SCHWARTZ**, *Lincoln Laboratory;* **KYLE SERNIAK**, *Lincoln Laboratory*, **JOEL I-JAN WANG**, *RLE;* **JONILYN YODER**, *Lincoln Laboratory*

“Broadband Squeezed Microwaves and Amplification with a Josephson Traveling-Wave Parametric Amplifier”
Jack Y. Qiu, Arne Grimsmo, Kaidong Peng, Bharath Kannan, Benjamin Lienhard, Youngkyu Sung, Philip Krantz, Vladimir Bolkhovsky, Greg Calusine, David Kim, Alex Melville, Bethany M. Niedzielski, Jonilyn Yoder, Mollie E. Schwartz, Terry P. Orlando, Irfan Siddiqi, Simon Gustavsson, Kevin P. O’Brien, William D. Oliver
arXiv:2201.11261 (2022)

“Distinguishing multi-spin interactions from lower-order effects”
T. R. Bergamaschi, T. Menke, W. P. Banner, A. Di Paolo, S. J. Weber, C. F. Hirjibehedin, A. J. Kerman, W. D. Oliver
arXiv:2111.12717 (2021)

“Mediated interactions beyond the nearest neighbor in an array of superconducting qubits”
Y. Yanay, J. Braumüller, T. P. Orlando, S. Gustavsson, C. Tahan, W. D. Oliver
arXiv:2110.01699 (2021)

“Building a quantum engineering undergraduate program”
A. Asfaw, A. Blais, K. R. Brown, J. Candelaria, C. Cantwell, L. D. Carr, J. Combes, D. M. Debroy, J. M. Donohue, S. E. Economou, E. Edwards, M. F. J. Fox, S. M. Girvin, A. Ho, H. M. Hurst, Z. Jacob, B. R. Johnson, E. Johnston-Halperin, R. Joynt, E. Kapit, J. Klein-Seetharaman, M. Laforest, H. J. Lewandowski, T. W. Lynn, C. R. H. McRae, C. Merzbacher, S. Michalakis, P. Narang, W. D. Oliver, J. Palsberg, D. P. Pappas, M. G. Raymer, D. J. Reilly, M. Saffman, T. A. Searles, J. H. Shapiro, C. Singh
arXiv:2108.01311 (2021)



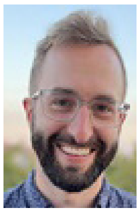

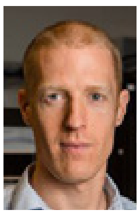


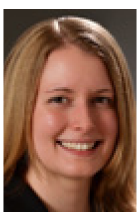

WILLIAM D. OLIVER, *EECS, Physics, Lincoln Laboratory;* **JEFF GROVER**, *RLE;*
SIMON GUSTAVSSON, *RLE;* **TERRY ORLANDO**, *EECS;* **MOLLIE SCHWARTZ**, *Lincoln Laboratory;*
KYLE SERNIAK, *Lincoln Laboratory*, **JOEL I-JAN WANG**, *RLE;* **JONILYN YODER**, *Lincoln Laboratory*

"Hexagonal Boron Nitride as a low-loss dielectric for superconducting quantum circuits and qubits"

J. I-J. Wang, M. A. Yamoah, Q. Li, A. Karamlou, T. Dinh, B. Kannan, J. Braumueller, D. Kim, A. J. Melville, S. E. Muschinske, B. M. Niedzielski, K. Serniak, Y. Sung, R. Winik, J. L. Yoder, M. Schwartz, K. Watanabe, T. Taniguchi, T. P. Orlando, S. Gustavsson, P. Jarillo-Herrero, W. D. Oliver

MIT News (2022) | Nature Materials (2022) | Phys.org (2022) | arXiv:2109.00015 (2021)

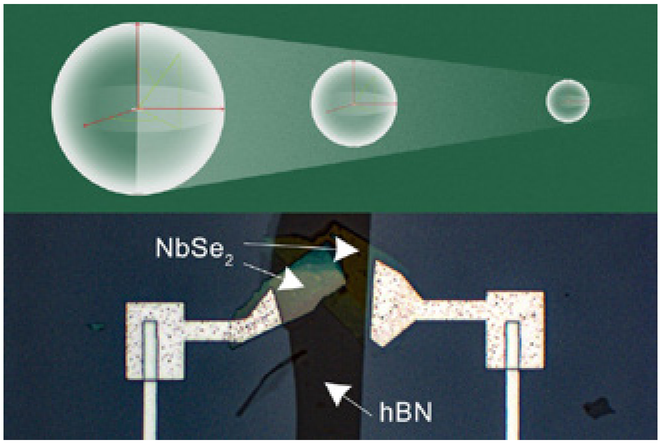

MIT Researchers used the 2D material hexagonal boron nitride to build much smaller capacitors for superconducting qubits, enabling them to shrink the footprint of a qubit by two orders of magnitude without sacrificing performance.

"Deep neural network discrimination of multiplexed superconducting qubit states"

B. Lienhard, A. Vepsäläinen, L. C. G. Govia, C. R. Hoffer, J. Y. Qiu, D. Ristè, M. Ware, D. Kim, R. Winik, A. Melville, B. Niedzielski, J. Yoder, G. J. Ribeill, T. A. Ohki, H. K. Krovi, T. P. Orlando, S. Gustavsson, W. D. Oliver

Phys. Rev. Applied 17, 014024 (2022) | arXiv:2102.12481 (2021)

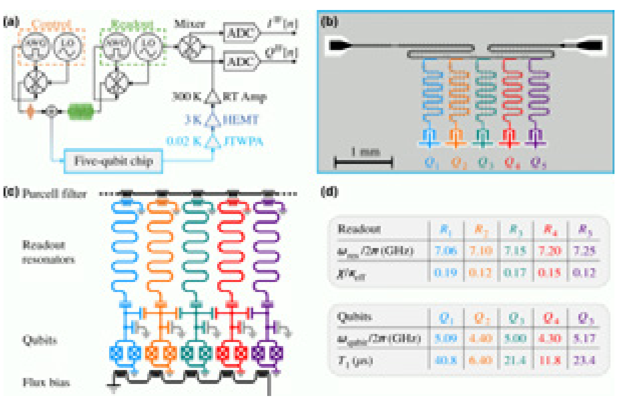

Measurement setup and chip. (a) Schematic of control and readout of superconducting qubits. The control and readout pulses, generated by an arbitrary waveform generator (AWG) and up-converted to GHz frequencies using a local oscillator (LO), are sent through attenuated signal lines to the readout resonator on the five-qubit chip. The transmitted readout signal is amplified by a Josephson traveling-wave parametric amplifier (JTWPA), a HEMT, and a room-temperature amplifier. Subsequently, the signal is down-converted to MHz frequencies and digitized—in-phase IIF[n] and quadrature QIF[n] sequences at intermediate frequencies (IF). Colored optical micrograph (b) and the circuit schematic (c) comprising five superconducting transmon qubits. The qubit transition frequencies are tuned via a global flux bias. Each qubit is capacitively coupled to a quarter-wave readout resonator that couples inductively to a bandpass (Purcell) filtered feedline. (d) The resonator frequencies ωres/2π are near 7 GHz with χ/κeff ratios ranging from 0.12 to 0.19, where χ and κeff are, respectively, the dispersive shift and the effective resonator decay rate through the feedline. Table of the qubit lifetimes (T1) and operating frequencies (ωqubit/2π). Qubit colors indicate the qubit operating frequency: red (purple) → lowest (highest) operating frequency.



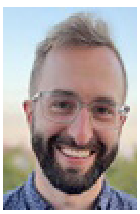

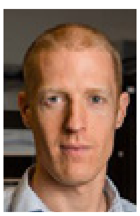


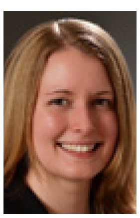

WILLIAM D. OLIVER, *EECS, Physics, Lincoln Laboratory;* **JEFF GROVER**, *RLE;*
SIMON GUSTAVSSON, *RLE;* **TERRY ORLANDO**, *EECS;* **MOLLIE SCHWARTZ**, *Lincoln Laboratory;*
KYLE SERNIAK, *Lincoln Laboratory*, **JOEL I-JAN WANG**, *RLE;* **JONILYN YODER**, *Lincoln Laboratory*

“Twist: sound reasoning for purity and entanglement in Quantum programs”
C. Yuan, C. McNally, M. Carbin
MIT News (2022) | Proc. ACM Program. Lang. 6, POPL, Article 30, 1-32 (2022)

“Demonstration of Density Matrix Exponentiation using a superconducting quantum processor”
M. Kjaergaard, M. E. Schwartz, A. Greene, G. O. Samach, A. Bengtsson, M. O’Keeffe, C. M. McNally, J. Braumüller, D. K. Kim, P. Krantz, M. Marvian, A. Melville, B. M. Niedzielski, Y. Sung, R. Winik, J. L. Yoder, D. Rosenberg, K. Obenland, S. Lloyd, T. P. Orlando, I. Marvian, S. Gustavsson, W. D. Oliver
Phys. Rev. X 12, 011005 (2022)| arXiv:2001.08838 (2020)

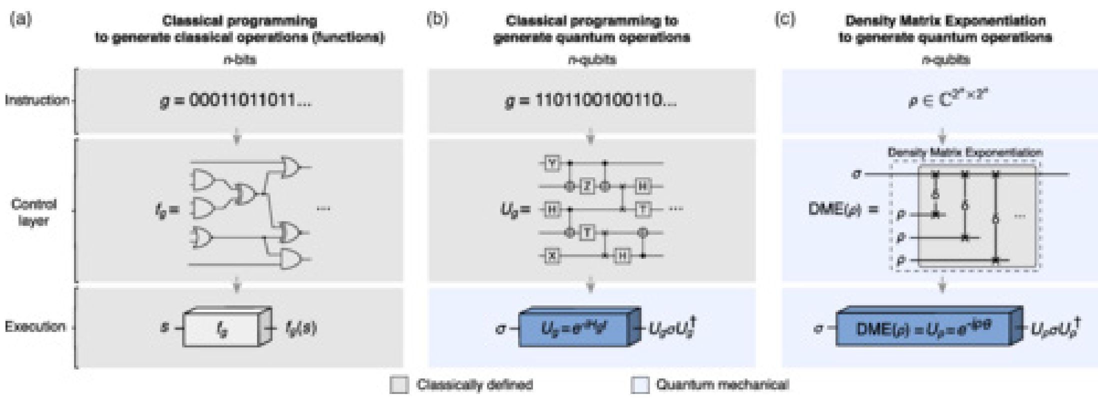

Schematic representations of computing architectures. (a) Classical programming to generate classical operations (functions). Instructions are defined by a classical bit string g that uniquely determines a Boolean logic function fg. The control layer executes the resulting circuit on data bits s to produce the output fg(s). (b) Classical programming to generate quantum operations. Instructions are defined by a classical bit string g that uniquely determines a unitary operation Ug. The gate sequence is applied to the quantum hardware (data qubits σ) to execute the unitary operation U=exp(−iHgt), where Hg is the quantum circuit Hamiltonian, to produce the output UgσU†g. If any components of the instruction string depend on information from previous steps in the algorithm, that information must be tomographically extracted from σ and then classically recompiled. (c) DME to generate quantum operations. In DME, the quantum operation is stored in the quantum instruction state ρ. Classical hardware generates N partial SWAP operations, a co-rotation enacted by a Heisenberg interaction between qubits σ and ρ (see text) along the same axis, over a small, classically chosen rotation angle δ=θ/N. These partial SWAP operations implement the unitary operation U=e−iρθ without first requiring classical compilation of the information contained in ρ.



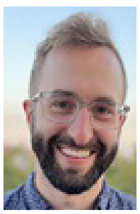

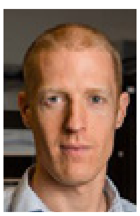


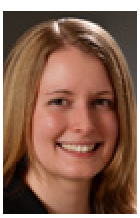

WILLIAM D. OLIVER, *EECS, Physics, Lincoln Laboratory;* **JEFF GROVER**, *RLE;* **SIMON GUSTAVSSON**, *RLE;* **TERRY ORLANDO**, *EECS;* **MOLLIE SCHWARTZ**, *Lincoln Laboratory;* **KYLE SERNIAK**, *Lincoln Laboratory*, **JOEL I-JAN WANG**, *RLE;* **JONILYN YODER**, *Lincoln Laboratory*

“Probing quantum information propagation with out-of-time-ordered correlators”
J. Braumüller, A. H. Karamlou, Y. Yanay, B. Kannan, D. Kim, M. Kjaergaard, A. Melville, B. M. Niedzielski, Y. Sung, A. Vepsäläinen, R. Winik, J. L. Yoder, T. P. Orlando, S. Gustavsson, C. Tahan, W. D. Oliver
Nat. Phys. (2021) | arXiv:2102.11751 (2021) See also: News and Views by Arghavan Safavi–Naini

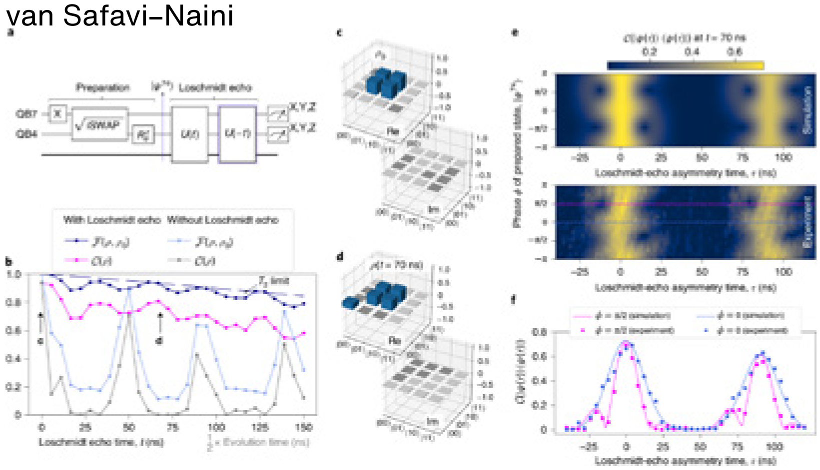

a, Pulse sequence used in the Loschmidt echo experiment. The notation X, Y, Z denotes tomographic qubit readout. b, Overlap fidelity FF of the extracted density matrix ρ after varying Loschmidt echo times t with the prepared entangled state ρ0 (dark blue) as measured immediately after state preparation. The coherence (T2) limit on F(ρ,ρ0) F(ρ,ρ0) due to qubit dephasing is plotted as a dashed line, based on net T2,eff = 0.88 μs (Supplementary Section 7). We also show the concurrence C(ρ) C(ρ) of the measured state after a Loschmidt echo (pink). For comparison, we show F(ρ,ρ0)F(ρ,ρ0) and C(ρ) C(ρ) without the time-reversal operator in the middle, but with two successive forward time evolution steps |Ψ(t)⟩ = U(t)U(t)|Ψ74⟩ (grey and light blue). c, Reconstructed density matrix of the experimentally prepared state ρ0, with F(ρ0,σ)F(ρ0,σ) = 95.3%. d, Reconstructed density matrix of the measured state ρ(t = 70 ns), with F(ρ,ρ0)F(ρ,ρ0) = 91.5%. e, Concurrence of the initially entangled subspace after a sequence with the reverse evolution time offset by τ, that is, |Ψ(t)⟩ = U(–70 ns – τ)U(70 ns)|Ψ74⟩. We observe an entanglement revival after a Loschmidt echo with τ = 0. The additional revival at τ = T reveals the lattice periodicity. f, Line-cuts from the dataset in e.

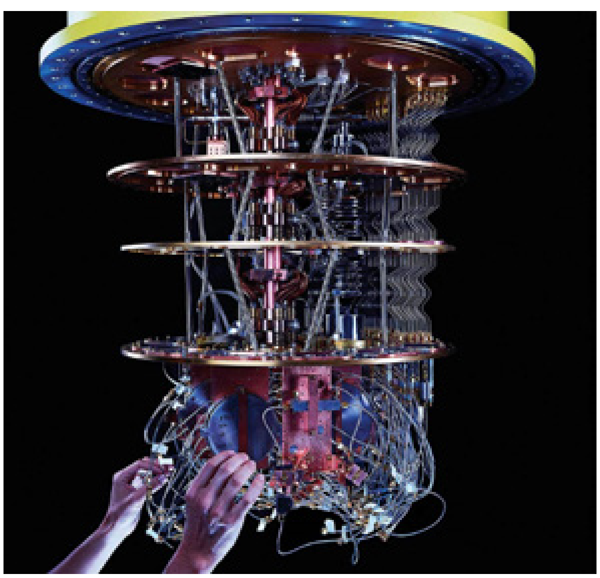

“Quantum computing for business leaders”
J. Ruane, A. McAfee, W. D. Oliver
Harvard Business Review, January-February (2022)



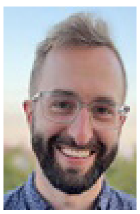

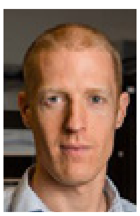


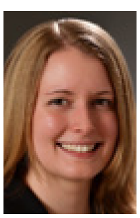

WILLIAM D. OLIVER, *EECS, Physics, Lincoln Laboratory;* **JEFF GROVER**, *RLE;*
SIMON GUSTAVSSON, *RLE;* **TERRY ORLANDO**, *EECS;* **MOLLIE SCHWARTZ**, *Lincoln Laboratory;*
KYLE SERNIAK, *Lincoln Laboratory*, **JOEL I-JAN WANG**, *RLE;* **JONILYN YODER**, *Lincoln Laboratory*

"Quantum-coherent nanoscience"

A. J. Heinrich, W. D. Oliver, L. M. K. Vandersypen, A. Ardavan, R. Sessoli, D. Loss, A. B. Jayich, J. Fernandez-Rossier, A. Laucht, A. Morello

Nat. Nanotechnol. (2021)

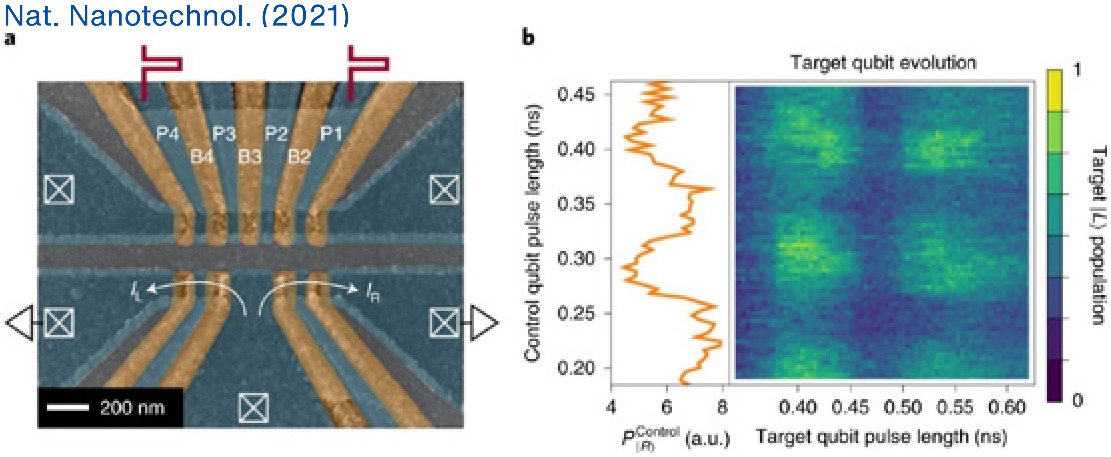

a, False-colour scanning electron micrograph of the device. Plunger (P) and barrier (B) gates are labelled, with P1 and P4 used for fast d.c. control of the quantum dots. IL (IR) is the left (right) charge sensor current. b, Demonstration of the coherent evolution of the target qubit based on the state of the control qubit. Left: a one-dimensional slice through the data. Right: the control and target qubits are controlled by pulses of varying length, where PControl|R⟩P|R⟩Control is the population of the control qubit. a.u., arbitrary units. This work represents an important step towards electrical quantum control of two coupled qubits. Figure reproduced with permission from ref. 127, under a Creative Commons licence CC BY 4.0.

"Quantum computer-aided design: digital quantum simulation of quantum processors"

T. H. Kyaw, T. Menke, S. Sim, N. P. D. Sawaya, W. D. Oliver, G. G. Guerreschi, A. Aspuru-Guzik

Phys. Rev. Applied 16, 044042 (2021) | arXiv:2006.03070 (2020)

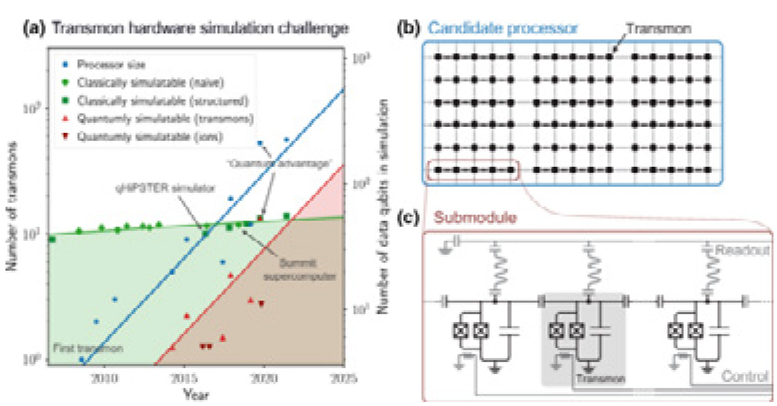

The challenge of simulating transmon quantum processors. (a) The historical numbers of transmons in a superconducting processor suggest an exponential growth in processor size, while classical supercomputer simulations will be limited to about ten transmons in the forseeable future. Quantum computers may soon be able to simulate larger transmon processors than their classical counterparts. The blue dots show the size of a selection of published transmon processors over time (Refs. [12, 13, 14, 15, 16, 17, 18, 19, 20, 21] chronologically). The green diamonds show the maximum number of transmons that



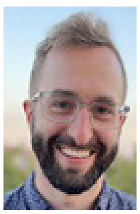

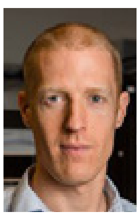


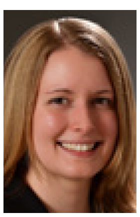

WILLIAM D. OLIVER, *EECS, Physics, Lincoln Laboratory;* **JEFF GROVER**, *RLE;* **SIMON GUSTAVSSON**, *RLE;* **TERRY ORLANDO**, *EECS;* **MOLLIE SCHWARTZ**, *Lincoln Laboratory;* **KYLE SERNIAK**, *Lincoln Laboratory*, **JOEL I-JAN WANG**, *RLE;* **JONILYN YODER**, *Lincoln Laboratory*

the best supercomputer at the given point in time could simulate based naïvely on its memory size, using a Hilbert state truncation of 16 states per transmon [22]. Another estimate for the classically simulatable processor size takes the maximum number of data qubits for which a quantum algorithm has been simulated on a supercomputer and scales it to the number of transmons that these qubits could encode (green squares, Refs. [20, 21, 23, 24, 25, 26] chronologically). An encoding scheme with four data qubits per transmons is assumed. The red triangles show the number of transmons that could be simulated on an experimentally demonstrated quantum computer that is made up of transmons themselves (triangles up, Refs. [15, 16, 17, 18, 19, 20, 21] chronologically) or of ions (triangles down, Refs. [27, 28, 29] chronologically). All solid lines are to guide the eyes along the general trend of the transmon processor size (blue), classically simulatable processor size (green), and quantumly simulatable processor size (red). Note that the cost of simulation is a constant offset in this log-linear plot and grows as fast as the available quantum processors. (b) Design proposals for new processors typically consist of tiled submodules (red box) that share common readout circuitry and that can be perceived as the unit cells of the processor. (c) This work considers the case in which the submodules are chains of capacitively coupled transmons, for which the circuit diagram including readout and flux control circuitry is shown here.

Reasserting U.S. leadership in microelectronics

Jesús A. del Alamo, Dimitri A. Antoniadis, Robert G. Atkins, Marc A. Baldo, Vladimir Bulović, Mark A. Gouker, Craig L. Keast, Hae-Seung Lee, William D. Oliver, Tomás Palacios, Max M. Shulaker, Carl V. Thompson

MIT News (2022) | A White Paper on the Role of Universities (2021) | CNET (2021)

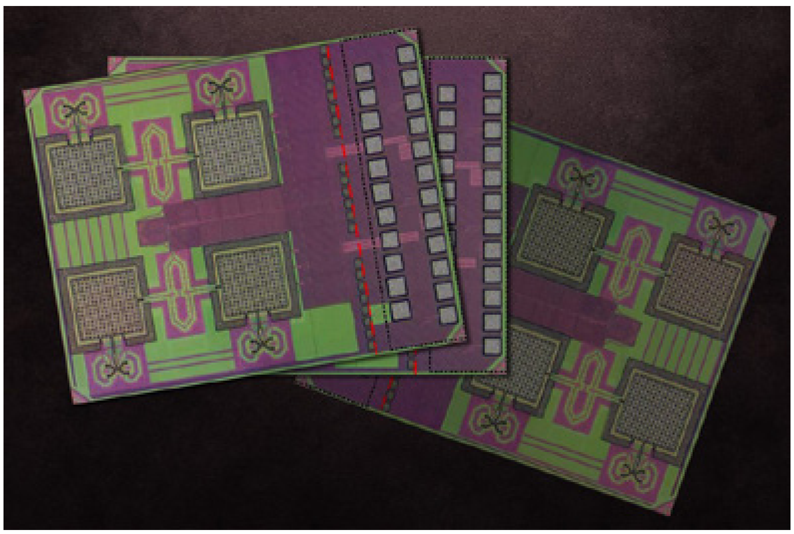

This image shows the CMOS THz-ID chip. The chip is a collaboration between Profs. Ruonan Han and Anantha P. Chandrakasan.

RAJEEV RAM, *EECS*

[“Computational polarized Raman microscopy on sub-surface nanostructures with sub-diffraction-limit resolution”]

Zheng Li, Nili Persits, Dodd J. Gray, and Rajeev J. Ram
[Optics Express 29 (23), 38027-38043 (2021)]

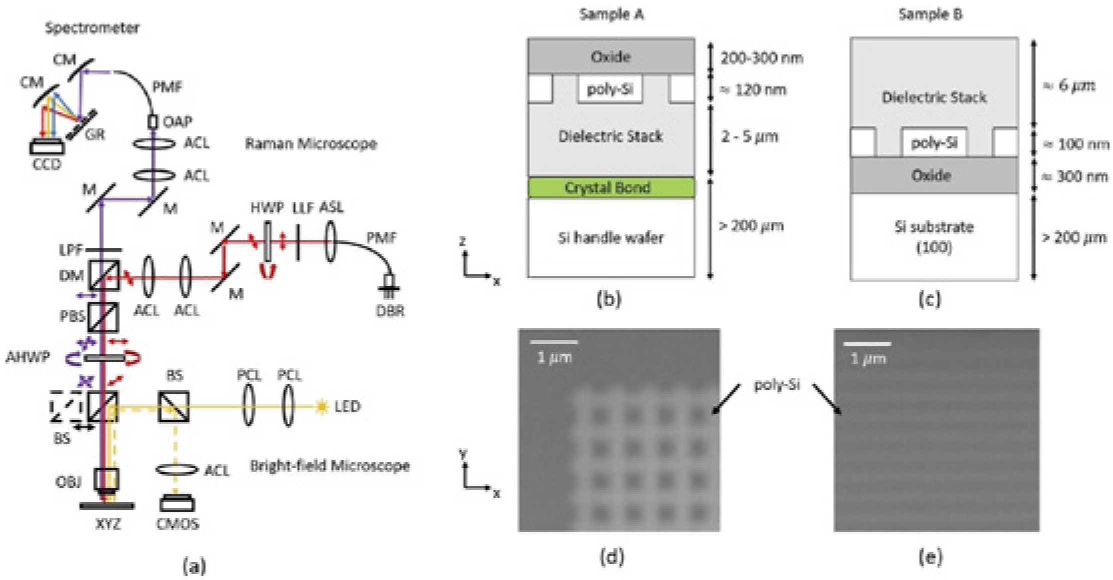

(a) The schematic plot of our polarized Raman microscope, the layer stacks of (b) sample A and (c) sample B, and the bright-field images of representative patterns on the poly-Si layer of (d) sample A and (e) sample B. In (a), the red and the purple arrows indicate the beam path of the excitation and the Raman light, respectively. The red and the purple double-headed arrows indicate the polarization directions in the corresponding beam path. The orange solid and dashed arrows indicate the beam path of the illumination and the reflection path of the bright-field microscope, respectively. The multi-colored arrows in the spectrometer indicate the dispersed spectrum. Labels in (a) are listed as follows. DBR: 785785 nm distributed Bragg reflector laser. PMF: polarization-maintaining fiber. ASL: aspherical lens. LLF: 785785 nm laser line filter. HWP: 785785 nm half-wave plate. M: mirror. ACL: achromatic lens. DM: dichroic mirror. PBS: polarization beam splitter. AHWP: achromatic half-wave plate. BS: 5050-5050 beam splitter. PCL: plano-convex lens. LED: 633 nm light-emitting diode. OBJ: objective. CMOS: CMOS camera. LPF: 785785 nm long-pass filter. OAP: off-axis parabolic mirror. CM: collimating mirror. GR: 600600 grooves per mm grating. CCD: liquid-nitrogen cooled CCD camera.

[“Machine Learning-Aided At-Line Detection of Bacterial marker NA for Cell Manufacturing”]

Jiayi Huang, Thiara Sana Ahmed, Maciej Baranski, Elizabeth Lee, Shruthi Pandi Chelvam, Ying Ying Wu, Rajeev Ram, Scott Rice, Derrick Yong, and Stacy Springs
[Frontiers in Optics, JTu1A. 93 (2021)]

KYLE SERNIAK, *Lincoln Laboratory*

[“Dark matter axion search using a Josephson traveling wave parametric amplifier”]
C.Bartram, T. Braine, R. Cervantes, N. Crisosto, N. Du, G. Leum, P. Mohapatra, T. Nitta, L. J Rosenberg, G. Rybka, J. Yang, J. Clarke, I. Siddiqi, A. Agrawal, A. V. Dixit, M. H. Awida, A. S. Chou, M. Hollister, S. Knirck, A. Sonnenschein, W. Wester, J. R. Gleason, A. T. Hipp, S. Jois, P. Sikivie, N. S. Sullivan, D. B. Tanner, E. Lentz, R. Khatiwada, G. Carosi, C. Cisneros, N. Robertson, N. Woollett, L. D. Duffy, C. Boutan, M. Jones, B. H. LaRoque, N. S. Oblath, M. S. Taubman, E. J. Daw, M. G. Perry, J. H. Buckley, C. Gaikwad, J. Hoffman, K. Murch, M. Goryachev, B. T. McAllister, A. Quiskamp, C. Thomson, M. E. Tobar, V. Bolkhovsky, G. Calusine, W.D. Oliver, K. Serniak
arXiv:2110.10262 (2021)

JEFFREY H. SHAPIRO, *EECS*

“Demonstration of quantum-limited discrimination of multi-copy pure versus mixed states”
Arunkumar Jagannathan, Olivia Brasher, Michael Grace, Jeffrey H. Shapiro, Saikat Guha, Jonathan L. Habif
arXiv:2111.14890 (2021)

“Ultimate accuracy limit of quantum pulse-compression ranging”
Quntao Zhuang and Jeffrey H. Shapiro
Phys. Rev. Lett. 128, 010501 (2022) | Phys.org (2022) | arXiv:2109.11079 (2021)

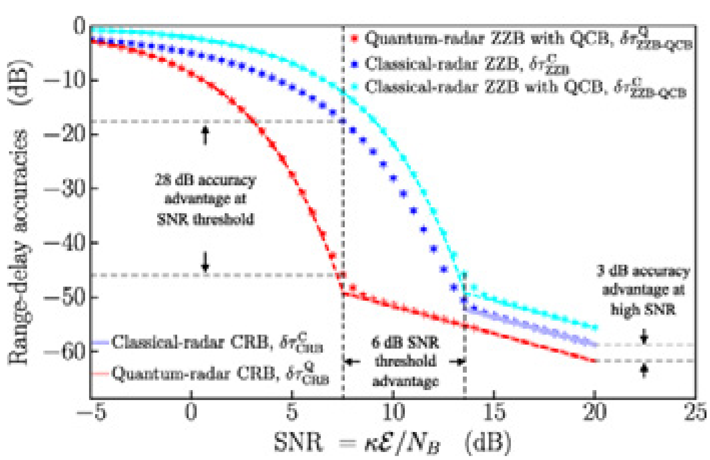

Normalized mean-squared range-delay accuracies in dB, 20log10(δτ/στ), versus SNR in dB. The plots assume Δω/2π=106 Hz and ΔR=5 km. Results are shown, top to bottom, for δτCZZB−QCB (cyan stars), δτCZZB (blue stars), and δτCZZB−QCB (red stars). Also plotted, in the corresponding colors, are their high-SNR and low-SNR asymptotic behaviors, along with vertical dashed lines showing their SNR thresholds, SNRCthresh and SNRQthresh, computed from the intersections of each radar's high-SNR and low-SNR asymptotic behaviors.

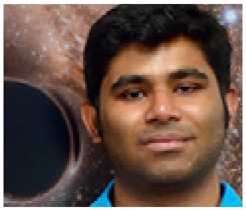

PETER SHOR, *Mathematics*

"Simultaneous Measurement and Entanglement"
Andrey Boris Khesin, Peter Shor
arXiv:2201.10667 (2022)

VIVISHEK SUDHIR, *ME*

"Thermorefringent noise in crystalline optical materials"
Serhii Kryhin, Evan D. Hall, Vivishek Sudhir
arXiv:2111.05433 (2021)

"Quantum theory of feedback cooling of an anelastic macro-mechanical oscillator"
Kentaro Komori, Dominika Ďurovčíková, Vivishek Sudhir
arXiv:2111.02412 (2021)

TIMOTHY SWAGER, *Chemistry*

“Molecular Platform for Fast Low-Voltage Nanoelectromechanical Switching”
Jinchi Han, Zachary Nelson, Matthew R. Chua, Timothy M. Swager, Farnaz Niroui, Jeffrey H. Lang, and Vladimir Bulović
Nano Lett. 21, 24, 10244–10251 (2021)

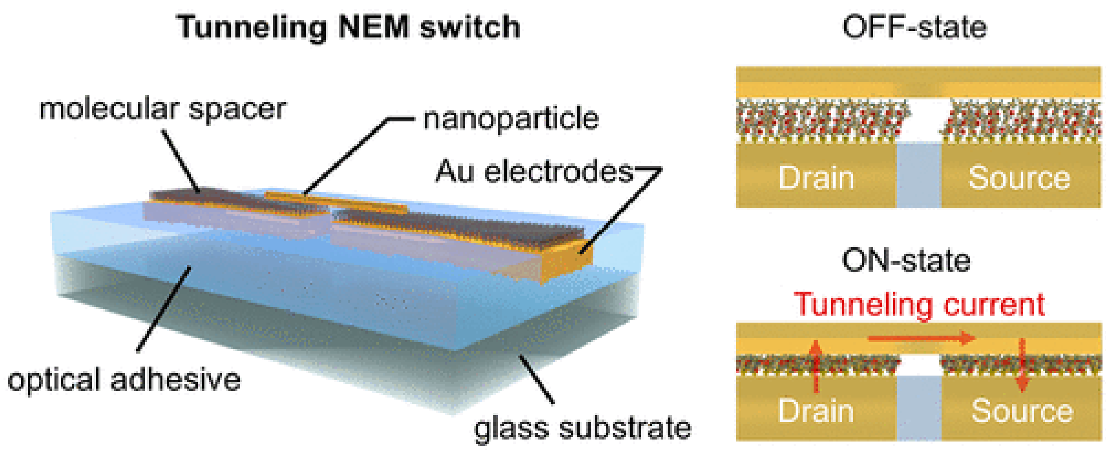

“Overhauser Dynamic Nuclear Polarization with Selectively Deuterated BDPA Radicals”
Léo Delage-Laurin, Ravi Shankar Palani, Natalie Golota, Michael Mardini, Yifu Ouyang, Kong Ooi Tan, Timothy M Swager, Robert G Griffin
J. Am. Chem. Soc. 143, 48, 20281–20290 (2021)

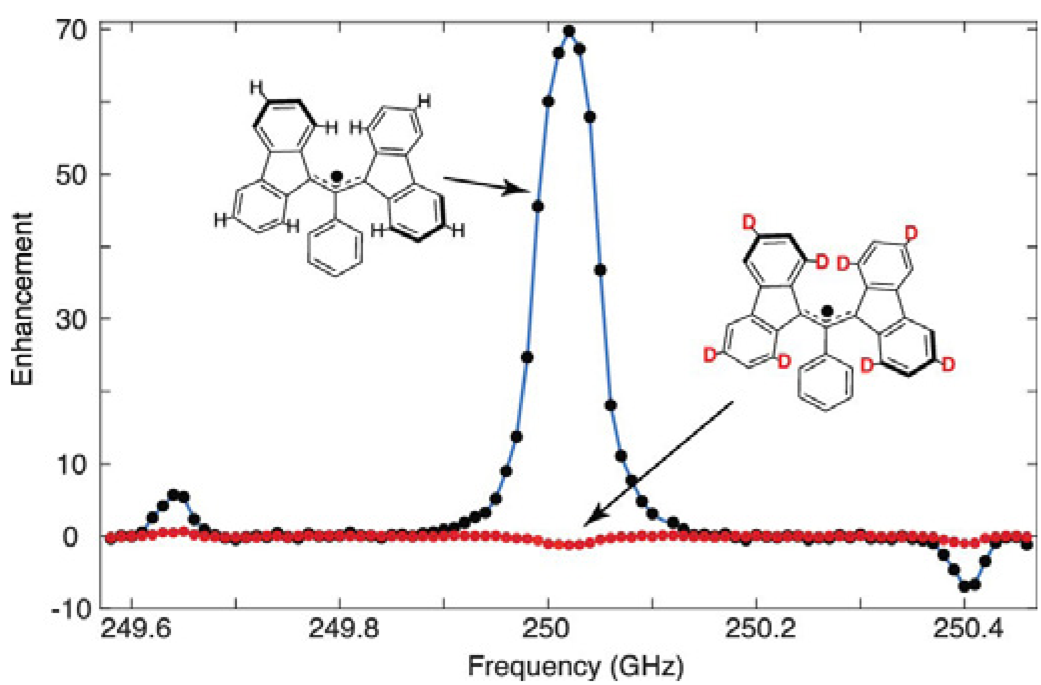

TIMOTHY SWAGER, *Chemistry*

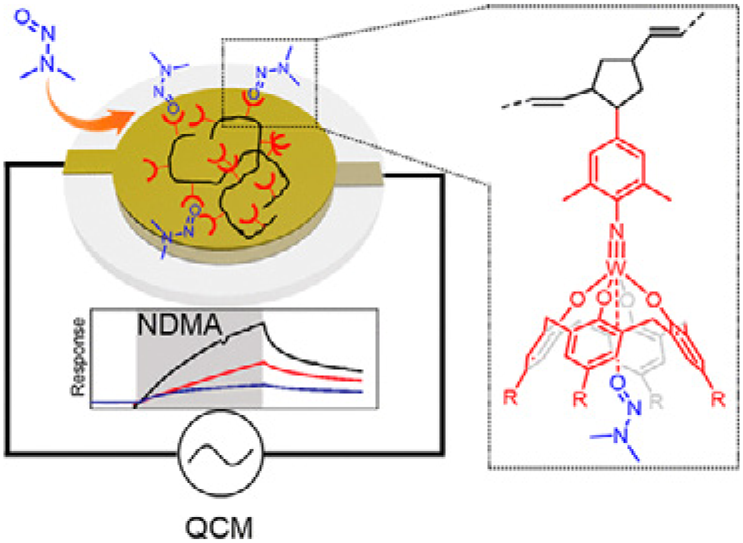

"Metallocalix[4]arene Polymers for Gravimetric Detection of N-Nitrosodialkylamines"
Ru-Qiang Lu, Weize Yuan, Robert G Croy, John M Essigmann, Timothy M Swager
J. Am. Chem. Soc. 143, 47, 19809–19815 (2021)

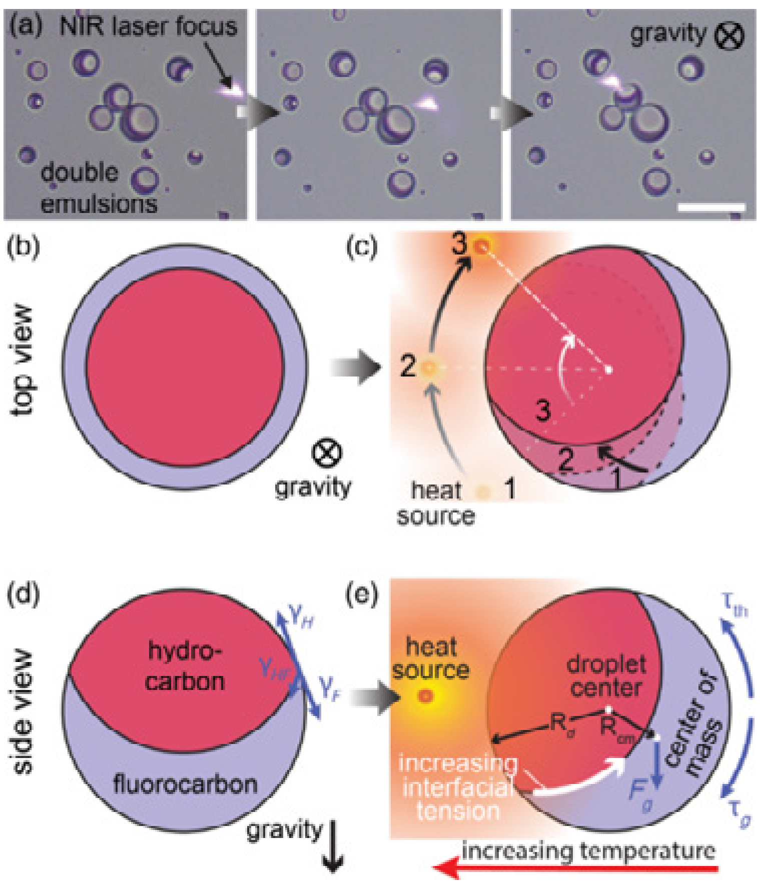

"Actuation of Janus Emulsion Droplets via Optothermally Induced Marangoni Forces"
Sara Nagelberg, Jan F Totz, Matthäus Mittasch, Vishnu Sresht, Lukas Zeininger, Timothy M Swager, Moritz Kreysing, Mathias Kolle
Phys. Rev. Lett. 127, 144503 (2021)

SENTHIL TODRARI, *Physics*

“The dipolar Bose-Hubbard model”
Ethan Lake, Michael Hermele, T. Senthil
arXiv:2201.04132 (2022)

“Theory of a Continuous Bandwidth-tuned Wigner-Mott Transition”
Seth Musser, T. Senthil, Debanjan Chowdhury
arXiv:2111.09894 (2021)

“Interpreting Angle Dependent Magnetoresistance in Layered Materials: Application to Cuprates”
Seth Musser, Debanjan Chowdhury, Patrick A. Lee, T. Senthil
arXiv:2111.08740 (2021)

“Lowest Landau level theory of the bosonic Jain states”
Hart Goldman, T. Senthil
arXiv:2110.03700 (2021)

“Critical drag as a mechanism for resistivity”
Dominic Else, T. Senthil
Phys. Rev. B 104, 205132 (2021) | arXiv:2106.15623 (2021)

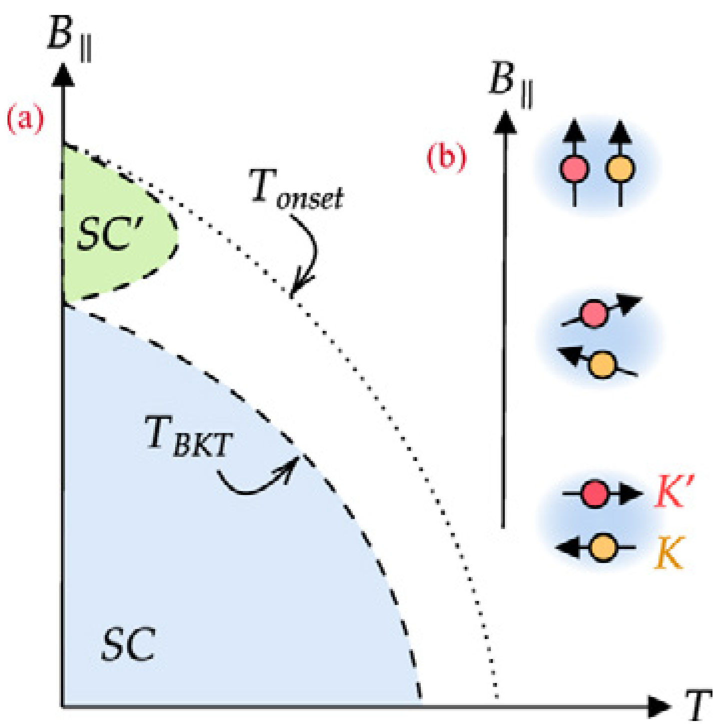

“Re-entrant Superconductivity Through a Quantum Lifshitz Transition in Twisted Trilayer Graphene”
Ethan Lake, T. Senthil
Phys. Rev. B 104, 174505 (2021) | arXiv:2104.13920 (2021)

(a) A schematic of the phase diagram in the B∥–T plane. SC denotes the low-field superconductor, and SC′ denotes the reentrant finite-momentum pairing phase. The inset (b) shows a schematic of how the pairing evolves in the field: the electrons in the Cooper pair have their spins oppositely aligned in the K,K′ valleys in zero field, with the spins smoothly rotating to point along the field at large B∥.

TROY VAN VOORHIS, *Chemistry*

"Heterogeneous Pair Approximation of Methanol Oxidation on TiO2 Reveals Two Reaction Pathways"

Changhae Andrew Kim, Troy Van Voorhis
J. Phys. Chem. C, 126, 4, 1845–1856 (2022)

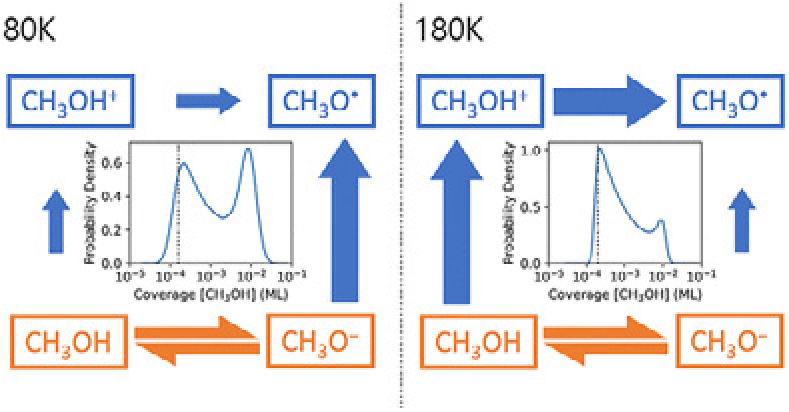

"Machine learning dynamic correlation in chemical kinetics"

Changhae Andrew Kim, Nathan D Ricke, Troy Van Voorhis
J. Chem. Phys. 155, 144107 (2021) | chemrxiv (2021)

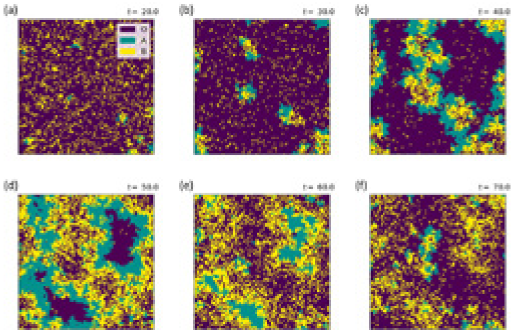

Snapshots of a 100 × 100 sublattice of a 500 × 500 lattice in a KMC simulation. The panels correspond to different times: (a) t = 20.0, (b) t = 30.0, (c) t = 40.0, (d) t = 50.0, (e) t = 60.0, and (f) t = 70.0. The rate constants were (k1, k2, k3) = (0.5, 0.3, 0.1), and the initial conditions were ([O], [A], [B]) = (0.2, 0.3, 0.5).

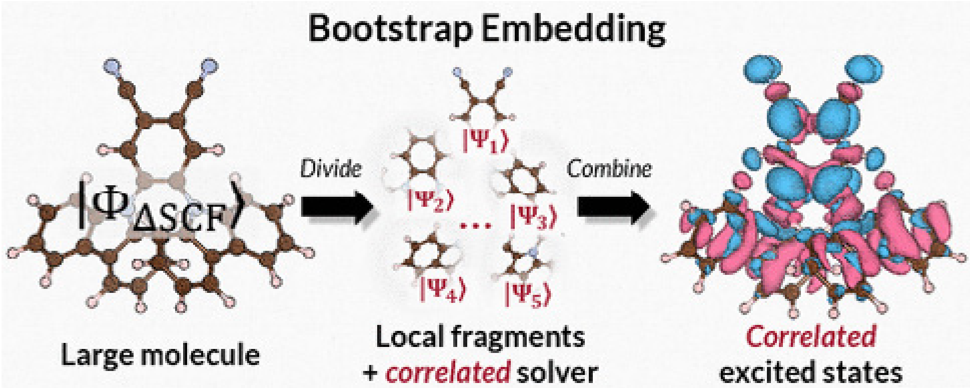

VLADAN VULETIC, *Physics*

"Evidence of Two-Source King Plot Nonlinearity in Spectroscopic Search for New Boson"
Joonseok Hur, Diana P. L. Aude Craik, Eugene Knyazev, Ian Counts, Luke Caldwell, Calvin Leung, Swadha Pandey, Julian C. Berengut, Amy Geddes, Witold Nazarewicz, Paul-Gerhard Reinhard, Akio Kawasaki, Honggi Jeon, Wonho Jhe, Vladan Vuletić
arXiv:2201.03578 (2022)

"Generating Extreme Spin Squeezing"
Sebastian C. Carrasco, Michael H. Goerz, Zeyang Li, Simone Colombo, Vladan Vuletić, Vladimir S. Malinovsky
arXiv:2201.01744 (2022)

"A quantum processor based on coherent transport of entangled atom arrays"
Dolev Bluvstein, Harry Levine, Giulia Semeghini, Tout T. Wang, Sepehr Ebadi, Marcin Kalinowski, Alexander Keesling, Nishad Maskara, Hannes Pichler, Markus Greiner, Vladan Vuletic, Mikhail D. Lukin
arXiv:2112.03923 (2021)

"Dispersive optical systems for scalable Raman driving of hyperfine qubits"
Harry Levine, Dolev Bluvstein, Alexander Keesling, Tout T. Wang, Sepehr Ebadi, Giulia Semeghini, Ahmed Omran, Markus Greiner, Vladan Vuletić, Mikhail D. Lukin
arXiv:2110.14645 (2021)

"Any-to-any connected cavity-mediated architecture for quantum computing with trapped ions or Rydberg arrays"
Joshua Ramette, Josiah Sinclair, Zachary Vendeiro, Alyssa Rudelis, Marko Cetina, Vladan Vuletić
arXiv:2109.11551 (2021)

"Probing Topological Spin Liquids on a Programmable Quantum Simulator"
Giulia Semeghini, Harry Levine, Alexander Keesling, Sepehr Ebadi, Tout T. Wang, Dolev Bluvstein, Ruben Verresen, Hannes Pichler, Marcin Kalinowski, Rhine Samajdar, Ahmed Omran, Subir Sachdev, Ashvin Vishwanath, Markus Greiner, Vladan Vuletic, Mikhail D. Lukin
SCIENCE • Vol 374, Issue 6572 • pp. 1242-1247 (2021) | arXiv:2104.04119

"Optimally squeezed atomic states for quantum metrology"
Sebastián C. Carrasco, Michael H. Goerz, Vladan Vuletić, and Vladimir S. Malinovsky
Quantum Information and Measurement (2021)

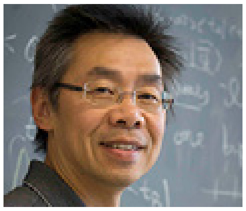

LINDLEY WINSLOW, *Physics*

"Limits on Astrophysical Antineutrinos with the KamLAND Experiment"
S Abe, S Asami, A Gando, ..., LA Winslow, et. Al
S. Abe et al ApJ 925 14 (2022)

"Search for Solar Flare Neutrinos with the KamLAND Detector"
S Abe, S Asami, A Gando, ..., LA Winslow, et. Al
S. Abe et al ApJ 924 103 (2022)

"CUORE opens the door to tonne-scale cryogenics experiments"
DQ Adams, C Alduino, F Alessandria, ..., LA Winslow, et. Al
Progress in Particle and Nuclear Physics Volume 122,103902 (2022)

"A search for correlated low-energy electron antineutrinos in KamLAND with gamma-ray bursts"
S Abe, S Asami, A Gando, ..., LA Winslow, et. Al
arxiv.org/abs/2112.04918 (2021)

"Ricochet Progress and Status"
Ricochet Collaboration, G. Beaulieu, V. Belov, ..., LA Winslow, et. Al
arXiv:2111.06745 (2021)

FRANCO N. C. WONG, *RLE*

"Spectral control of nonclassical light using an integrated thin-film lithium niobate modulator"
Di Zhu, Changchen Chen, Mengjie Yu, Linbo Shao, Yaowen Hu, C. J. Xin, Matthew Yeh, Soumya Ghosh, Lingyan He, Christian Reimer, Neil Sinclair, Franco N. C. Wong, Mian Zhang, Marko Lončar
arXiv:2112.09961 (2021)

BILGE YILDIZ, *NSE MSE*

"Bulk and surface exsolution produces a variety of Fe-rich and Fe-depleted ellipsoidal nanostructures in La0.6Sr0.4FeO3 thin films"
Komal Syed, Jiayue Wang, Bilge Yildiz, William Bowman
Nanoscale, Advance Article. (2022)

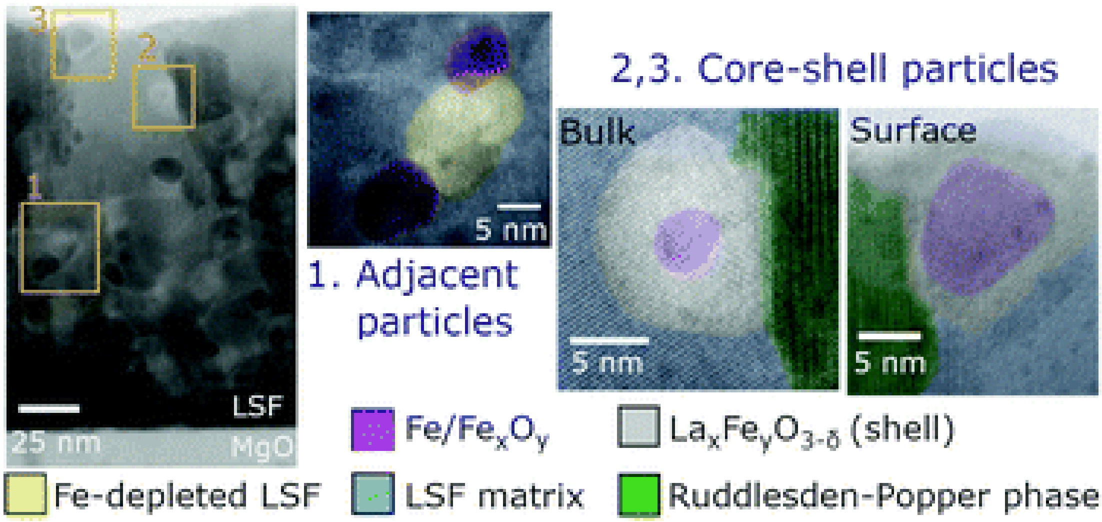

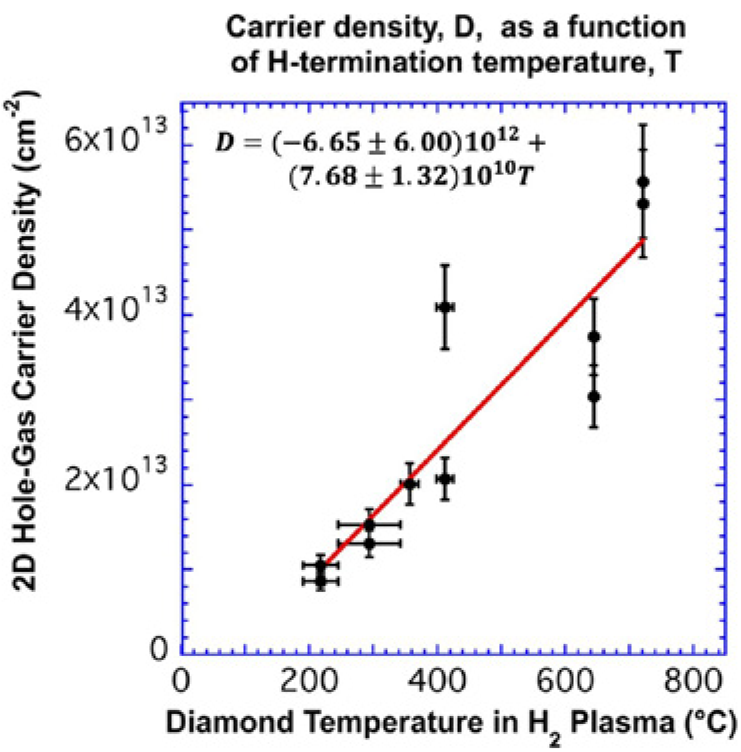

"Controlling the carrier density of surface conductive diamond"
M.W.Geis, M.A.Hollis, G.W.Turner, J. Daulton, J.O.Varghese, K.Klyukin, J. Wang, B.Yildiz, B.Zhang
Diamond and Related Materials, 108775, (2021)

BILGE YILDIZ, *NSE MSE*

[“Complex Oxides under Simulated Electric Field: Determinants of Defect Polarization in ABO3 Perovskites”]

Yen-Ting Chi, Krystyn J. Van Vliet, Mostafa Youssef, Bilge Yildiz

[Advanced Science, 2104476 (2021)]

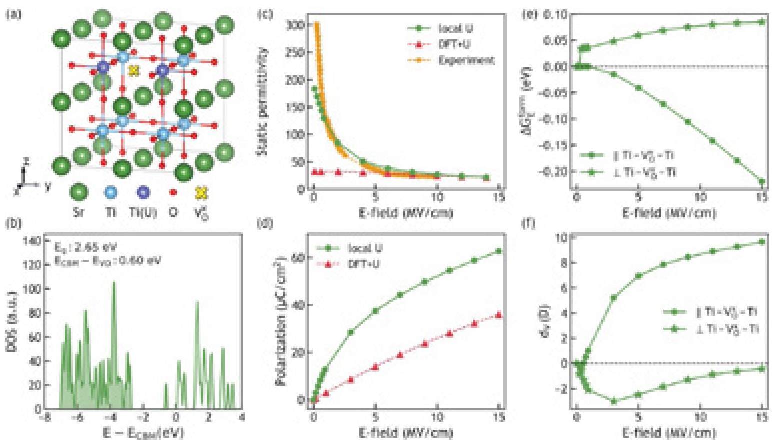

Density of states, dielectric properties and defect formation energy predicted for neutral oxygen vacancy VxOVOx in SrTiO3, using density functional theory with local Hubbard U. a) A 2 × 2 × 2 SrTiO3 super cell with VxOVOx. Green, light blue, and red spheres represent Sr, Ti, and O ions, respectively. Dark blue spheres indicate the two Ti ions with local Hubbard U, adjacent to the trapped electrons in the oxygen vacancy site represented by a yellow cross. All crystals in this work were visualized by VESTA.[41] b) Density of states for defected SrTiO3 under 3 MV cm−1 with shaded area representing occupied states. Eg and ECBM are the band gap and the minimum energy of conduction band, respectively. ECBM is set to be zero. Static dielectric permittivity (c) and polarization (d) of defected SrTiO3 with respect to applied electric field parallel to the Ti4+−VxO−Ti4+Ti4+−VOx−Ti4+ chain direction, from 0 to 15 MV cm−1, using the local Hubbard U method (green circles), standard DFT + U method (red triangles), and the experimental values (orange stars). The non-linear polarization predicted by local Hubbard U better reflects the high static permittivity of SrTiO3 under low field. Comparison of relative electric Gibbs free energy of formation of VxOVOx (e), and the vacancy dipole dV in units of Debye (f) with respect to applied field parallel to (circles) and perpendicular to (stars) the Ti4+−VxO−Ti4+Ti4+−VOx−Ti4+ chain.

[“Exsolution synthesis of nanocomposite perovskites with tunable electrical and magnetic properties”]

Jiayue Wang, Komal Syed, Shuai Ning, Iradwikanari Waluyo, Adrian Hunt, Ethan J. Crumlin, Alexander K. Opitz, Caroline A. Ross, William Bowman, Bilge Yildiz

[Advanced Functional Materials, 2108005, (2021)]

[“Antisite defects stabilized by antiphase boundaries in YFeO3 thin films”]

Abinash Kumar, Konstantin Klyukin, Shuai Ning, Cigdem Ozsoy-Keskinbora, Mikhail Ovsyanko, Felix van Uden, Ruud Krijnen, Bilge Yildiz, Caroline A. Ross, James M. LeBeau

[Advanced Functional Materials, 202107017, (2021)] | [arXiv:2107.09152v1 (2021)]

JONILYN YODER, *Lincoln Laboratory*

[“Calibration of Flux Crosstalk in Large-Scale Flux-Tunable Superconducting Quantum Circuits”]

X. Dai, D.M. Tennant, R. Trappen, A.J. Martinez, D. Melanson, M.A. Yurtalan, Y. Tang, S. Novikov, J.A. Grover, S.M. Disseler, J.I. Basham, R. Das, D.K. Kim, A.J. Melville, B.M. Niedzielski, S.J. Weber, J.L. Yoder, D.A. Lidar, and A. Lupascu
PRX Quantum 2, 040313 (2021) | arXiv:2105.14360

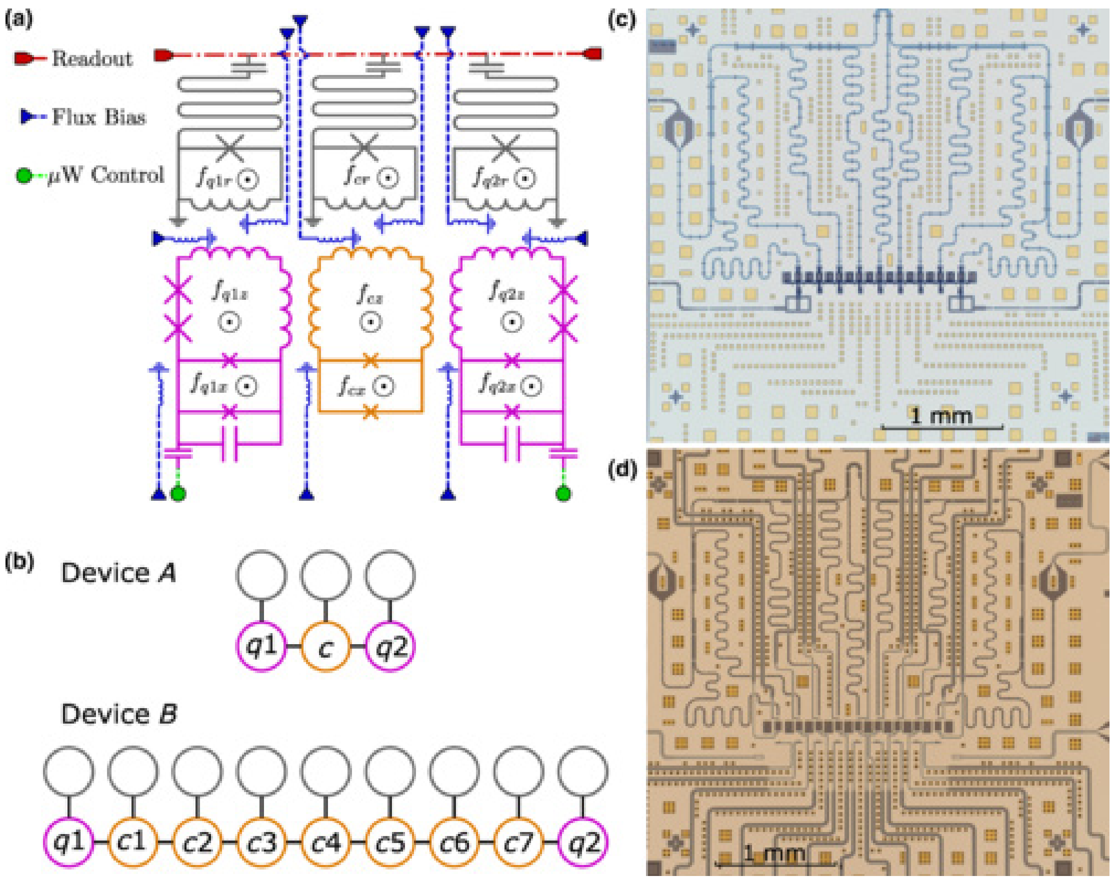

(a) Circuit schematic of device A. The qubit circuits (left and right, purple) are tunable CSFQs. The coupler circuit (middle, orange) is a tunable rf SQUID. Each qubit and coupler has two control loops and is coupled to a tunable resonator (top, gray). All resonators are coupled to a joint feedline (top, red). Fluxes in each loop are controlled via the on-chip bias lines (triangles, blue). The design also includes microwave control by capacitively coupling microwave lines (circle, green) to the qubit, allowing for spectroscopy measurement of the device (not used in this work). (b) Diagram representation of devices A and B. Device A contains two qubits (left and right units, purple), the coupler (insider cell, orange) and a tunable resonator for each cell (top, gray). Device B contains two qubits and seven couplers. Device B has the same qubit and coupler circuit schematic and control capabilities as device A, shown in (a). (c),(d) Microscope image of the qubit and interposer chips of device B. The qubit chip (c) hosts the qubit and readout circuitry and the interposer chip (d) hosts the flux-bias lines. The square features (yellow boxes) correspond to indium bumps used to connect the two chips.

From the Director
CQE PI Feature
CQE Student Feature
Around the Institute
Beyond the Institute
Quantum Conferences

MARTIN ZWIERLEIN, *Physics*

"Crystallization of Bosonic Quantum Hall States"

Biswaroop Mukherjee, Airlia Shaffer, Parth B. Patel, Zhenjie Yan, Cedric C. Wilson, Valentin Crépel, Richard J. Fletcher, Martin Zwierlein

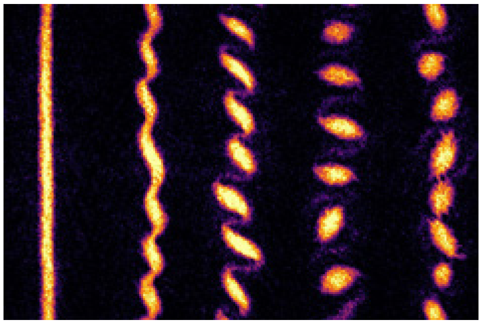

MIT News (2022) | Nature/s41586-021-04170-2 (2022) | Popular Science (2022)| Smithsonian Magazine (2022) | arXiv:2106.11300 (2021)

Just like the formation of weather patterns on Earth, here a spinning fluid of quantum particles breaks up into a crystal formed from swirling, tornado-like structures.

"Quantum register of fermion pairs"

Thomas Hartke, Botond Oreg, Ningyuan Jia & Martin Zwierlein

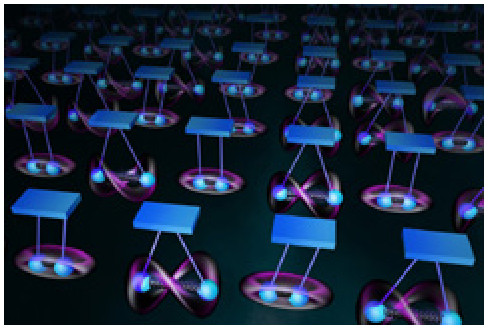

MIT News (2022) | Nature (2022) | Ars Technica (2022) | arXiv:2103.13992 (2021)

Image credit – Sampson Wilcox
MIT researchers have found a way to store quantum information in the vibrational motion of atom pairs, similar to the swinging of two pendula, connected by a spring. The quantum register contains hundreds of pairs of vibrating qubits that researchers can coherently control for over ten seconds.

"Spectroscopic probes of quantum gases"

Chris J. Vale & Martin Zwierlein
Nature s41567-021-01434-6 (2021)

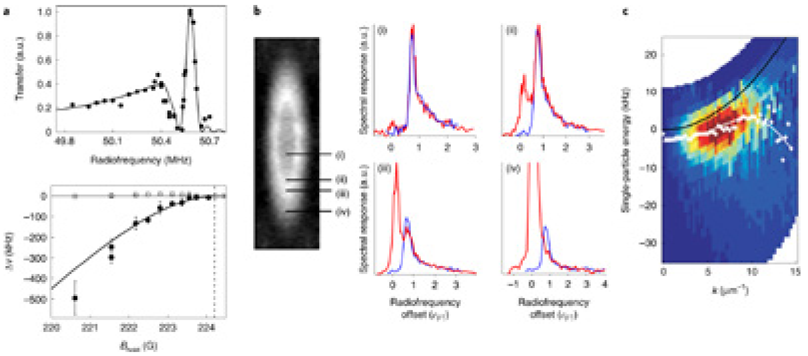

a, Top: radiofrequency spectrum showing a bare atomic transition (sharp peak) and the characteristic asymmetric spectral feature associated with molecular dissociation. Bottom: EB determined from the shift between the bare atomic (open squares) and molecular features (filled circles) as a function of the magnetic field Bhold8. b, Spatially resolved radiofrequency response of a spin-imbalanced two-component Fermi gas, where εF↑ is the Fermi energy of the majority spin component. Majority (red) and minority (blue) spectra from the indicated positions reveal a paired superfluid core with a peak shift that allows the pairing gap to be determined12. c, Angle-resolved photo-emission spectra of a two-component Fermi gas at unitarity provide momentum-resolved measurements of the single-particle spectral function A(k, ω) (false colour image), along with a fitted BCS-like dispersion (white line) to the peak of the spectral response (white symbols) 13. Panels reproduced with permission from: a, ref. 8, Springer Nature Limited; c, ref. 13, Springer Nature Limited. Panel b adapted with permission from ref. 12, APS.

Publications

Information scrambling in quantum circuits
Xiao Mi, et. al., including MIT-CQE member Edward H. Farhi
Science/10.1126/science.abg5029

The Efficient Preparation of Normal Distributions in Quantum Registers
Our algorithm employs a repeat-until-success scheme, and only requires a constant-bounded number of repetitions in expectation. In the experiments presented, the use of MCMR enables up to a 862.6x reduction in required qubits. [arXiv]

Relaxation of stationary states on a quantum computer yields a unique spectroscopic fingerprint of the computer's noise
In this paper, we simulate the relaxation of stationary quantum states on a quantum computer to obtain a unique spectroscopic fingerprint of the computer's noise. In contrast to traditional approaches, we obtain the frequency profile of the noise as it is experienced by the simulated stationary quantum states. [Communication Physics]

The impact of hardware specifications on reaching quantum advantage in the fault tolerant regime featured
We show that in certain situations, architectures with considerably slower code cycle times will still be able to reach desirable run times, provided enough physical qubits are available. [AVS Quantum Sci.]

Quantum computing in silicon hits 99 per cent accuracy
Australian researchers have proven that near error-free quantum computing is possible, paving the way to build silicon-based quantum devices compatible with current semiconductor manufacturing technology. [Nature]

Discovery could pave the way to high speed, low-energy quantum computing
Hovden explains that exotic quantum properties—like the ability to switch from a conductor to an insulator—could be key to the next generation of computing, providing more ways to store information and faster switching between states. [Nature Communications]

Faster technique for resetting quantum circuits proposed
The best current lab record for resetting a qubit is 280 nanoseconds, with 99.0% fidelity. "Our simulations suggest we could reset the qubit in 80 nanoseconds, with 99.0% fidelity," says Yoshioka. [Applied Physics Letters]

Major improvements in quantum fidelity
The researchers used quantum state tomography, which estimates the properties of a quantum state based on the properties of similar states, to keep track of values and correct for errors upon completion. The results showed a 23 percent improvement in quantum state fidelity—one of

the most successful refinements for a quantum problem so far. [Nature Physics]

A Survey of Quantum Computing for Finance

This survey paper presents a comprehensive summary of the state of the art of quantum computing for financial applications, with particular emphasis on Monte Carlo integration, optimization, and machine learning, showing how these solutions, adapted to work on a quantum computer, can help solve more efficiently and accurately problems such as derivative pricing, risk analysis, portfolio optimization, natural language processing, and fraud detection. [arXiv]

Qubits Can Be as Safe as Bits, Researchers Show

The result means that quantum codes now match classical codes in their combination of properties. It also provides a means to make quantum computers more efficient, since their ability to correct errors can now (theoretically) remain constant as they are made larger. [arXiv]

EPFL engineers find promising way to boost computing power of quantum computers

Engineers at EPFL have developed a method for reading several qubits—the smallest unit of quantum data—at the same time. Their discovery paves the way to a new generation of even more powerful quantum computers. [Nature Electronics]

Magnetic Surprise Revealed in "Magic-Angle" Graphene—Potential Quantum Computing Applications

"We've shown that we can create magnetism in a system that originally hosts superconductivity. This gives us a new way to study the interplay between superconductivity and magnetism, and provides exciting new possibilities for quantum science research." [Science]

Electron's wave nature constructed in the lab at last

Because the light and heavy holes accelerate at different rates in the electric field, their respective Bloch wavefunctions acquire different quantum phases before they recombine with the electrons. Thanks to this phase difference, their wavefunctions interfere to produce the final emission, which can then be measured. [Nature]

Experimental quantum teleportation of propagating microwaves

A team of scientists in Germany, Finland and Japan demonstrated unconditional quantum teleportation to propagate coherent microwave states by exploring two-mode squeezing and analog feedforward across a distance of 0.42 m. The researchers achieved a teleportation fidelity of $F = 0.689 \pm 0.004$. [Science Advances]

Research Team Reaches Milestone in Quantum Computing with Error Correction

They have integrated high-fidelity operations on encoded quantum data with a scalable scheme for repeated data stabilization. "We do three types of logical-qubit operations: initializing the logical qubit in any state, transforming it with gates, and measuring it." [Nature Physics]

Geometric entanglement of a photon and spin qubits in diamond
Here we show that geometric photon and spin qubits are entangled upon spontaneous emission with the help of the spin—orbit entanglement inherent in a nitrogen-vacancy center in diamond. The geometric spin qubit is defined in a degenerate subsystem of spin triplet electrons and manipulated with a polarized microwave.
[Communication Physics]

SQMS researchers discover performance-limiting nanohydrides in superconducting qubits
The new technological discovery is a variant of Q-disease—a strong degradation of cavity performance, which SRF scientists discovered several decades ago in niobium superconducting radio-frequency cavities built for particle accelerators.
[arXiv]

Algorithmic Ground-State Cooling of Weakly Coupled Oscillators Using Quantum Logic
Here, we introduce a novel algorithmic cooling protocol for transferring phonons from poorly to efficiently cooled modes. We reach the lowest temperature reported for a highly charged ion, with a residual temperature of only $T \lesssim 200\ \mu K$ in each of the two modes. [Phys. Rev. X 11, 041049]

Real-Time Error Correction for Quantum Computing
The team showed that they could perform multiple rounds of error detection and correction on each data qubit in the circuit and that they could detect two distinct types of qubit errors. "Essentially, we have demonstrated for the first time all of the elements needed for a single [error-tolerant] logical qubit," says Ryan-Anderson. [Phys. Rev X]

Princeton researchers develop world's purest sample of gallium arsenide
"The new samples/materials have only about 1 part per 10 billion impurities, meaning there is only one unwanted atom (impurity) for every 10 billion wanted atoms," Shayegan wrote. "This is like having only one bad person on Earth!" [Nature Materials]

Researchers disentangle quantum machine learning
"While entanglement is necessary for quantum speedups, the research indicates the need for careful design of which qubits should be entangled and how much," says co-author Dr Maria Kieferova, Research Fellow at the ARC Centre for Quantum Computation and Communication Technology based at the University of Technology Sydney. [PRXQ]

SU(2) hadrons on a quantum computer via a variational approach
The SU(2) gauge group considered here represents an important first step towards ultimately studying quantum chromodynamics, the theory that describes the properties

of protons, neutrons and other hadrons. [Video] [Nature Communications]

An optical lattice with sound
Here, we create an optical lattice with phonon modes using a Bose–Einstein condensate (BEC) coupled to a confocal optical resonator. Playing the role of an active quantum gas microscope, the multimode cavity QED system both images the phonons and induces the crystallization that supports phonons via short-range, photon-mediated atom–atom interactions. [Nature]

Many-body-localized discrete time crystal with a programmable spin-based quantum simulator
Here, we observe the hallmark signatures of the many-body-localized discrete time crystal using a novel quantum simulation platform based on individually controllable 13-C nuclear spins in diamond. [Science]

New Platform for Quantum Computing? Artificial Material Mimics Quantum Entangled Rare Earth Compounds
One layer behaves like a metal, conducting electrons, while the other layer has a structural change that causes electrons to be localized into a regular lattice. The combination of the two results in the appearance of heavy fermion physics, which neither layer exhibits alone. [Nature]

Realization of Modularized Quantum Light Source Toward Fault-tolerant Large-scale Universal Optical Quantum Computers
In this study, we have developed a new optical fiber-coupled quantum light source that operates at optical communication wavelengths. [Applied Physics Letters]

New algorithms advance the computing power of early-stage quantum computers
A group of scientists at the U.S. Department of Energy's Ames Laboratory has developed computational quantum algorithms that are capable of efficient and highly accurate simulations of static and dynamic properties of quantum systems. [PRX Quantum | Advanced Quantum Technologies]

A potential hangup for quantum computing: Cosmic rays
The problem is that the quasiparticles won't end up localized; instead, they should spread out around their site of origin and end up affecting multiple qubits. And that should be enough to interfere with error correction. [Nature Physics]

New Standards Rolling Out for Clocking Quantum-Computer Performance
"It's surprisingly difficult to benchmark state-of-the-art quantum computers, because most bench-marks rely on comparing the results of a quantum computation with the correct output, computed on a

conventional computer," says study lead author Tim Proctor. [Nature Physics]

Race Not Over Between Classical and Quantum Computers

The team behind that advantage claim had asserted that a classical computation of Gaussian boson sampling would take 600 million years on the world's fastest super-computer. But Bulmer, Bell, and colleagues show that their classical algorithm can do it in just 73 days. [Science Advances]

IBM Quantum Debuts Classical Entanglement Forging to Expand Simulation Capabilities

BM last week reported a new technique—entanglement forging—that uses both quantum and classical computing resources to double the size of select simulation problems that can be solved on current quantum computers. [PRXQ]

Math may have caught up with Google's quantum-supremacy claims

Over the intervening time, a few options have been explored that do perform better. Now, Feng Pan, Keyang Chen, and Pan Zhang are describing a specific method that allows a GPU-based cluster to produce an equivalent output in only 15 hours. Run it on a leading super-computer, and they estimate that it would outperform the Sycamore quantum processor. [arXiv]

Cryogenic Chip Is Big Step To Scale Up Quantum Computing

Microsoft Senior Hardware Engineer, Dr. Kushal Das, a joint inventor of the chip, said: "Our device does away with all those cables. With just two wires carrying information as input, it can generate control signals for thousands of qubits.[Nature Electronics]

Duke University and IonQ Develop New Quantum Computing Gate

The new gate family includes the N-qubit Toffoli gate, which flips a select qubit if and only if all the other qubits are in a particular state. Unlike standard two-qubit quantum computing gates, the N-qubit Toffoli gate acts on many qubits at once, leading to more efficient operations. [arXiv]

A-List Candidate for Fault-Free Quantum Computing Delivers Puzzling Surprise

The promise is that if you have a spin-triplet superconductor, it can potentially be used to make topological qubits," said Dai. "You can't do that with spin-singlet superconductors. So, that's why people are extremely interested in this." [Nature]

Sandia Designs a Faster and More Accurate Quantum Computing Benchmark

"It is standard practice in the quantum computing community to use only random, disordered programs to measure performance, and our results show that this is not a good thing to do," said computer scientist Timothy Proctor. With a mirror circuit, however, the output should always be the same as the input or some intentional modification. [Nature Physics]

Shrinking qubits for quantum computing with atom-thin materials
Using 2D materials, researchers have built superconducting qubits that are a fraction of previous sizes, paving the way for smaller quantum computers. [Nano Lett.]

Stanford engineers propose a simpler design for quantum computers
Their proposed design uses a laser to manipulate a single atom that, in turn, can modify the state of the photons via a phenomenon called "quantum teleportation." [Optica]

Quantum computers getting connected
"With our approach, we could demonstrate that the excellent spin-optical properties of our colour centres are maintained after nanophotonic integration." says Florian Kaiser, Assistant Professor at the University of Stuttgart. [Nature Materials]

Key Witness Helps Scientists Detect 'Spooky' Quantum Entanglement in Solid Materials
"The quantum Fisher information, or QFI, witness showed a close overlap between theory and experiment, which makes it a robust and reliable way to quantify entanglement," said Allen Scheie, a postdoctoral research associate at ORNL and a lead author. [Physical Review B].

Politics and Funding

Congress Passes National Defense Authorization Act for Fiscal Year 2022
DOD is directed to "establish a set of activities to accelerate the development and deployment of a useful, large-scale, dual-use quantum computing capability," and to provide funding through DARPA to "one or more organizations" to advance that goal.

US-Japan alliance restricting vital tech exports to China risks 'major impact' on trade, supply chains
Japan and the US are mulling the establishment of a multilateral framework to regulate the trade of advanced technology, which includes semiconductor manufacturing equipment, quantum cryptography and artificial intelligence.

Japan steps up quantum push as U.S. and China forge ahead
An expert panel met Monday to start mapping out the changes, which the government aims to approve by June.

Quantum Computing Governance Principles
This report lays out the first set of principles for the responsible design and adoption of quantum computing technologies to drive positive outcomes for society; it also outlines the key actions to be taken by stakeholders to incentivize the development of the technology while mitigating the possible risks.

Memorandum on Improving the Cybersecurity of National Security, Department of Defense, and Intelligence Community Systems
Within 60 days of the date of this memorandum, the NSA shall revise and make available to Chief Information Officers the CNSS Advisory Memorandum 01-07 and any associated enclosures and relevant references regarding modernization planning, use of unsupported encryption, approved mission unique protocols, quantum resistant protocols, and planning for use of quantum resistant cryptography where necessary.

Quantum Annealer With More Than 5,000 Qubits Launched
The annealing quantum computer is part of the Jülich UNified Infrastructure for Quantum computing (JUNIQ), which was established in autumn 2019 to provide researchers in Germany and Europe with access to various quantum systems.

Incentives, Infrastructure, and Research and Development Needs To Support a Strong Domestic Semi-conductor Industry
The Department of Commerce (Department), with the assistance of the National Institute of Standards and Technology (NIST), is seeking information in order to inform the planning and design of potential programs to: Incentivize investment in semiconductor manufacturing facilities and associated ecosystems

DOE Announces $420 Million to Advance Clean Energy Breakthroughs at Energy Research Centers Across America
This funding will advance climate solutions through early-stage research on clean energy technology, advanced and low-carbon manufacturing, and quantum information science.

Japan to conceal key patents to boost economic security
The main targets of the concealment of patents are nuclear-related and other advanced technologies such as quantum cryptography, which enhances the security of data communications.

DOE Announces $18M for Research to Advance Particle Accelerator Technology
Research will focus both on laying the R&D groundwork for next-generation accelerators and on potential upgrades to existing facilities that will advance our understanding of the building blocks of matter, discovering the origins of nuclei, and identifying the forces that transform matter.

France opens access to quantum computing to researchers, start-ups
The French government launched a new programme to link quantum machines and supercomputers on Tuesday (4 January). The resources will have to be made available to researchers and companies to ensure France is up to speed with the technological revolutions to come.

US blocks export of quantum computing tech to Chinese organizations
The Commerce Department on Wednesday barred US firms from exporting quantum computing technology to eight Chinese companies and labs to try to keep the country from decrypting sensitive US communications and developing new military technology. [PDF]

Australia, US agree to protect sensitive quantum tech, share knowledge
The two nations signed a statement of intent on Friday, recognising that the "critical emerging technology" presents significant opportunities for economic prosperity and security. [Statement]

Study To Advance a More Productive Tech Economy
This Request for Information (RFI) is seeking comments to help identify, understand, refine, and guide the development of the current and future state of technology in the eight emerging technology areas named above. The information will inform a final report that will be submitted to Congress.

Taiwan to invest big in quantum computing
Taiwan will set aside an NT$8 billion (US$288 million) budget for the development of quantum computing technology and talent nurturing, Premier Su Tseng-chang (蘇貞昌) announced Thursday (Dec. 2).

[FY22 Budget Outlook: Department of Defense]

The Senate proposes to provide $60 million above the requested amount within DARPA's budget for quantum computing, specifically to "evaluate disruptive designs for utility-scale, fault-tolerant quantum computers, with a specific focus on systems that can be constructed in less than 10 years using non-traditional quantum computing approaches."

[The United States and United Kingdom Issue Joint Statement to Enhance Cooperation on Quantum Information Science and Technology]

The quantum cooperation statement articulates a shared vision to promote collaborative research efforts, enhance training opportunities for scientists and engineers, and grow the market for quantum technologies. [Statement]

[Two of World's Biggest Quantum Computers Made in China]

Quantum computers Zuchongzi and Jiuzhang 2.0 may both display "quantum primacy" over classical computers. Although the sampling task used in experiments with Zuchongzi has no known practical value, the Gaussian boson sampling problem on which Jiuzhang 2.0 was tested potentially has many practical applications, such as identifying which pairs of molecules are the best fits for each other.

MIT Center for Quantum Engineering
MIT Quantum Science and Engineering Consortium

Pronouncements and Commentary

First quantum computer to pack 100 qubits enters crowded race
The 'Eagle' chip is a step towards IBM's goal of creating a 433-qubit quantum processor next year, followed by one with 1,121 qubits named Condor by 2023. [Nature]

Quantum computing use cases are getting real—what you need to know
In 2021 alone, announced investments in quantum-computing start-ups have surpassed $1.7 billion, more than double the amount raised in 2020. Experts disagree on whether quantum computers can create significant business value before they are fully fault tolerant.

What To Expect From Quantum Computing In The Next Two Years
The quantum ecosystem will look very different in 2023 than it does now. In large part, this will be the result of quantum computers with more qubits and with less noise.

China's Sunway exascale supercomputer team wins top prize for closing Google's quantum supremacy gap
The Sunway exascale computer had reached the speed of 4.4 exaflops, or quintillion calculations per second with more than 10 million CPU cores, Zhejiang Lab said on its social media account on Friday.

Strangeworks And Quantinuum Partner To Integrate Quantum-Enhanced Cryptographic Key Service
Quantum Origin is the world's first commercial product to generate cryptographic keys using quantum computers, and will become an important component of the eco-system, providing its users seamless access to superior cryptographic keys and helping to protect against current security threats.

Quantum computing study finds rising budgets, growing competitive significance
The study, based on a survey of 300 corporate enterprise leaders conducted by Wakefield Research, revealed that 28% of enterprises surveyed now have quantum computing budgets over $1 million, a major departure from the $100,000 "toe in the water" budgets of the recent past, according to Zapata.

What Europe's $48 billion chips plan could do for quantum computing
The European Chips Act, which still has to be approved by EU member states and lawmakers, would temporarily re-write strict rules that regulate when and how individual countries are allowed to subsidize industries within their borders.

ColdQuanta to develop atomic clocks for Office of Naval Research

ColdQuanta has been awarded a 5-year subcontract to develop portable atomic clocks for the Office of Naval Research. ColdQuanta will serve as a subcontractor to Vescent Photonics, which secured the $15.6 million total award.

Q-CTRL Awarded DOE Grant to Automate Quantum Computers with Sandia National Labs

Q-CTRL will leverage the grant to fund a project automating quantum computer hardware through AI in collaboration with Sandia National Laboratories, a U.S. Department of Energy science and engineering lab for national security and technology innovation.

Rigetti and Zapata to Build First Commercial Hybrid Quantum-Classical Compilation Stack

The integration provides access to Rigetti QPUs, including the company's recently announced 80Q Aspen-M system. This new, full-stack combination is designed to optimize access to the new device and speed up execution of hybrid applications.

D-Wave to Go Public Via Transaction with DPCM Capital

Upon closing of the transaction, shares of D-Wave Quantum Inc., a newly formed parent company of D-Wave and DPCM Capital, are expected to trade on the NYSE under the symbol "QBTS."

How Quantum Computers Will Correct Their Errors

A fault-tolerant code can deal with errors introduced by the environment, by imperfect operations on those qubits, and even by the error-correction steps themselves—provided the rate at which these errors occur is below a certain threshold.

USRA Teams with Rigetti Computing and NASA to Deliver Technology for Phase 2 of the DARPA ONISQ Program

The project will continue to employ Rigetti Computing quantum p rocessors, including the company's recently announced 80-qubit system, for the purpose of increasing the quantum computing capabilities available to program variational quantum algorithms developed by the team.

NASA's JPL uses Microsoft's Azure Quantum to manage communication with space missions

The Azure Quantum team developed a solution for a version of JPL's scheduling problem with a limited feature set with the eventual goal to incorporate a broader set of require-ments. This is intended to reduce the need for lengthy negotiations and speed up the overall process.

Menten Ai Partners With Xanadu To Develop Quantum Machine Learning For Protein-Based Drug Discovery

Menten AI partners with Xanadu to build solutions on top of Xanadu's open-source software, PennyLane, to design novel drug molecules that can efficiently bind to a specific target of interest.

MIT Center for Quantum Engineering

MIT Quantum Science and Engineering Consortium

Cisco chases quantum tech
The company is investing in photonics development, which will enable quantum communications as well as other hardware and software technologies for quantum computing, networking, and cryptography.

Hyundai Motor, IonQ team up on next-generation batteries
The partnership will allow Hyundai to use IonQ's quantum computers to develop high-performance lithium batteries with better energy efficiency at lower costs.

Google's Australia investment could be a big boost for the nation's A.I. scene
Google announced Monday that it plans to set up a new Google Research Australia lab in Sydney as part of a 1 billion Australian dollar ($729 million) investment in Australia. The lab will research everything from AI to quantum computing.

New platform opens quantum networking to everyone
Starting today, everyone can freely access Quantum Network Explorer (QNE) to experiment with quantum networks. Right now, your programs will run on our simulation platforms NetSquid or SimulaQron.

Quantum science & technology: Highlights of 2021
No list of quantum highlights would be complete without a few results to remind us just how wonderfully strange the quantum world can be.

Inside Google's Quantum Computing Data Center
The facility in Santa Barbara, Calif. is where Google hopes to create the first error-corrected quantum computer, a key milestone in applying the technology.

Why quantum 'utility' should replace quantum advantage
Because what may be a more valuable goal for this still-nascent industry is achieving quantum "utility," or usefulness, as soon as possible. Quantum utility is defined as a quantum system outperforming classical processors of comparable size, weight and power in similar environments.

Honeywell Just Launched The World's Largest Quantum Computing Company
With the deal's completion, Quantinuum is now the largest, standalone quantum computing enterprise anywhere, according to the new company. The new company has 400 employees and offices in Cambridge, U.K., and Colorado.

New Quantum Intermediate Representation Alliance Serves as Common Interface for Quantum Computing Development
The Linux Foundation announced the QIR Alliance, a joint effort to establish an intermediate representation with the goal to facilitate interoperability within the quantum ecosystem. Founding members include Honeywell, Microsoft, Oak Ridge National Laboratory, Quantum Circuits Inc. and Rigetti Computing.

Amazon quantum computing comes to Europe with OQC

OQC 8 qubit quantum computer called Lucy will debut on Amazon Braket and be available to customers to access from Europe and around the world from February 2022.

Rigetti Enhances Predictive Weather Modeling with Quantum Machine Learning

Building on existing machine learning workflows, the company applied a combination of classical and quantum machine learning techniques to produce high-quality synthetic weather radar data and improve classical models for storm prediction.

IDC Forecasts Worldwide Quantum Computing Market to Grow to $8.6B in 2027

This represents a 6-year compound annual growth rate (CAGR) of 50.9% over the 2021-2027 forecast period. The forecast includes core quantum computing as a service as well as enabling and adjacent quantum computing as a service.

Cambridge Quantum and Deutsche Bahn Netz AG Leverage Latest Quantum Algorithms to Optimise Train Scheduling

The team re-optimised realistic train timetables after simulated delays and are now identifying areas for continued study. This collaboration evidences how innovations in both quantum algorithms and domain-specific modelling can inform a long-term vision for a faster and greener transportation network.

2022:

1–3 Apr: Quantum Computing Applications in Chemical and Biochemical Engineering Workshop, Copenhagen, Denmark

3–7 Apr: Security, Robustness, and Trust in Artificial Intelligence and Distributed Architectures, Orlando, Florida

11–13 Apr: Topological Materials: From Weak to Strong Correlations

25–28 Apr: Simulating Quantum Many-Body Systems on Noisy Intermediate-Scale Quantum Computers

15–20 May: CLEO

16-20 May: IEEE International Conference on Communications

29 May–2 Jun: ISC High Performance, Hamburg, Germany

30 May–3 Jun: Division of Atomic, Molecular & Optical Physics, Orlando, Florida

14–15 Jun: Quantum.Tech, Boston, United States of America

19–24 Jun: International Workshop on Quantum Systems in Chemistry, Physics and Biology

20–24 Jun: New Perspectives in Quantum Information

21–23 Jun: International Conference on Quantum Matter & Information, Barcelona, Spain

21–23 Jun: Quantum Computing Thematic Track, London

27 Jun–1 Jul: Quantum Thermodynamics Conference

11–14 Jul: Conference on the Theory of Quantum Computation, Communication, and Cryptography

11–15 Jul: International Conference on Quantum Communication, Measurement and Computing, Lisbon, Portugal

11–15 Jul: Supercomputing Frontiers, Warsaw, Poland

21–25 Aug: SPIE Quantum Communication and Quantum Imaging Conference, San Diego

29 Aug–2 Sep: Conference on Quantum Information and Quantum Control IX

29–31 Aug: Solvay Workshop on Quantum Simulation 2021, Brussels